Advanced Polysiloxane Waveguide Components for Telecommunications

A thesis submitted for the degree of Master of Philosophy
of the Australian National University

Yang Zhang

April 2007

the Australian National University
the Research School of Physics & Science Engineering
Laser Physics Centre

This thesis is entirely my own work,
except where explicitly indicated.

Yang Zhang

Laser Physics Centre
Research School of Physical Sciences and Engineering
The Australian National University
Canberra, ACT 0200, Australia

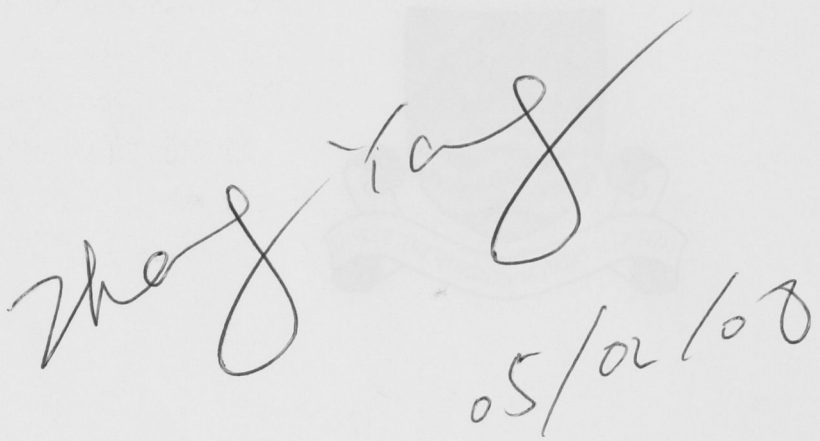

Acknowledgements

Throughout the research undertaken between January 2005 and February 2007 at the Laser Physics Centre, I have had the opportunity to work and communicate with a lot of people. These interactions have been the best memory of my research work and study. However, I cannot possibly express my appreciation to them individually in my thesis, but I wish to acknowledge some that have been particularly helpful and inspiring.

Professor Barry Lurther-Davies has fully supported the project from its beginning with great vigor. His energy and optimism have sustained both the project and myself, for which I am very grateful.

Dr. Steve Madden has graciously acted as a supervisor in this project. I am extremely thankful for his support, guidance and the direction that he has provided to the project from the beginning. I also acknowledge his great efforts on my thesis, as he often has to work on it till midnight.

Dr. Robbie Charters has provided many important insights, and have aided in the direction of the research. For his support and help I am grateful. And his colleagues, Ben Cornish, Dr. Graham Atkins, Dr. Graeme Gordon, Warwick Holloway and Maureen Brauers have been a great support throughout this work. I very much appreciate their generous help in materials fabrication and instrumentation.

It has been a pleasure to work with the people in the Laser Physics Center, Dr. Duk Choi, Maryla Krolikowski, John Bottega, Craig McCleod, Anita Smith on this project. I appreciate the willing and capable help of both Josephine McKeon and Klaus Webber in Engineering Department, who have helped with many of the experiments where aluminum deposition was needed and our system was unavailable. Finally, I especially appreciate the help of Dr. Shad Roundy, who gave me an opportunity to study at ANU.

I also greatly appreciate Department of Applied Math and Department of Electronic Material Engineering in Research School of Physical Sciences and Engineering at the Australian National University for giving assistance in AFM

measurements. Dr. Cheng Huang at Electronic Microscopy Unit gave many useful suggestions in FESEM application, which helped a lot. I also gratefully acknowledge Dr. Li Weitang at Plasma Centre for his advice and support in this project.

Specially, I am very thankful for Redfern Polymer Optics Pty. Ltd in Canberra to provide the experimental materials and all kinds of helps.

Finally, I am ever grateful to my parents for their endless love and confidence in me. They gave me not only complete financial support but also great understanding while I have been studying in Australia. To them, I am always in debt.

Abstract

Telecommunications is one of the worlds rapidly growing industries and is today founded on optical transmission technology with its ever growing pervasiveness, currently moving towards direct optical connection of the home. The desired and required size and cost reduction of optical components to enable this success has led to a large research effort based around the vision of integrated planar style fabrication with novel materials. Whilst planar integrated components have been available for a number of years, there is still a strong cost and size driver that has not yet been satisfied.

In this thesis, we first look at different non-polymer and polymer material systems. Then we review the most commonly used classes of technology and present their pros and cons as well as the functions achieved to date in each. The characteristics of Inorganic Polymer Glasses (IPGs), which is commercialized by RPO Pty Ltd in Canberra, Australia, are examined. A comprehensive survey of novel and conventional optical polymer systems and their processing techniques is also presented.

In IPG based waveguide fabrication, there are three problems in the project requiring resolution: (a) waveguides below about 5 micron are not directly UV patternable in IPG, and need alternative fabrication methods, (b) need masking and dry etch technology for small guides and etched gratings etc, is needed, (c) severe problems with direct metallization of IPG and surface roughness have to be overcome for several different applications. In order to eliminate these problems, this dissertation explores the possible fabrication methods of IPG based waveguides for the creation of photonic integrated devices.

Metallization of IPG films was extensively investigated due to the unusual effects observed with IPG. Issues associated with direct metallization and metallization onto a buffer atop the IPG film were overcome successfully. An extensive study of new dry etching methods for fabricating IPG based waveguides was conducted using $CHF_3/O_2/Ar$ or CHF_3/O_2 gas mixtures to determine the optimum process conditions for the waveguides with Aluminum or silicon dioxide

etching masks. It was found that a silicon dioxide mask is a simpler option for etching small dimension (< 3 μm) IPG based waveguides and produced near vertical sidewalls with a smooth profile. However, when considering the selectivity, an Aluminum mask has obvious advantages for deep etching to make waveguide facets or trenches for other waveguide applications, etc. In measurement, the minimum waveguide loss attained with dry etched waveguides was 0.73 dB/cm at 1550 nm and 0.40 dB/cm at 1310 nm.

This thesis also presents an alternative novel method of patterning IPG by soft lithography. Although, these techniques have been used with inorganic glasses or other materials, IPG posed some special challenges. The possible release treatments required for the etched silicon dioxide master and soft lithography processes were presented. Finally, both theory and test results demonstrate that soft lithography are capable of 3 micron or submicron IPG based waveguide fabrication.

Contents

List of Figures

List of Tables

List of Acronyms

A.....Angstrom

AFM.....Atomic Force Microscope

Al.....Aluminum

Au.....Gold

BARC.....Bottom Anti-Reflection Coating

CCD.....Charge-coupled Device

CD.....Critical Dimension

Cr.....Chromium

CTE.....Coefficient of Thermal Expansion

DC.....Direct Current

DIC.....Differential Interference Contrast

d-PFMA.....deuterated Polyfluoromethacrylate

ECR.....Electron Cyclotron Resonance

FESEM.....Field Emission Scanning Electron Microscope

FOV.....Fields of View

HMDS.....Hexamethyldisilizane

IAD.....Ion Assisted Deposition

ICP.....Inductively Coupled Plasma

InP.....Indium Phosphide

IP.....Intellectual Property

IPGs.....Inorganic Polymer Glasses

$LiNbO_3$.....Lithium Niobate

MEMS.....Microelectromechanical Systems

MFD.....Mode Field Diameter

MIMIC.....Micro Molding in Capillaries

PC.....Polycarbonate

PDMS.....Polydimethylsiloxane

PECVD.....Plasma Enhanced Chemical Vapor Deposition

PFCB.....Perfluorocyclobutyl

PICs.....Photonic Integrated Circuits

PMMA.....Polymethylmethacrylate or Acrylic glass

PS.....Polystyrene

PTFE.....Polytetrafluoroethylene

PU.....Polyurethane

RF.....Radio Frequency

RI.....Refractive Index

RIE.....Reactive Ion Etching

RPM.....Rotation per Minute

RPO.....Redfern Polymer Optics Pty. Ltd

SCCM.....Standard Cubic Centimeters per Minute

SOI.....Silicon on Insulator

TE.....Transverse Electric

T_g.....Glass Transition Temperature

TM.....Transverse Magnetic

UV.....Ultraviolet

VLSI.....Very-large-scale integration

Chapter 1

Introduction

1.1 Background and Motivation

Optical fiber technology revolutionized the communications industry upon its introduction and has continued to mature and push deeper and deeper into the network. Today, even fiber to the home systems are in active mass scale commercial deployment in a small number of countries. However, the main barrier to the widespread use of optical technologies in our societies is rather the high cost of most optical technology than any purely technical issues.

Photonic devices, which are embedded deep in the network, are shared by many subscribers who collectively absorb the relatively high component or sub-system costs. However, the real costs of increasingly sophisticated and high speed technologies spiraled and exceeded revenues from subscribers, triggering the collapse of the industry bubble in 2002. Thus, the desire to push optical technology right out to customers, and opportunities in the enterprise market has created an interest in low cost componentry as the primary driver for the future telecommunication markets.

There are two technologies developed in the 20^{th} century which may create low cost photonic products. The first one is the development and understanding of plastics and polymers; and the second one is the rapid development of silicon integrated circuit technology and processing methods. Plastics comprise a versatile range of inexpensive materials that can be engineered at the molecular level to provide desirable physical properties and are easily shaped to create most microstructures. The silicon chip introduced the concepts of integration of many devices on a chip and the manufacture of many chips in parallel which led to miniaturization of complex electronic circuits and enabled efficient mass-manufacturing techniques at low cost. Clearly the concept of integration and the use of plastics are both relevant to photonic devices when a combination of low cost and high performance is required. This has motivated many

researchers to study polymer photonic integrated circuits.

Unfortunately the most transparent and homogeneous optical polymers often have physical properties that are inadequate for photonic applications. For example most of acrylates (such as PMMA) display excellent optical clarity but have very low glass transition temperature making them thermally unstable and susceptible to moisture absorption. The polyimides, which are widely used in the electronics industry, whilst having excellent thermal properties are strongly birefringent when prepared as thin films which make them of limited value for optical circuits. Polymers are also often subject to slow degradation when exposed to light — a particularly undesirable property for an optical device. As a result only a few polymer materials used for photonic integrated circuits have proved capable of passing the rigorous Telcordia GR1209 and GR1221 tests probing long term reliability and performance under severe environmental conditions. This is very important as it is essentially impossible to market devices to the telecommunications industry without passing these tests.

Suitable polymers will offer significant advantages beyond their low cost for photonics compared with the traditional inorganic glasses such as silica. Silica has so far been the material of choice for photonic integrated circuits (PICs). It is very stable, can be produced as high quality thin films and patterned to create optical waveguides using a variety of techniques. Furthermore it is compatible with the standard optical transmission medium — silica optical fibers. Unfortunately, silica has some fundamental limitations. Firstly obtaining high index contrast between the core and cladding is difficult. High contrast allows the used of much smaller radii in waveguide bends resulting in more than an order of magnitude reduction in the overall size of the optical circuits and this will be essential for future low cost devices. Furthermore, the absence of significant electro-optic activity, the material's low thermo-optic sensitivity and low third-order nonlinearity makes chip-sized active and non-linear components in silica difficult to achieve. Finally the cost of the materials, the processing and the

associated safety equipment is high for the silica system. None of these restrictions, however, are fundamental to polymers.

Over the past few years, hybrid organic-inorganic siloxane polymers have emerged as commercially viable PIC materials. Siloxanes are macromolecules comprised of a polymer backbone of alternating silicon and oxygen atoms (siloxane bonds) with organic side groups, such as methyl, phenyl or vinyl, attached to the silicon. By adjusting the -Si-O-Si-O- chain length, the functionality of the side groups and the cross-linking between molecular chains, siloxanes can be synthesized into an almost infinite variety of materials, each with unique chemical properties and performance characteristics. They display properties intermediate between inorganic glasses and plastics. Their thermal stability, low moisture absorption, wide operating temperature range, and versatility make them excellent materials for photonics applications compared with most organic polymers. The main challenge for optical applications was thus identifying the appropriate chain structure or variety of structures that allow the production of siloxane resins with stable but tunable properties for waveguide fabrication.

A novel range of siloxane resins was developed in the late 1990s at the Australian National University as result of research funded by the Australian Photonics Cooperative Research Centre. The IP developed during this program was licensed to a start-up company RPO Pty Ltd for the production of poly-siloxane optical waveguides. The materials developed by RPO have been trade-marked as Inorganic Polymer Glasses^{TM} (IPGs^{TM}).

Whilst RPO's initial market focus was telecommunications, the massive down turn in this market since 2001 led RPO to seek alternative applications for the technology. To achieve low cost in device production, RPO's IPGs film patterning process mirrors that of a negative photo resist. The material is exposed to UV light through a mask, rendering the exposed regions insoluble in developer thereby creating a pattern of waveguide cores. This approach

provides remarkably inexpensive and high quality waveguides but has limitations. Waveguides narrower than about 5 microns or other features below a few microns can not be accurately reproduced. This severely limits the usable index contrast and hence the range of possible devices that can be fabricated for telecommunications markets. The materials themselves can support index contrasts much higher than the current approach to patterning allows and hence new patterning methods allowing higher contrast and complex device fabrication must be developed.

It was therefore the aim of this project to research alternative methods of patterning IPGs and demonstrates the fabrication of high index contrast single mode waveguides for future telecommunications markets.

1.2 Outline

This thesis is investigating the fabrication of waveguide devices based on inorganic polymer glasses. The main purpose of this thesis and our project is on the fabrication of low loss high index contrast waveguides and the optimization of the fabrication processes.

In chapter 2, a survey of optical polymer systems, their processing techniques, and the integrated optical waveguide components and circuits derived from these materials is summarized. The first part is focused on discussing the characteristics of several important classes of optical polymers, such as their refractive index, optical loss, processibility/mechanical properties, and environmental performance. The aim of this chapter should give reader an idea of current state of polymer based waveguide research and the motivation behind this thesis. This chapter also gives a review of waveguides and other photonic devices derived from polymers.

In chapter 3, the emphasis is placed on versatile processing technologies commonly used for fabricating waveguides and how they can be used with IPGs.

Metallization approaches for IPG are discussed in detail due to the unusual effects observed with IPG. Direct metallization and metallization on a buffer layer are presented. Different etching approaches using inductively coupled plasma and reactive ion etching (ICP and RIE) are demonstrated using hard masks such as silicon dioxide and aluminum, as standard photo-resists have a chemical compatibility issue when used directly on top of IPG. Finally, the loss and sidewall profiles of the etched IPG waveguides were characterized.

Chapter 4 details novel soft lithography (nanoimprint) technologies for IPG. The current status of soft lithography methods is reviewed first. Afterwards, we investigate the possible release treatments required for the etched silicon dioxide master and soft lithography processes. Demonstrations of the capability of the technology are then presented indicating that this will be an inexpensive route to high quality device fabrication given appropriate tools.

In final chapter, conclusions drawn from the work are presented along with an outline of further work required to attain the goals of low cost generic device fabrication.

Chapter 2

Overview of Waveguide Materials

In this chapter, an overview of current practical optical materials for waveguide fabrication will be presented. Special properties of conventional and novel polymers including IPGs will be discussed. The focus in this chapter will be on refractive index, optical loss and other properties of various polymers. Characteristics of IPGs will be addressed as well.

2.1 Introduction

Over the last twenty years, the revolution in electronics resulting from semiconductor integration has essentially commoditized high speed electronic devices. Simultaneously, the developments in optical communications have enabled high speed communications at attainable prices, although even with the advent of planar optical integration, the industry is still arguably a step away from the level of commoditization attained in the electronics industry. Breaching this gap and enabling the potential union of these two technologies in even consumer products requires a true low cost mass producible optical technology.

In waveguide fabrication, the desirable requirements for materials are low cost, low optical loss, low birefringence, high thermal stability and stable optical properties. Low cost generally will only be achieved using cheap raw materials, simple high yield wafer scale processing using only non-cutting-edge fabrication tools with batch processing capabilities, and by designing compact devices (i.e. more to a wafer). Low optical loss is a key characteristic and has been a barrier to the application of many materials and approaches for waveguide fabrication. Other concerns are related to the environmental stability, such as thermal and humidity stability, of the materials.

An additional revolution that has impacted our lives over the past 50 years

has stemmed from the development of polymer materials that have provided low cost products of considerable complexity. Polymers, therefore, may also have much to offer as an enabler for low cost optical communications devices. Polymer waveguide devices, due to their potentially simple fabrication and low cost, may therefore be set to play an important role in the growing broadband communication arena, especially in enterprise networking, computer interconnects in addition to telecommunications. Furthermore, there are reliability-proven polymer devices on the market today thereby overcoming the "traditional" resistance to market acceptance of polymer optical devices. This chapter will address the alternative proven waveguide materials, the general characteristics of polymers, and a brief review of prior work on polymer waveguides.

2.2 Brief History of Waveguide Materials

There are several material groups commonly used in planar waveguide fabrication. The most widely used for waveguide fabrication is silica on silicon. Other market proven and reliable potential materials for waveguide fabrication are systems such as other oxide glasses, Lithium Niobate ($LiNbO_3$), Silicon, Indium Phosphide (InP), and Polymers.

Silica (SiO_2) and other oxide based glasses

Silica has long been the benchmark material for integrated optics globally and can be considered the most mature integrated optics platform. The propagation loss for silica optical fiber is about 0.15 dB/km at 1550 nm wavelength due to the low intrinsic absorption of silica, and the absence of surface roughness on the fiber core/cladding interface. Planar silica waveguides have not yet approached this level of loss, but have achieved losses around

0.005 dB/cm at 1550nm with optimized materials, geometries, and processes. Silica has excellent stability and environmental resistance; is photosensitive when appropriately doped; can exhibit optical gain when appropriately doped and pumped; and has low temperature dependence compared to most materials. When grown on a silicon substrate, wafers up to 300mm can be processed (i.e. many devices from one wafer). It is a good platform for hybrid integration with other technologies (e.g. laser chips, etc to make full functionality sub-systems on a chip) and can have self aligned V-grooves built in to make for low cost passive fiber pig tailing. These features have been demonstrated by many research and industry groups. [1]

Whilst it has proven an excellent materials system for building devices and there are many reliable commercial devices on the market using this technology, one of the main issues with the silica system is how to attain the high refractive index contrast necessary to build very compact devices. Additionally the process, raw materials, and tool costs for silica on silicon waveguides are high.

Other glass technologies are also currently on the market. One approach uses ion exchange in borosilicate type glasses to fabricate passive and Erbium doped waveguide devices (e.g. Teem Photonics, Grenoble, France). Whilst this has proven to be an effective and relatively low cost approach compared to the traditional silica on silicon method, one of its main drawbacks is that the substrate is a piece of glass which effectively bars the method from either having any future Hybrid integration potential or from realizing self aligned fiber pig tailing which introduces therefore a substantial cost barrier. [2]

Another approach used chemical vapor deposition to make high index glass on silica and thereby achieves the high index contrast required to make compact devices (Little Optics Inc., now Nomadics, Baltimore, USA). The waveguide losses are higher at 0.15dB/cm at 1550nm, but this is also countered by the fact that the higher index contrasts shrink the device substantially. However the cost structure of this method is essentially identical to that of the standard silica on silicon approach (although it can achieve much higher chip counts per wafer). [3]

Other non-polymer materials

A number of other technology platforms have made it to commercial production and passed reliability testing. Several of these are semiconductor based approaches. Foremost amongst those was Silicon on Insulator (SOI), a technology commercialized by Bookham Technology. The substrate is a silicon wafer with a buried silica layer. A core rib is patterned in the top silicon layer, and silica over cladding layer is grown on top. The waveguide structure needs to be a rib as opposed to a channel due to the high index contrast between silica and silicon. A channel waveguide would have to be extremely small (< 0.25 μm) to be single mode, and coupling that structure to a standard single-mode fiber would be highly inefficient. Despite progressing the technology to the commercial level and developing and selling Hybrid integrated components, Bookham shut down its SOI business in 2003. The technical challenges involved in SOI are clearly greater than that for conventional Silica on Silicon (for example the issue of surface scatter at the very high index core/cladding interface), and the cost structures for the substrate also somewhat greater. Thus it looks unlikely that SOI would ever be a true low cost technology. [4, 5]

Indium Phosphide is another well researched and proven semiconductor material in commercial production, both as laser diode devices and for integrated optics chips (Infinera, California, US). [6] However, InP is a high cost material that is only available in small substrate sizes typically 3", and it is difficult to manufacture circuits of even modest complexity with high yield and low cost. It seems very unlikely that it could ever compete with some of the lower cost technologies for mass market type applications.

Lithium Niobate is another materials system which has market dominance in a specific area, namely high speed electro-optic modulators. Whilst the fabrication of waveguides by processes such as Titanium indiffusion is an inherently low cost process, the material itself is not and matters are further

complicated by the fragility and anisotropic nature of the material. Tight waveguide bends are also difficult, and as with glass substrates, Hybrid integration of actives and self aligned pig tailing are difficult again meaning that Lithium Niobate is unlikely to be a realistic low cost device option. [7]

Thus it appears that there are no obvious low cost contenders in the non-glass arena which have a proven track record. Certainly there are many other options in the research arena, but it is a big jump from research to reliability proven product.

Polymers

The main advantages of polymeric optical devices are low cost materials, potentially low cost processing, high yields, environmental stability, and tunablilty of properties. Polymer waveguides can even be made by simple spin-coating and UV-exposure with relatively simple exposure tools – certainly a fast and inexpensive fabrication route. However, waveguides cannot be photo-defined in all polymers (such as some polyimides), and resolution issues also exist so processing by other methods is also used. Moreover, the absorption loss of polymers can be less than 0.1 dB/cm at all the key communication wavelengths (840, 1310, and 1550 nm) [8]. Tunability of the refractive index difference between the core and the cladding is easily achieved and large index contrasts ($n_{core} - n_{clad}$ of up to ~0.1) are straightforward. The tunability of the refractive index enables compact high index contrast compact waveguiding structures employing tight bend radii [9]. Most polymers possess large thermo-optic coefficients meaning that active devices (switches, variable optical attenuators, etc) with response times down to a few microseconds can be made. Low or high birefringence can be attained in polymeric films, optical gain, and electro-optic effects are possible though not currently commercialized. Using silicon as the substrate material opens up the opportunities of processing large wafers, hybrid integration and self-aligned pigtailing. Finally, the unique properties of polymers

allow them to be made by special techniques such as micro molding and soft embossing, helping rapid processing and introducing new opportunities for low cost waveguide fabrication.

2.3 General Polymer Characteristics

The important general characteristics of polymers are: their molecular weight; the applicable thermal transitions and where they lie; crystallinity; inter-chain interaction and structure; and method of hardening/curing. Generally, single polymer molecules typically have molecular weights between 10,000 and 1,000,000 g/mol. More than 2000 repeating units can be found in polymerized chains depending on the polymer structure. The mechanical properties of a polymer are significantly affected by the molecular weight, normally, with better engineering properties at higher molecular weights. The polymer glass transition point and the melting point/decomposition temperature will determine which application it is suitable for. As for crystallinity, polymers generally have a combination of crystalline and amorphous structures. Where integrated optics is concerned, there are several additional crucial characteristics:

2.3.1 Refractive Index

According to the requirements for waveguide design and geometry, the polymer acting as the core in the waveguides must generally have a higher refractive index than any other cladding material. The appropriate index difference between core and cladding is related to the operating wavelength, the necessity for single mode operation, the required bending radius, and the need to have efficient coupling to sources and outgoing/ incoming optical connections. Besides the actual desired value of refractive index, there are also factors that cause it to vary and this has to be within acceptable bounds to prevent

degrading the performance of certain types of optical devices.

The refractive index of a material is not a single unvarying constant. It is variable for light of different frequencies. This phenomenon is termed refractive index dispersion, which is an important property of a waveguide. In general, most polymers have significantly larger dispersion than silica, which can be both a problem and a benefit depending on the circumstances. This is clearly a property which has to be factored into device designs, but is not generally a limiting factor. Refractive index is not only a function of wavelength, but also of temperature, humidity, light exposure, and ultimately time. Polymer-based waveguides have in the past been especially sensitive to the last two effects (yellowing and long term stability), especially at elevated temperatures. A fundamental difference between many conventional optical materials and polymer is their larger temperature dependence, that is to say, the refractive index of polymers varies more rapidly than other materials with temperature. The refractive index of many polymers of interest for optical waveguides decreases at a rate of $\sim 10^{-4}/\ ^{\circ}C$, which is one order of magnitude larger than that of inorganic glasses. This can be used to make active devices or to athermalise inorganic glass waveguides, where the small, positive thermo-optic effect in, the core is canceled out using the negative thermo-optic coefficient of the polymer cladding.

Humidity induced changes of the refractive index can be problematic in several types of devices. For polymers, the refractive index changes are ascribed to the counterbalance between moisture absorption and swelling. For example, the refractive index of deutero-PMMA increases as the humidity increases at temperatures higher than $60^{\circ}C$. Although the humidity dependence of deutero-PMMA is as large as 10^{-5} % $(RH)^{-1}$, some hydrophobic polymers, such as silicone polymer, are affected by humidity to a much lesser and acceptable degree than acrylic polymers. [10]

Tuning of the refractive index can be accomplished in a family of polymers via several methods. The incorporation of fluorine atoms into polymers in place

of hydrogen can affect the refractive index in three ways simultaneously. Firstly, the increase in free volume which often accompanies fluorine substitution (attributed to the greater steric volume of fluorine relative to hydrogen interfering with efficient chain packing), may decrease the refractive index via the density. Secondly, the electronic polarizability is always lowered with fluorine substitution because of the smaller electronic polarization of the C-F bond relative to C-H bond. Lastly the blue-shifting of the short wavelength absorption from fluorine substitution also contributes to the lowering of the refractive index.

Another means of varying both the refractive index and in fact other properties of polymers is to vary the side groups that branch off the main polymer backbone. It is this capability which gives polymers their wide range of tunable properties.

As a result, an important feature of polymers is the controllability of the refractive index contrast, enabling high density compact wave guiding structures with small waveguide bend radii. Compact structures are critical for the achievement of large-scale photonic integration. [11]

The birefringence ($n_{TE} - n_{TM}$, TE= transverse electric to planar surface, TM= transverse magnetic to planar surface) indicates the optical anisotropy of a material. In a normally isotropic material, birefringence is also related to the stress build-up within the material due to processing or thermal treatment. Unlike inorganic crystals or glasses, polymers can be molecularly engineered to achieve either low or high birefringence. Some aromatic polymers, such as polyimides, exhibit a very large birefringence (up to 0.24) that is attributed to the strong preference of aromatic moieties to align with their planes along the film surfaces. [12] However, the birefringence can be extremely low (10^{-5} to 10^{-6}) in polymers that undergo little molecular orientation during processing, as is common in three dimensionally cross linked polymers [13].

2.3.2 *Optical loss*

Attenuation or loss is an important characteristic of a waveguide. The loss is generally attributable to several different mechanisms: absorption, scattering, radiation loss, etc. In general, all waveguide devices need to have low optical loss, especially, at the major telecom wavelengths (1310 and 1550 nm) and data communication wavelengths (840 nm). With the utilization of fiber-optic telecommunications in the S-band (1450 to 1510 nm), C-band (1525 to 1560 nm), and L-band (1570 to 1620 nm), all waveguide devices should possess low loss in these bands. [14] Optical polymers have promising characteristics which should enable the reduction of all these loss sources to acceptable levels, including absorption loss, scattering loss, radiation loss, and fiber pigtail loss, etc.

For polymer materials, generally, there are large absorptions in the ultraviolet because of fundamental electronic transitions across the band gap. These absorptions tend to be in the deep ultraviolet (less than 200 nm) for polymers with predominantly aliphatic hydrogen atoms, and in the near UV (200 to 400 nm) for polymers with significant numbers of aromatic hydrogen atoms. Partially or fully fluorinated polymers tend to have their UV absorptions deeper in the UV also. In general, though these UV bands are important in determining the refractive index and dispersion of the material, electronic absorptions in polymers contribute minimally to optical loss in the major telecommunication windows near 1300 nm and 1500 nm. In the 1300 to 1600nm range, however, absorptions appear from the overtones of fundamental molecular vibrations [15, 16]. Since the strength of the absorption tends to decrease by approximately an order of magnitude between each harmonic order, higher harmonics are generally weak enough to not be of concern. Both C-H and O-H overtones are seen to be highly absorptive in the telecommunications windows, whereas C-F overtones, for example, show extremely low absorption throughout the range of

interest, due to their higher harmonic order. Table 2.1 provides a comparison of the positions and intensities of these vibrational overtone absorptions of interest when considering optical polymer.

Bond	Overtone order	Wavelength (nm)	Intensity (relative)
C-H	1	3390	1
C-H	2	1729	7.2×10^{-2}
C-H	3	1176	6.8×10^{-3}
C-F	5	1626	6.4×10^{-6}
C-F	6	1361	1.9×10^{-7}
C-F	7	1171	6.4×10^{-9}
O-H	2	1438	7.2×10^{-2}

Table 2.1. Wavelengths and intensities of some important vibrational overtones. [17]

As hydrogen atoms are substituted through partial fluorination, the absorption of optical polymers in the telecommunication band therefore reduces significantly. In general, it is difficult to accurately determine the pure absorption component of loss in an optical material, since scattering also contributes to the overall attenuation and is difficult to separate from the absorption terms. [17]

There are numerous extrinsic contributions to scattering loss in optical materials. Primaries are large inclusions such as particles, voids, cracks, and bubbles. Generally, an inclusion is considered large if it is greater than 1 μm in diameter, in which case the scattering intensity is largely wavelength independent. Extrinsic scattering in polymers can result from unfiltered particles, dust, dissolved bubbles, and untreated monomer. In order to eliminate extrinsic scattering, it is important to follow clean procedures in the preparation of polymer formulations, and to perform all coating operations in a clean room.

Moreover, polymer waveguides are typically formed by spin-coating processes in which polymers are deposited from solution and dried by heating in an oven or hot plate. The resulting films are generally uniform, but can have

surface roughness that will contribute to scattering loss. This is not generally a major issue as spin coated polymer films routinely achieve low surface roughness as will be shown later. However, the fabrication of single-mode channel waveguides involves additional photolithographic processes where wet or dry etching defines the waveguide channel. Hence scattering can occur from the etched side-walls as well as the original film surface. Therefore, etching must be performed in a manner which minimizes the surface roughness to obtain waveguides with low propagation losses.

2.3.3 Environmental Performance

The environmental stability of optical polymers is crucial and most polymers do not have good enough stability for use in telecommunications devices. An important characteristic is the thermal stability of optical polymers, since polymeric materials subjected to thermal aging can "yellow"; change their refractive index; harden and become brittle; amongst other effects. Typically, such aging results from the formation of partially conjugated molecular groups characterized by broad ultraviolet absorption bands, which tail off in intensity through the visible region [18]. This yellowing is strongly dependent on the chemical structure of the original polymer. In fully halogenated materials, yellowing becomes almost negligible at any wavelength because the absence of hydrogen prohibits the formation of H-halogen products that will result in carbon double bonds. These unsaturated double bonds are the major cause of yellowing when they are slowly oxidized under long-term thermal aging.

Requirements for telecommunications devices have been developed with the goal of assuring operation for 20 to 25 years. The major governing documents for passive optical components are two monographs from Telecordia, the GR 1209 and GR 1221. The Telecordia GR 1209 focuses primarily on optical performance tests and short-term reliability data that would apply to any manufactured lot of devices. The Telecordia GR 1221 is a document that

focuses on comprehensive reliability assurance, in particular vendor and device qualification, lot-to-lot quality and reliability control, storage, and handling. [19]

2.3.4 Overview of Conventional and Novel Optical Polymers

A large number of polymer compositions already exist and many more are certain to yet be invented that possess interesting optical characteristics. However as discussed above it is hard to synthesize a polymer that meets all the requirements for optical networking applications.

Polymers have been used for light guided films since the 1970s. [20] In the literature, "conventional" optical polymers generally are PMMA (polymethyl methacrylate or Acrylic glass) and acrylate derivates, Epoxy-based materials, PS (polystyrene), PC (polycarbonate) and PU (polyurethane).

In the past twenty years, several major families of novel optical polymers have been developed in academic and industrial laboratories. In addition to the review articles [21] some recent updates on developed materials will be given in this section. A summary is presented in Table 2.2. Currently, the avaible optical polymers are highly transparent with absorption loss values close to 0.1 - 0.5dB/cm at all major communication wavelengths (840 nm, 1310 nm and 1550 nm). The propagation loss given in Table 2.2 are for multimode wavegudies (for datacom) and for single mode wavegudie (for telecom).

Polyacrylates

The absorption-limited loss of polymethylmethacrylate (PMMA) has been reported as ≈ 0.25 dB/cm at 1300 nm and ≈ 0.75 dB/cm at 1550 nm, respectively [22]. The index of refraction at 1550 nm is 1.48. The major drawback of PMMA is that the T_g (85 -115 ℃) is uncomfortably close to the specifi ed operating temperature range for deployed devices. As the material properties undergo large changes around T_g, this is an undesirable characteristic of PMMA based

compounds. Another difficulty with PMMA is the control of viscosity, which is crucial when thicker films are needed. PMMA has been utilized for the manufacture of thermo-optic switches, where it has been directly photo-patterned in a thickness of 5 µm onto a SiO_2 layer [23] after mixing with a photo initiator. Operating at 1550 nm, an attenuation of 1 dB/cm was reported [23].

Epoxy-based material

The SU-8 family of materials plays a major role in microsystems technology, particularly for microelectromechanical systems (MEMS) [27]. These epoxy-based polymers are directly UV patternable upon cationic initiation, exhibiting negative-photo resist properties. Refractive indices of 1.596 at 633 nm and 1.575 at 1550 nm, respectively, have been reported [25]. Patterned SU-8 waveguides exhibited optical losses of 0.5 dB/cm at 1300 nm [26]. A high absorption of 3 dB/cm at 1550 nm, however, makes SU-8 a poor candidate for application in the third telecom window.

Polysiloxanes

Polysiloxanes are highly suitable materials for optical applications. The siloxane network (full siloxane chain) not only accounts for mechanical and thermal rigidity, but also reduces the organic C-H concentration resulting in low absorption losses at 1310 nm and 1550 nm due to minimized overtone absorption. However, as (Si-)O-H also effects optical losses, especially around 1550 nm, the build-up of the inorganic network has to be thoroughly controlled in order to minimize residual Si-OH content.

Inorganic polymers and polysiloxanes have been developed to a commercial stage by NTT (deuterated siloxanes), Fraunhofer Institute (Ormocer), RPO (Inorganic Polymer Glasses), etc.

Inorganic polymer glass™ developed by RPO Pty Ltd is a reactive branched-chained polysiloxane. Georgia Institute of Technology reported IPG waveguide losses of 0.24 dB/cm at 1322 nm and 0.52 dB/cm at 1548 nm. [28] More details about this material will be presented in the section 2.4, together with the process parameters for application of the optical layers.

NTT synthesized deuterated phenylsilyl chloride monomers as the starting material for the waveguide core polymer. The structure of the synthesized polymers has two distinctive characteristics. One is the adoption of a polysiloxane backbone (-Si-O-) to provide high heat resistance compared with carbon-carbon (C-C) bonds. The other is the adoption of a deuterated substituent in the phenyl group with lower absorption at both 1300 and 1550 nm compare to that of normal (non-deuterated) phenylsilyl chloride. On the other hand, since a phenyl group has a large molecular refraction, the refractive index of the polymer can be changed by controlling the content of the phenyl group. The propagation loss of the channel waveguides was 0.17 dB/cm at 1310 nm and 0.43 dB/cm at 1550 nm. The thermal and environmental stability of the waveguides was demonstrated by the fact that the propagation loss remained unchanged after testing at >200 ℃ for 30 minutes, at > 120 ℃ for 1000 hours, and at > 75 ℃ and 90% relative humidity (RH) for 1 000 hours. [29, 30]

The Ormocer (Organic Modified Ceramics), developed by Fraunhofer Institute are synthesized by organic crosslinking of polycondensed alkoxysilanes (sol-gel processing). Its transmission losses in the near infrared range are 0.05 @ 830 nm, 0.2 @ 1310 nm and 0.6 @ 1550nm. For optical applications, their thermal performance is good enough for most of the technological applications (decomposition temperature > 270 ℃). [31]

A cross-linked silicone with a propagation loss of 0.5 dB/cm and a refractive index of 1.49 at 1550 nm and with long-term environmental stability has been reported. [32] RIE needs to be employed in the fabrication of patterned structures. The chemical composition of the material, however, has not been further specified by the authors.

A number of materials were prepared by co-polymerization of pentadeuterophenyltrichlorosilane and methyltrichlorosilane in various monomer ratios [33]. The authors state that in the case of methyl groups, deuteration by way of exception leads to a higher absorption at 1550 nm than C-H bonds. From the silicones, single mode optical waveguides were fabricated by spin-coating, lithography and dry-etching techniques. In case of a formulation containing 95 mol. % deuterated phenylsilane, a propagation loss as low as 0.23 dB/cm at 1550 nm was found. Glass transition temperatures above 300 ℃ for all different formulations indicated thermal stability.

Fluorinated polyimides

Fluorinated polyimides have good thermal stability (up to ~300 ℃) and advantageous mechanical and dielectric properties [34]. In the past loss was a problem, for which there are two main causes in waveguides. The first is ordering processes, which can produce scattering loss (domain formation/phase separation). The other is rapid curing, which can lead to voids in waveguides. However, in the past several years, some fluorinated polymers have achieved low optical loss and a quite good refractive index control, such as Ultradel (Amoco), Ultem (General Electric), NTT and Hitachi fluorinated polyimides. Fluorinated polyimides can suppress refractive index fluctuations and the presence of the pinholes, two main causes for the observed waveguide losses in the conventional polyimides. One intrinsic problem that is still difficult to aviod is that the large birefringence and polarization dependent loss. At 830 nm, Ultem shows an optical loss of 0.24dB/cm, it is mostly combined with BCB as a cladding layer [35].

Perfluorocyclobutyl (PFCB) aryl ether polymers

Another popular high performance polymer is perfluorocyclobutyl (PFCB) aryl

ether polymers developed by Dow Chemical. This sort of polymer has a unique combination of properties, which is very suitable for optical application. Actually, PFCB polymers have a high temperature stability, precisely controlled refractive index, low moisture absorption, and low absorption at the major telecom wavelengths. The standard methods or soft lithography can be used for processing this material. Moreover, these polymers from Dow Corning possess high performance properties and processibility, high temperature stability (T_g from 120 °C to 250 °C), precisely controlled refractive index, low moisture absorption, and losses at 1300 and 1550nm <0.25 dB/cm. [36] However, PFCB materials are not photopatternable. The fabrication processes includes patterning (lithography/RIE) of an inverse structure into the substrate silicon, then thermal growth of silicon oxide as the buffer layer and afterwards spin-coating of the polymer resin into the so-prepared grooves and thermal curing. This multi-step process makes waveguide fabrication from PFCB very expensive and presents a major drawback of this class of materials.

Polynorbornenes

Recently, BFGoodrich has developed a novel catalyst system that allows addition polymerization of norbornene-type monomers. The innovation of this catalyst system led to a new generation of polycyclic olefins, which enable cyclic olefin based waveguide polymers with intrinsically good optical, mechanical and moisture absorption properties. The intrinsic properties of the polynorbornenes system include low transmission loss (<0.1 dB/cm at 820 nm), wide spectral range (<0.4dB/cm at 450nm and <0.1 dB/cm at 515-870 nm), low birefringence, consistent difference in index over a wide temperature range, long-term stability (2000 hours at 125 °C), high glass transition temperature (> 280 °C), and low moisture absorption (<0.1%). Candidate materials have been identified as core and cladding components for optical waveguides. The refractive index of a typical core material is 1.53 and at of a typical cladding material is 1.50 at 820nm.

[37] But polynorbornenes exhibit poor adhesion to common substrate materials, including silicon, silicon dioxide, aluminum, gold, and copper. In addition, it is brittle, yielding less than 1% elongation-to-break values.

Deuterated and halogenated polyacrylates

Deuterated and halogenated polyacrylates were developed by several companies. Allied-signal developed a wide varity of photo-crosslinkable, optically transparent polymers based on combinations of multifunctional halogenated acrylate monomers and oligomers in addition to various additives. [38] These polymers allows the creation of waveguides with low scattering losses and low polarization-dependent losses. Upon UV-expsoure, these monomer systems form highly crosslinked networks, which exhibit low intrinsic absorption in the waveglegth range extending from 400 to 1600 nm. At 840 nm, losses can be as low as 0.02 dB/cm, and 0.01 dB/cm for the halogenated acrylates. By blending and copolymerizing with selected miscible monomers, this approach allows precise tailoring of the refractive index over a very broad range from 1.3 to 1.6, although it can be difficult to simultaneously achieve a given refractive index and low intrinsic absorption at the same time. It is possible to tailor other physical properties such as flexibility, toughness, surface energy, and adhesion to specific applications.

NTT has developed deuterated polyfluoromethacrylate (d-PFMA) with high transparency, low birefringence, and good processibility. They have also developed processes to fabricate low optical loss single-mode and multi-mode optical waveguides with these polymers. The propagation loss and waveguide birefringence of the single-mode waveguides were as low as 0.10 dB/cm and -5.5×10^{-6} at 1310 nm. Main disadvantage of d-PFMA is poor thermal stability. This characteristic limits the d-PFMA waveguides to usage under restricted conditions.

Polyguide, developed by DuPont has shown excellent layer quality and

thickness control. Polyguide can be machined using excimer laser to form mechanical structures with high degree of accuracy allowing for connection to a mechanically transferable (MT-type) ferrule packaged with push/pull housing connected to a multichannel standard ribbon fiber. [39] Polyguide possesses moderate refractive indices (1.48 to 1.51) and moderate optical loss (0.18 dB/cm at 800 nm, 0.2 dB/cm at 1300 nm, and 0.6 dB/cm at 1550 nm) due to its non-halogenated acrylate structures. [40] But, its thermal stability is only up to 85°C, which restricts its application in the telecommunications field.

2.4 Inorganic Polymer Glasses (IPGs ™)

The materials

Inorganic polymer glasses (IPGs) from RPO Pty Ltd are a familly of superior quality photocurable spin-on polysiloxane based optical polymers. They are a group of highly stable inorganic polymers with the processing and design properties of a flexible organic polymer. It is made through a unique process. IPG films have low stress and high uniformity. IPGs materials are well suited to the fabrication of high quality optical films and waveguides.

For waveguide fabrication, two IPGs are employed as cladding (L-3) and core (L-11) layer. Both of them contain photo-initiator and must be handled under UV-free illumination. They are quite similar materials. Thermo-optic coefficients (dn/dT) are around -3×10^{-4} /℃, coefficient of thermal expansion is about 600×10^{-6}/℃. The decomposition temperature is larger than 3 00 ℃, which is high enough for almost all optical applications. The viscosities of IPGs are both 2300 centipoises. The only difference is the refractive index.

A schemiatic of Inorganic ploymer glasses is shown in Figure 2.1.

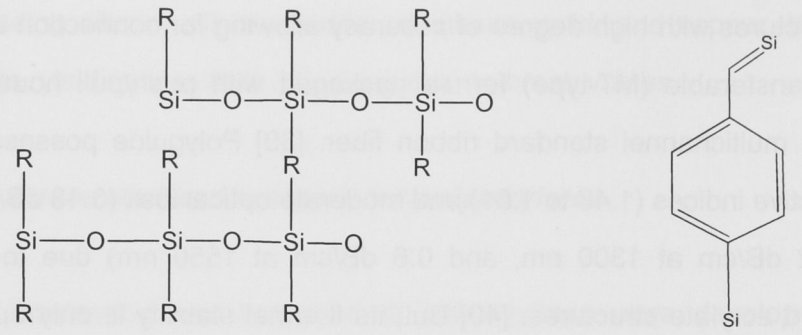

Figure 2.1: (a) Schematic of inorganic polymer glass. (b) The chemical structures of R.

Processing

The two primary processes for IPGs are spin-coating and UV exposure. Post fabrication a vacuum bake is required to fully stabilize the material.

The normal spin-coating processes are:

1. Apply between 3 and 5 mL (for 3-inch to 4-inch diameter substrates) of IPG on centre of substrate.

2. Spin coat at 2500 rpm for 45 seconds for a film thickness of about 20 μm.

3. Edge bead removal may be accomplished using the solvents MIBK or acetone.

However, for waveguide fabrication, we need 10μm L-3 and 3 μm L-11. Therefore, high speed spin-coating for thin layers needed to be addressed. More technical details about this will be explained in next chapter.

The general UV exposure processes are:

1. Purge exposure chamber with N_2 for several minutes (ensure adequate time for several volume replacements + 1-2 minutes equilibrium).

2. UV expose IPGs film at $\geqslant$ 20 mW/cm^2 (measured at 405 nm) for 60 seconds using broadband UV source.

3. Film/pattern development may be accomplished with the solvents IPA and MIBK mixed in a 50:50 volume ratio, using spin-spray develop or

bath-develop techniques. Rinse in pure IPA.

Stabilization baking requires vacuum bake (or under N_2 atmosphere if vacuum is not available) for 3 hours at 180 ℃ (ens ure uniform plate temperature).

SCI FilmTek 4000 system

The Scientific Computing International FilmTek 4000 is one of the most advanced thick and thin film metrology tools available. It incorporates multiple detectors positioned at different angles of incidence to accurately measure the index of refraction with a resolution of 0.00002. That is 100 times the performance of the best non-contact method, 10 times that of the best prism coupler contact systems. A prime application for this system is measuring the index of refraction and thickness of planar waveguide films. [41]

Using generalized material models in combination with advanced global optimization algorithms and power spectral density analysis, FilmTek can simultaneously determine multiple layer thickness, Indices of refraction [n(λ)], extinction (absorption) coefficients [k(λ)], energy band gap [Eg], composition, crystallinity and surface roughness.

In measurement of refractive index, the film's spectroscopic reflection data are gathered at normal incidence (0 degrees) and 70 degrees. PSD (Power Spectral Density) processing results in two peaks in the PSD domain. The ratio of their positions is a function of the index of refraction of the film, and the angle of incidence of the oblique measurement. This ratio is used to calculate the index. Once the index is known, the thickness can be calculated from the optical thickness of the normal incidence peak. [41]. Generalized materials models are used to represent the films for these calculations.

In measurements, the SCI (damped Lorentz Oscillator model) was used for silicon dioxide, and a Tauc-Lorenz model was used for IPG materials. A snapshot of the FilmTek system is shown in Figure 2.2.

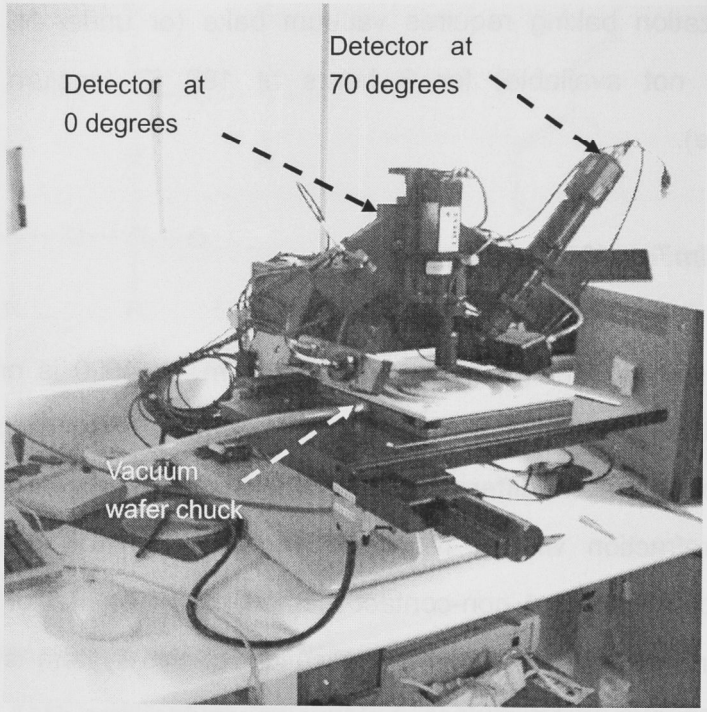

Figure 2.2. A snapshot of SCI FlimTek 4000 system in the cleanroom

Cured IPG films have refractive index in the range 1.474 to 1.528 at 1550 nm wavelength and room temperature. At 633 nm, the possible refractive index is from 1.491 to1.543. In the work reported in this thesis, two particular IPG polymers developed by RPO Pty Ltd were used for waveguide fabrication. The first, termed L-11, has a refractive index of 1.507 (standard exposure/bake conditions) at a wavelength of 1550 nm at room temperature. The other one, termed L-3, has a refractive index of 1.478 under the same conditions. Hence the core/clad refractive index difference is 0.029. These data were obtained by using an SCI FilmTek 4000 thin film measurement system with NIR measurement option installed and using a fully fitted Tauc-Lorenz model with 3 oscillators.

Figure 2.3 show 10 μm IPG film (L-3 and L-11) on silicon wafer does not have hysteresis in index or thickness when thermally cycled (returns to starting point as measured by Filmtek 4000 with hot chuck):

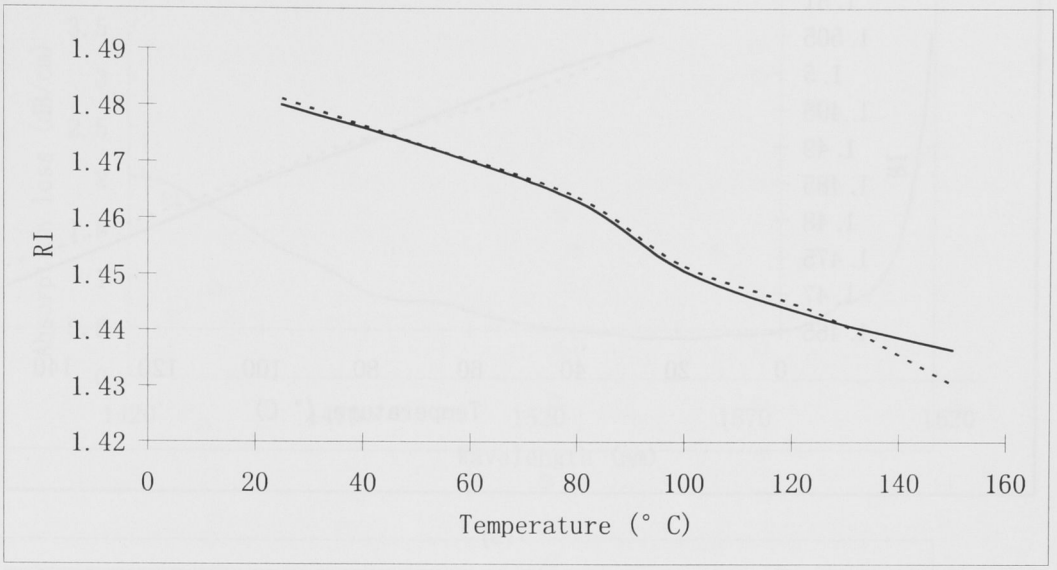
1.49
1.48
1.47
1.46
1.45
1.44
1.43
1.42
RI
0
20
40
60
80
100
120
140
160
Temperature (° C)

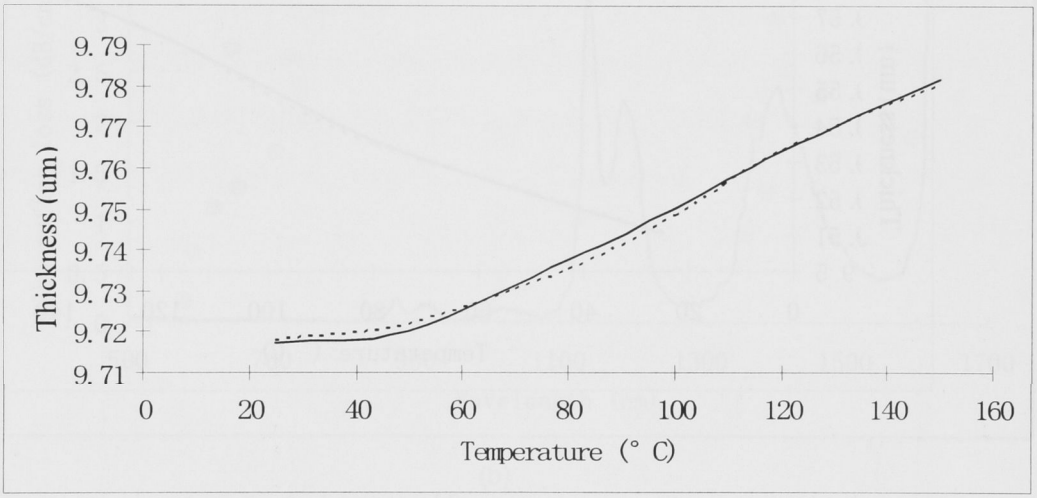
9.79
9.78
9.77
9.76
9.75
9.74
9.73
9.72
9.71
Thickness (um)
0
20
40
60
80
100
120
140
160
Temperature (° C)

(a)

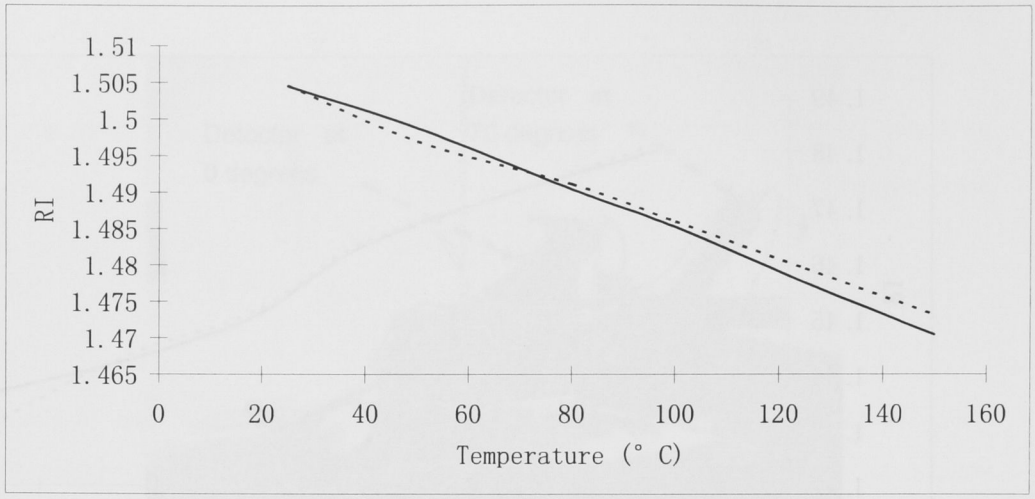

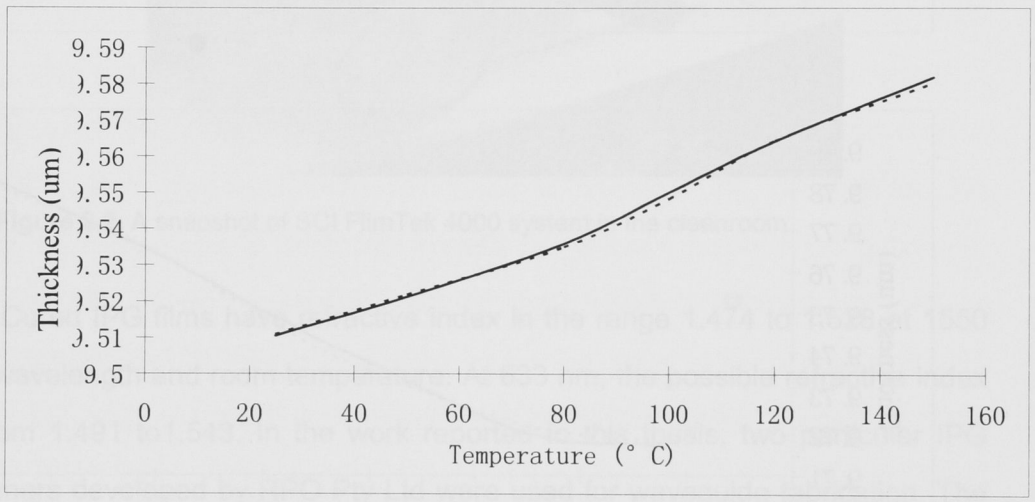

(b)

Figure 2.3: Hysteresis in refractive index (@1550 nm) and thickness of IPGs. (a) is L-3; (b) is L-11. Dot line represents temperature increase; Dark line represents temperature decrease.

The birefringence of a cured IPG film is about 10^{-4}. The IPG resin absorption loss varies with wavelength and the degree of fluorination. At wavelengths below 850 nm, it is generally substantially less than 0.1 dB/cm. For IPG L-11 resin, at wavelengths of 1310 nm and 1550 nm, its absorption losses are 0.2 dB/cm and 0.41 dB/cm respectively in Figure 2.4.

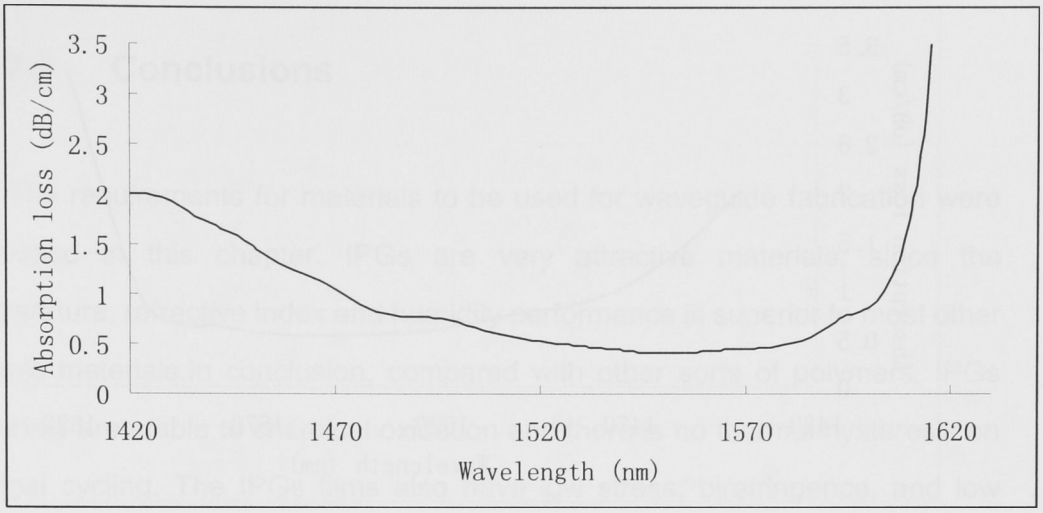

(a)

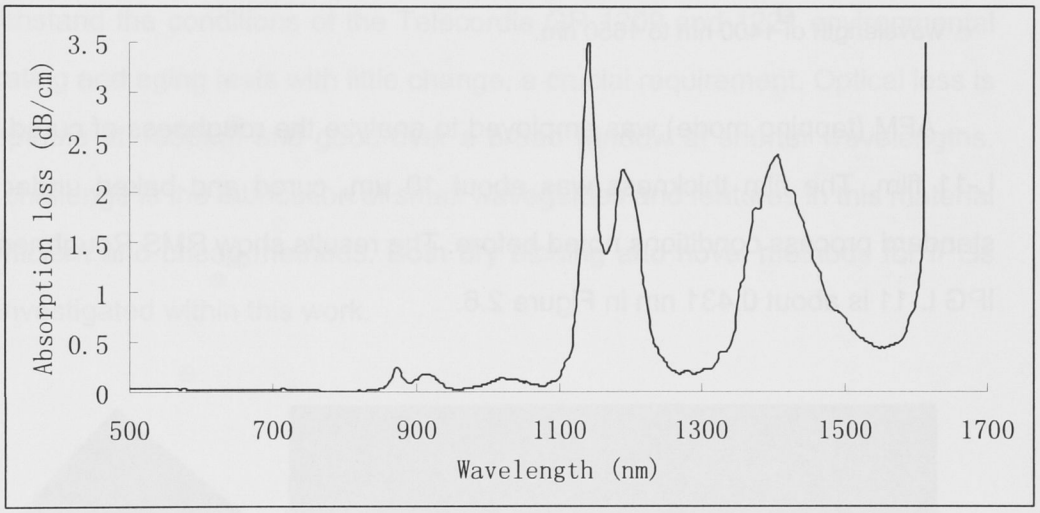

(b)

Figure 2.4: Absorption loss of IPG L-11 resin in different wavelength ranges. (a) From wavelength of 1400 nm to 1650 nm. (b) From wavelength of 500 nm to 1700 nm.

The absorption loss of photo patterned IPG waveguides measured from wavelength of 1400 nm to 1650 nm is illustrated in Figure 2.5. The dimensions are 5 μm x 5 μm. Whilst the loss of the most standard materials are not especially low at 1550nm, they are in the acceptable range for compact devices, and the materials are clearly good performers at shorter wavelength where price is even more of an issue.

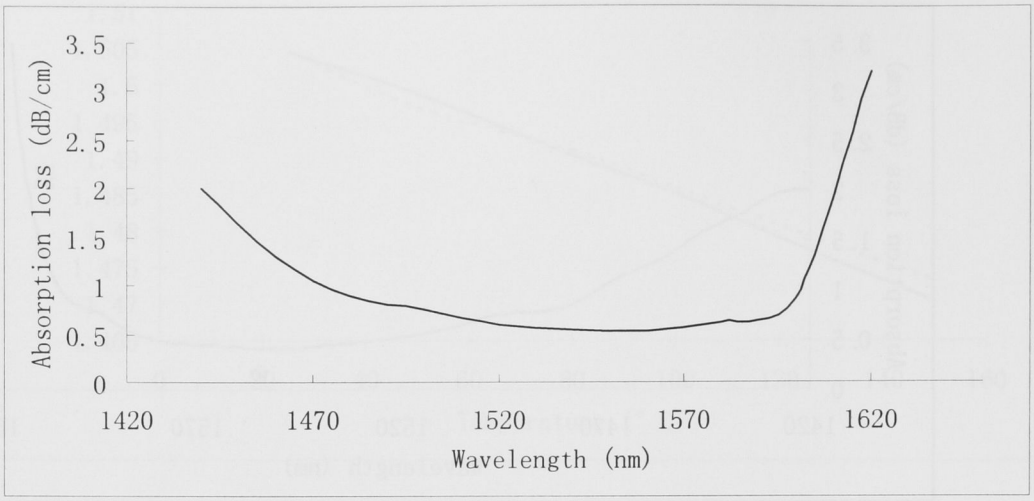

Figure 2.5: Absorption loss of directly photo patterned IPG waveguides from wavelength of 1400 nm to 1650 nm.

AFM (tapping mode) was employed to analyze the roughness of cured IPG L-11 film. The film thickness was about 10 μm, cured and baked under the standard process conditions noted before. The results show RMS Roughness of IPG L-11 is about 0.431 nm in Figure 2.6.

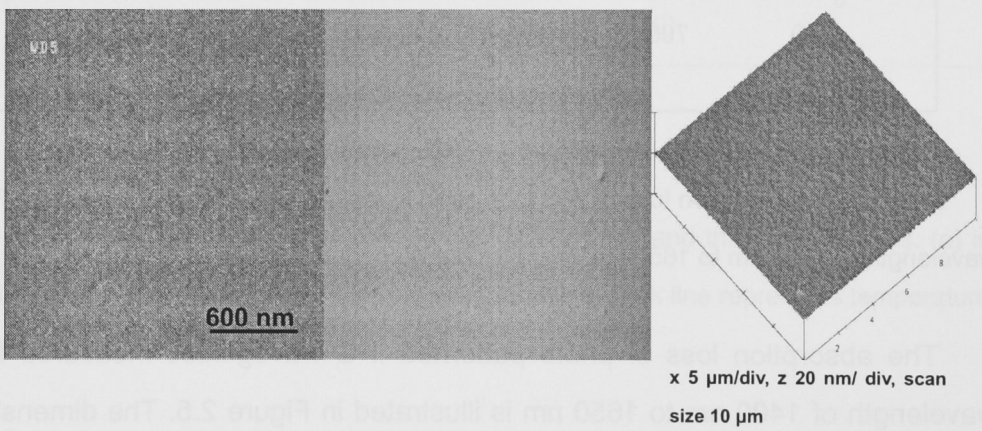

Figure 2.6: Surface measurement and observation of IPGs from FESEM (left) microscope (middle) and AFM (right). The AFM scan rate is 5 Hz. Normarski DIC FOV is 95x70 μm.

2.5 Conclusions

The requirements for materials to be used for waveguide fabrication were discussed in this chapter. IPGs are very attractive materials, since the temperature, refractive index and humidity performance is superior to most other organic materials.In conclusion, compared with other sorts of polymers, IPGs materials are stable to chemical oxidation and there is no thermal hysteresis on thermal cycling. The IPGs films also have low stress, birefringence, and low polarization dependent loss values. The materials have also been demonstrated to withstand the conditions of the Telecordia GR 1209 and 1221 environmental operating and aging tests with little change, a crucial requirement. Optical loss is acceptable at 1550nm and good over a broad window at shorter wavelengths. The challenge is the fabrication of small waveguides and features in this material by efficient and cheap methods. Both dry etching and novel methods for IPGs are investigated within this work.

Table

Manufacturer	Polymer Type (Trade Name)	Pattering Techniques	Propagation Loss, Single Mode waveguide, dB/cm (wavelength, nm)	Other Properties (wavelength, nm)
Amoco	Fluorinated polyimide (Ultadel ^{TM})	Photo exposure / wet etch	0.4 (1300) 1.0 (1550)	Birefringence: 0.025, Crosslinked, Thermally stable
Corning (formerly AlliedSignal)	Acrylate	Photo exposure / wet etch, RIE, laser ablation	0.02 (840) 0.3 (1300) 0.8 (1550)	Birefringence: 0.0002 (1550), Crosslinked, T_g=25 C°, environmentally stable
	Halogenated acrylate	Photo exposure / wet etch, RIE, laser ablation	<0.01 (840) 0.06 (1300) 0.2 (1550)	Birefringence: 0.000001 (1550), Crosslinked, T_g= -50 C°, environmentally stable

Dow Chemical	Benzocyclobutene (Cyclotene ™)	RIE	0.8 (1300) 1.5 (1550)	T_g> 350 C°
	Perfluorocyclobutene (XU 35121)	Photo exposure / wet etch	0.25 (1300) 0.25 (1550)	T_g= 400 C°
Gemfire	(Gemfire)	Photo exposure / wet etch	1.0 (1550)	Birefringence: 0.0002 (1550), Crosslinked
General Electric	Polyetherimide (Ultem ™)	RIE, laser ablation	0.24 (830)	Thermally stable
Hitachi	Fluorinated polyimide	Photo exposure / wet etch	TE: 0.5, TM :0.6 (1300)	Birefringence: 0.009 (1300), PDL: 0.1 dB/cm (1300), T_g= 310 C°, Thermally stable
Hoechst Celanese	PMMA copolymer (P2ANS)	Photo bleaching	1.0 (1300)	NLO polymer
Ipitek	Poly(methylmethacrylate) with CLD-1 chromophore (PMMA-CLD-1)	RIE	5.0 (1300)	NLO polymer r_{33} =60 pm/V (1300) Pigtail loss= 3.5 dB/facet
JDS Uniphase (formerly Akzo Nobel)	Polycarbnate (BeamBox ™)	RIE	0.6 (1550)	Thermally stable
K-JIST	Fluorinated poly(arylene ether sulfide) (FPAESI)	RIE	TE: 0.42, TM: 0.4 (1550)	PDL : 0.02 dB/cm (1550), Birefringence:

				0.0003 (1550), Crosslinked, Thermally stable
Lumera	Polyurethane with FTC chromophore	RIE	2.0 (1300)	NLO polymer r_{33} =25 pm/V (1310) Pigtail loss= 5 dB/facet
NTT	Halogenated acrylate	RIE	0.02(830) 0.07(1310) 1.7 (1550)	Birefringence: 0.000006 (1310) , T_g= 110 C°
	Deuterated polysiloxane	RIE	0.17 (1310) 0.43 (1550)	Environmentally stable
	Fluorinated polyimide	RIE	TE: 0.3, TM: 0.7 (1310)	PDL: 0.4 dB/cm (1310) Environmentally stable
Optical Crosslinks	Acrylate (Polyguide ™)	Diffusion	0.18 (800) 0.2 (1300) 0.6 (1550)	Laminated sheets, excimer laser machinable
PacificWave	Polycarbonate with CLD-1 chromophore (PC-CLD-1)	RIE	1.8 (1550)	NLO polymer r_{33} =70 pm/V (1310) Pigtail loss= 1.5 dB/facet
Redfern (currently	Inorganic polymer glasses	Photo exposure /	0.24 (1322) 0.52 (1548)	Environmentally stable

RPO)	(IPGs ™)	RIE		
Telephotonics	(OASIC ™)	Photo exposure / wet etch, RIE, laser ablation	<0.01 (840) 0,03 (1300) 0.1 (1550)	Environmentally stable
Micro Resist Technology	Ormocer	Photo exposure / wet etch, RIE, laser ablation	0.05 (830) 0.02 (1310) 0.6 (1550)	Environmentally stable
	cross-linked silicone	RIE	0.5 dB/cm (1550)	
	deuterated organopolysiloxanes		0.23 dB/cm (1550)	T_g: >300 ℃

Table 2.2 Characteristics of optical polymers developed globally by companies. Where NLO means second order nonlinear optic, r_{33} is value of macroscopic electro optic activity. PDL means polarization dependent loss. [21]

Reference

[1]. T. Miya, "Silica-based planar lightwave circuits: passive and thermally active devices," IEEE J. Sel. Top. Quantum Electron. 6, 38 (2000).

[2]. Jarmila Spirkova, Pavlina Tresnakova-Nebolova and Martin Mika, "Optical waveguides fabricated by transition element ions exchange in some commercial and special optical glasses", Optical Materials 25,101, (2004)

[3]. A. Kilian, J. Kirchhof, B. Kuhlow, G. Przyrembel, and W. Wischmann, "Birefringence free planar optical waveguide made by flame hydrolysis deposition (FHD) through tailoring of the overcladding," J. Lightwave Technol. 18, 193 (2000).

[4]. A. G. Rickman, G. T. Reed, and F. Namavar, "Silicon-on-insulator optical rib waveguide circuits for fiber optic sensors," Proc. SPIE 2071, 190 (1993).

[5]. A. G. Rickman, G. T. Reed, and F. Namavar, "Silicon-on-insulator optical rib waveguide loss and mode characteristics," J. Lightwave Technol. 12, 1771 (1994).

[6]. L. Moller, C. R. Doerr, C. H. Joyner, and M. Zirngibl, "Multifrequency laser based in integrated Vernier-Michelson cavity for mode stabilization," Electron. Lett. 36, 540 (2000).

[7]. R. Alferness, "Titanium-diffused lithium niobate waveguide devices," in Guided-wave optoelectronics, 2nd ed., pp. 145, T. Tamir, Ed., Springer-Verlag, New York (1990).

[8]. L. Eldada and L. W. Shacklette, "Advances in polymer integrated optics", IEEE J. Sel. Top. Quantum Electron. 6, 54 (2000).

[9]. L. Eldada, "Advances in telecom and datacom optical component", Opt Eng, 40(7), 1165-1178, July (2001).

[10]. T.Watanabe, N.Ooba, Y.Hida, M.Hikita, Appl.Phys.Lett. 72, 1533 (1998).

[11].G.Hougham,G.Tesoro,A.Viehbeck,J.D.Chapple-Sokol, Macromollecules 1994,27,5964.

[12]. S.Herminghaus, D.Boese, D. Y. Yoon, B. A. Smith, Appl. Phys. Lett. 58, 1043 (1991).

[13]. Polymers for Electronic and Photonic Applications (Ed:C.P.Wang), Academic Press, New York (1993).

[14]. R. A Norwood, R. Y. Gao, J, Sharma, C. C. Teng, In Design, Manufacturing, and

Testing of Planar Optical Waveguide Devices (Ed: R. A. Norwood), Vol.4439, SPIE, Bellingham,p.19, (2001).

[15]. A. Skumanich and C.R.Moylan. The vibrational overtone spectrum of a thin polymer film. Chemical Physics Letters, 174 (2): 129-144, Nov 2 (1990).

[16].W.Groh. Overtone absorption in macromolecules for polymer optical fibers. Macromolecular Chemistry and Physics, 189(12):2861-2874, Dec (1988).

[17]. W.B.Jackson, N.M.Amer, A.C.Boccara, D.Fournier, Appl. Opt. 20, 1333, (1981).

[18]. H.Ma, A.K.Y.Jen, and L.R.Dalton. Polymer-based optical waveguides: materials, processing, and devices. Advanced Materials, 14(9): 1339-1365, Oct (2002).

[19]. Generic Reliability Assurance Requirements for Fiber Optic Branching Components, Bellcore GR-1221-CORE, Bellcore, HJ (1994).

[20]. J.H.Harris, R.Shubert, J.N.Polky, J.Opt.Soc.Am. 60,1007, (1970).

[21]. L.Eldada, WDM Solutions. April, 21, (2002).

[22]. J.P.D.Cook, G.O.,Este, F.R. Shepherd, W.D. Westwood, J.Arrington, W. Moyer, J. Nurse, S.Powell, Appl. Opt.37,1220, (1998).

[23]. N. Keil, B. Strebel, R. Türck, H.H. Yao, C. Zawadzki in Micro System Technologies '94 / 4th International Conference on Micro Electro, Opto, Mechanical Systems and Components, Berlin, October 19-21, 1994 (eds.: H. Reichl, A. Heuberger). vde-Verlag GmbH, Berlin (1994), 1097-1106.

[24]. C.L. Callender, J.-F. Viens, J.P. Noad, L. Eldada, Electron. Lett. 1999, 35, 1839-1840.

[25]. T.C. Sum, A.A. Bettiol, J.A. van Kan, F. Watt, E.Y.B. Pun, K.K. Tung, Appl. Phys. Lett. (2003), 83, 1707-1709.

[26]. A. Borreman, S. Musa, A.A.M. Kok, M.B.J. Diemeer, A. Driessen, Proc. Symp. IEEE/LEOS Benelux Chapter, Amsterdam (2002), 83-86.

[27]. N. LaBianca, J.D. Gelorme in Advances in Resist Technology and Processing XII (ed.: R.D. Allen). Proc. SPIE (1995), 2438, 846-852.

[28].V.Sundaram, R.Tummala, G.White, K.Lim, L.Wan, D. Guidotti, F.Liu, S.Bhattacharya, R.M.Pulugurtha, I.R. Abothu, R.Doraiswami, R.V.Pucha, J.Laskar, M.Tentzeris,G.K.Chang, and M.Swaminathan. System-on-a-package (sop) substrate and module with digital, rf and optical integration. In ECTC'04, Proceedings Electronic Components and Technology

Conference, pages 17-23, May (2004).

[29]. M.Usui, M. Hikita, T. Watanabe, M. Amano, S. Sugawara, S. Hayashida, and S. Imamura. Low-loss passive polymer optical waveguides with high enviromental stability. Journal of Lightwave Technology, 14(10): 2338-2343, Oct (1996).

[30]. T. Watanabe, N.Ooba, S. Hayashida, T. Kurihara, and S. Imamura. Polymeric optical waveguide circuits formed using silicone resin. Journal of Lightwave Technology, 16(6): 1049-1055, June (1998)

[31]. K.-H. Haas, S. Amberg-Schwab, T. Ballweg in Advances in Science and Technology (ed.: P. Vincenzini) (2003), 31, 581-592.

[32]. T. Watanabe, N. Ooba, S. Hayashida, T. Kurihara, S. Imamura, J. Lightwave Technol. (1998), 16, 1049-1055.

[33]. S. Toyoda, N. Ooba, M. Hikita, T. Kurihara, S. Imamura, Thin Solid Films (2000), 370, 311-314.

[34]. J. Kobayashi, T. Matsuura, S. Sasaki, T. Maruno, Appl. Opt. (1998), 37, 1032-1037.

[35]. S.Y.Cho, M.A.Brooke, and N.M.Jokerst. Optical interconnections on electrical boards using embedded active optoelectronic components. IEEE Journal of Selected Topics In Quantum Electronics, 9(2):465-476, Mar-Apr (2003).

[36]. D.W. Smith, Jr., S. Chen, S.M. Kumar, J. Ballato, C. Topping, H.V. Shah, S.H. Foulger, Adv. Mater. (2002), 14, 1585-1589.

[37]. R.H. Woudenberg, T.O. Boonstra, US 6,376,639 B1. JDS Uniphase Photonics C.V., Arnhem (NL) (2002).

[38]. L.W. Shacklette, R.A. Norwood, L.Eldada, C.Glass, D. Nguyen, C. Poga, B.P.Xu, S. Yon, J.T. Yardley, Proc. SPIE-Int. Soc. Opt. Eng. (1997).3147,222

[39]. Optical Crosslinks. http://www.opticalcrossliks.com.

[40]. B.L. Booth, J.E. Marchegiano, C.T. Chang, R.J. Furmanak, D.M. Graham, R.G. Wagner, in Optoelectronic Interconnects and Packaging (eds.: R.T. Chen, P.S. Guilfoyle). Proc. SPIE (1997), 3005, 238-253.

[41]. SCI FilmTek 4000 operation manual.

Chapter 3

Waveguide Fabrication: Deposition and Etching

This chapter describes the development of a process for waveguide fabrication and high quality plasma etching of IPGs using both metal and silica masks. Experimental results and discussions on IPG etching and metallization are presented. The main focus is on metal mask deposition and the optimization of the sidewall roughness and selectivity. Comparisons between silicon dioxide and Aluminum etch masks are also presented. Insertion loss measurement results are given for finished waveguides.

3.1 Introduction

The major barrier to market acceptance of polymer waveguides devices has long been material reliability. The RPO IPG material has essentially passed Telcordia reliability testing, and so the question arises as to how to fabricate suitable types of high quality compact devices in IPG at low cost. As noted earlier, the standard IPG photolithography method where the material acts as a negative photo-resist is not suitable for waveguide dimensions below about 5 micron, and a reasonable option is to pursue the industry standard dry etch method for waveguide patterning. However, this raises a number of issues. Firstly, here is a chemical compatibility issue between IPG and photo resist meaning direct photo resist masking will not work. Secondly, it was already known that there are issues with surface roughness when metalising IPGs, making metal etch masks problematic. Lastly, there is little previous published work on dry etching of IPGs. Therefore, resolutions to each of these issues were sought to enable dry etched waveguides to be fabricated.

3.2 IPG Coating

The first normal process for IPG waveguide fabrication is spin coating. IPG is applied onto the substrate (generally a 4-inch silicon wafer) lying on a vacuum chuck in a spinner. A sufficient volume of IPG is poured to give a pool about 25 mm in diameter. The wafer is then accelerated to the trial spin speed and maintained there for a fixed period. But, in contrast to solvent based coating, IPGs do not dry during the spin process. Therefore, the final film thickness is dependant on both the spin speed and spin time. At speed, centrifugal force causes the solution to flow to the edges, where it builds up until expelled when surface tension is exceeded. The resulting IPG thickness is a function of spin speed, viscosity, temperature, and spin time.

Firstly, a process to coat 10 μm of L-3 IPG (cladding) on a silicon wafer was developed. Figure 3.1 (a) shows the spin speed curve measurement for a 90 second spin time. The spin program comprises several steps: firstly, the wafer is accelerated to 4000 rpm to thin the coating to the desired thickness. Then the wafer is spun to 2500 rpm for 13 seconds for topside and backside edge bead removal. Finally, 2000 rpm for 5 seconds and 1000 rpm for 1 second are applied to dry off the edge bead solvent. Given the coating is wet throughout the spin curve shown therefore includes the edge bead processing. In Figure 3.1, on a bare silicon wafer, the required spin speed for a 10 micron film is evidently 4000 rpm.

After spin coating, the L-3 film is cured by a UV exposure process, as described earlier in section 2.4. Baking at 180 ℃ in vacuum was employed after cure to stabilize the film. The curing and baking processes are also the same for the L-11 core layer.

The next process after curing and baking the cladding is to spin a 3 μm L-11 core layer onto the L-3 layer. Figure 3.1 (b) shows the measured spin speed

curve for a 180 seconds spin. (The spin program is same as the L-3 coating, but the time and speed is increased to 180 seconds at 9000 rpm). The measurements of L-3 on bare silicon and L-11 on L-3 film were both carried out with a SCI FilmTek 4000.

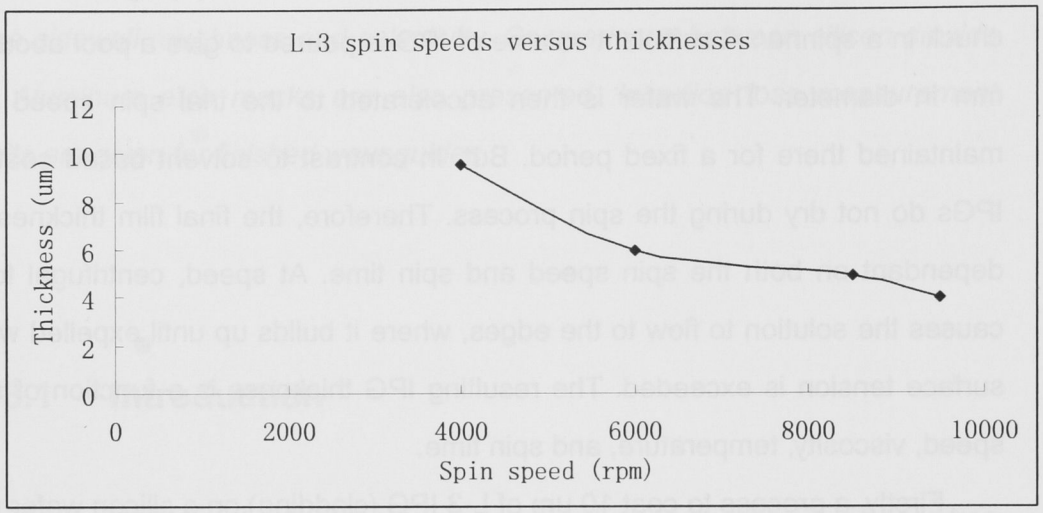

(a)

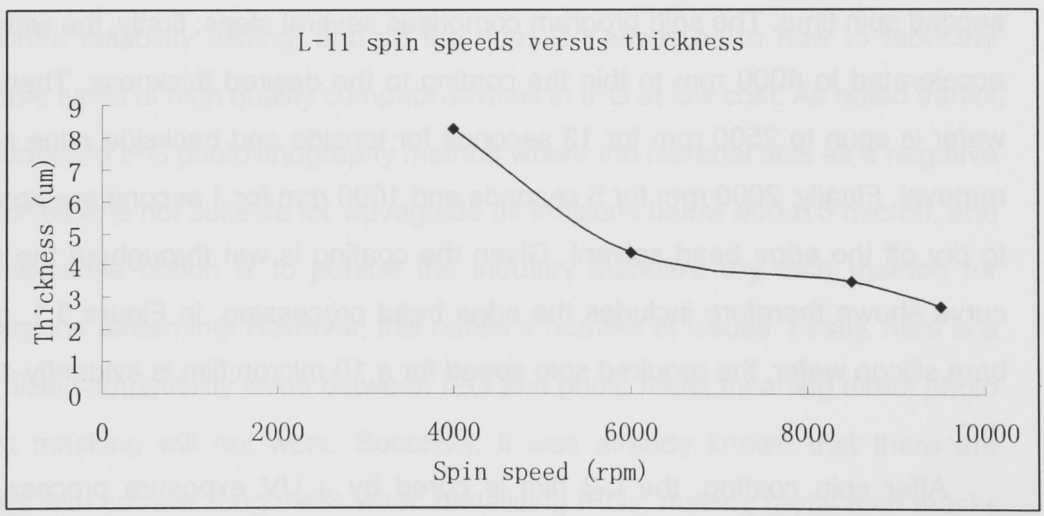

(b)

Figure 3.1 (a) Spin speeds versus thicknesses on bare silicon wafer for 90 seconds. (b) L-11 is spun on L-3 IPG film for 180 seconds.

Short spin times are desirable to reduce the risk of airborne contamination.

However, shorter time results in higher spin speeds, and higher spin speeds can cause poorer uniformity. Thus, there should be a balance between spin time and speed. For L-11 on L-3 film with silicon underneath, the desired 3 μm thickness can not be reached for a spin time below 180 seconds, which is not ideal. For a future production process a lower viscosity resin would be the solution to this issue.

Therefore, from figures above, the coating conditions were set as: 10 μm L-3 should be spun at 4000 rpm for 90 seconds. 3 μm L-11 should be spun at 9000 rpm for 180 seconds.

3.3 Deposition and Etching Processes Employed

3.3.1 Etch Mask Selection

The selection of the mask layer is important in dry etching to ensure sufficient selectivity is attained for the etch depth required. For IPG or other polymers, their similar composition to standard polymer-based photo resists poses a challenge as it is hard to obtain a sufficiently high etch selectivity between IPG and a photo resist mask. Thus, a mask layer, which can offer high selectivity, needs to be developed. Moreover, a smooth, vertical profile is required in the mask also, meaning generally it is advantageous if the mask material is itself dry etchable with high selectivity over the material to be etched. This poses yet another challenge.

Dry etching of waveguides using different masking materials has been reported before using masks such as Aluminum (Al) [1], photo resist [8], Chromium (Cr) [3], silicon dioxide [4] and amorphous silicon (a-Si) [5], etc.

Cr is widely used as a mask material, because it allows a very high waveguide/Cr etching selectivity and good adhesion to most waveguide materials. Whilst it is the standard material for photo masks and a lot of research

and development has consequently gone into dry etching chrome, the process is not an easy one and is aggressive being an approximately equal flow of Chlorine and Oxygen, something likely to attack polymers rapidly. Aluminum has the benefit of being easiest to dry etch at very high selectivity, which allows deep etch processing such as may be required for low resistance electrode fabrication, for example. Silicon dioxide is another potential option for the mask layer. Its etching properties are also widely understood since it is used widely in both electronics (as an insulator) and photonics (for waveguides). It is known to have high selectivity to polymer and standard processes exist for etching it.

The more details about choice of mask layer will be discussed further in the following sections.

3.3.2 Metal Coating

Previous experience of metallization of IPGs suggested that in order to obtain a smooth coating, the deposition needed to occur on a cold substrate. The optimum method for this was to use sputtering, where the thermal load on the wafer is minimal.

In this project, a sputtering system was utilized to deposit Aluminum, Chromium and gold. The system is illustrated in Figure 3.2. It is a DC magnetron sputter coating system, a PFEIFFER Classic 250. The system details are below:

- Deposition chamber approx. (W× D× H) 290 mm × 275 mm × 470 mm (useable space)
- Dry backing pump and turbo pump, base pressure is about 10^{-7} Torr, working pressure is about 10^{-3} Torr
- Target-sample distance variable from 5 to 25 cm
- The Argon gas supply is up to 7.0 sccm

Normally, it took approx. 20 minutes of pumping time to reach an operating pressure of 10^{-6} Torr. There are a number of variables that impact the properties of the films produced by DC magnetron sputtering. Details of the influence of

deposition parameters will be discussed in section 3.4.

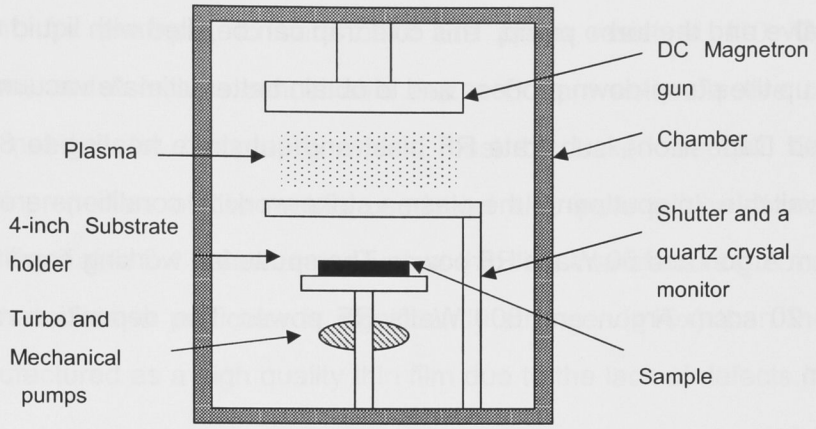

Figure 3.2: Schematic of sputtering apparatus.

3.3.3 Dielectric Deposition

It became clear during the project that deposition of silicon dioxide or silicon nitride layers would be advantageous. Two methods were used for this, low temperature PECVD (Plasma Enhanced Chemical Vapor Deposition) and RF sputtering. In our laboratory, an Oxford Plasmalab 80 Plus was used for silicon dioxide or silicon nitride deposition. It is a double chamber system, which uses 13.56 MHz driven parallel plate reactors (one for etching, the other for deposition). The available gas supplies for PECVD are NH_3, NO_2, SiH_4 and Oxygen. More PECVD deposition experimental details will be given in section 5.

Silica deposition using an AJA International magnetron sputtering system became available late in the project. This system is equipped with six guns which can all be operated simultaneously if desired to sputter in either DC or RF mode. Two separate gas lines are available. The first gas line goes to the chamber and can be used to provide for example an oxygen ambient for reactive sputtering. The second gas line feeds to the chimney of the guns and is usually fed with Argon for the sputtering plasma. The system is pumped by a turbo molecular pump backed by a dry mechanical pump. A pressure controlling gate

valve separates the vacuum chamber from the pump allowing independent setting of the chamber pressure for processing. There is a cold trap between the gate valve and the turbo pump. This cold trap can be filled with liquid nitrogen to speed up the pump-down process and to obtain better ultimate vacuum. IAD (Ion Assisted Deposition), substrate RF bias, and substrate heating to 800 ℃ are also available. In sputtering, the plasma strike working conditions are 25 mTorr, 20 sccm Argon and 60 Watts RF power. The sputtering working conditions are 4 mTorr, 20 sccm Argon and 300 Watts RF power. The deposition rate was 2 nm/min.

3.4 Metallization of IPGs

Metallization of IPGs is an essential and fundamental process for both hard etch mask fabrication and as electrodes for active devices. Three kinds of metal: Aluminum, Chromium and Gold were trialed on IPG. In the experiments, the DC sputtering system with argon gas supply was employed to deposit these metals. With simple DC sputtering, there are three parameters which impact the properties of the films: (a) The chamber pressure (gas flow rate), (b) the power (current), and (c) the target-sample distance. Because the target-sample distance (about 100 mm) was fixed in our sputtering system, this parameter was not investigated.

Metallization was carried out at different deposition rates around an operating pressure of approx 10^{-3} mbar. The thicknesses of metal layers were from 100 nm to 300 nm thick. Aluminum deposition rates were generally from 1.0 angstrom/second to 5.0 angstrom/second (measured on the system's quartz crystal monitor, the distance from the target to sample was the same as that to the crystal); Chromium deposition rates were between 0.4 angstrom/second and 60 angstrom/second; Gold deposition rates normally were tested from 1.3 angstrom/second to 2.0 angstrom/second. The working voltage range was from

200 to 400 Volts. A series of baking tests were run on a hotplate on films deposited on IPG for prospective applications from 90 ℃ to 150 ℃. There is a requirement, for example, to hard bake the photo resist at 110 ℃ after metallization, and it is also conceivable that a Bottom anti reflective coating would be needed for lithography which must be baked at 150 ℃. The mechanical properties of the metals used and also pure silicon dioxide are outlined in the Table 3.1 below under typical thin film manufacturing conditions [6]. Note that silica in particular is significantly stronger (>10x) than the bulk when manufactured as a high quality thin film due to the lack of defects in such films.

	Young's Modulus (GPa)	Modulus of Rigidity (GPa)	Compressive Yield Strength (MPa)	Tensile Yield Strength (MPa)	CTE ($\times 10^{-6}$/℃)	Poisson Ratio	Bulk Compression Modulus (GPa)
Al	70	26	7-40	7-40	23	0.35	76
Cr	279	115	362	362	4.9	0.21	160
Au	78	27	100	100	14.2	0.44	220
Silica	73	26	1100	5000	0.59	0.17	37

Table 3.1: Properties of Al, Cr, Au and Silicon dioxide. Coefficient of thermal expansion (CTE). [6]

3.4.1 Direct Metallization with Aluminum

Aluminum was the first material sputtered on IPGs. With care, smooth Al films could be deposited by DC sputtering. The deposition rate range to obtain a good coating is quite small, from 1.0 to 1.5 angstrom/second, compared to the minimum rate for sputtering of 1.0 angstrom/second. The sputtering conditions were 0.4 sccm Argon or around 1.0 angstrom/second at a pressure of 2.2×10^{-3} mbar. The working voltage was 290 Volts and current 0.09 A. which appeared to produce the best quality films. Outside this process range, the films had

significant topology with wrinkled surfaces and other defects. Post sputtering optical, FESEM and AFM (Atomic Force Microscope) images of good quality films were obtained and are shown below in Figure 3.3.

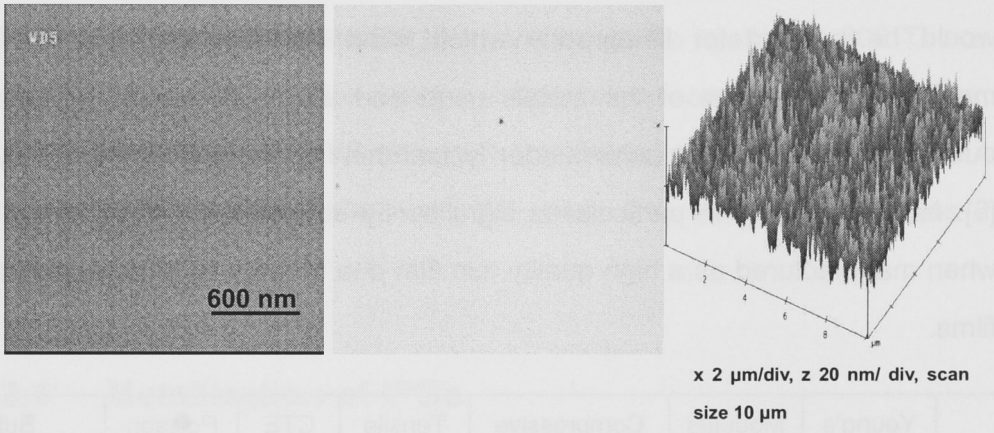

Figure 3.3: Aluminum sputtered on IPG film. No thermal cycling of Al/IPG sample. Images from FESEM (left), AFM (right) and microscope (middle).The RMS Roughness is about 1.0 nm. The AFM scan rate is 5 Hz. Normarski DIC FOV is 95x70 µm.

Baking tests were then run by placing the films on a hotplate for half an hour. Finally, the samples were inspected on a microscope and scanned by the AFM. After heating, the film above approx. 100 ℃ wrinkl ing of the film occurred. Figure 3.4 shows a typical example.

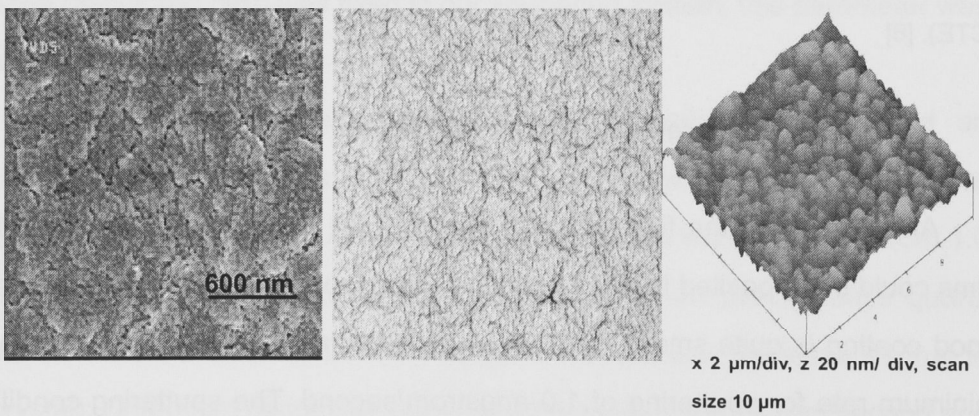

Figure 3.4: Post-heating Aluminum on IPG film. Images from FESEM (left), AFM (right) and microscope (middle). The AFM scan rate is 5 Hz. Normarski DIC FOV is 95x70 µm.

This effect is believed to be analogous to the "hillocking" behavior seen in Aluminum films in VLSI interconnects, where the film extrudes the weakest crystal planes due to differential thermal expansion with the substrate (compression in this case). Looking in Table 3.1, it is notable that Aluminum has by far the lowest yield stress. We believe that on IPG films, Aluminum is more likely "stretched" during the heating phase, and on cooling it cannot recompress so that it causes the relatively soft IPG surface to wrinkle. The thermal expansion coefficient of Aluminum and IPG are 23 $\times 10^{-6}$ / ℃ for Aluminum and 600 $\times 10^{-6}$ / ℃ for IPG.

Samples were also baked at 150 ℃ for half an hour in a vacuum oven and cooled down to room temperature to ensure there were no oxidation or thermal shock effects causing the wrinkling. Clearly visible wrinkles appear on the surface after such thermal cycling.

After thermal cycling, the Aluminum was removed by wet etching (by HPO_4: HNO_3: CH_3OOH=16: 1: 1 at 20 - 30 ℃) in order to check the IPG film underneath. It was clear from FESEM images that the IPG was roughened. A comparison between IPG with wet etched Aluminum and direct wet etched IPG is made in Figure 3.5. These two images show a completely different surface morphology. Therefore the roughening observed in the Al coated samples were not caused by attack of the IPG by the etchant. This tends to suggest some sort of chemical interaction occurred between Aluminum and the IPG. However time was not available to investigate this further.

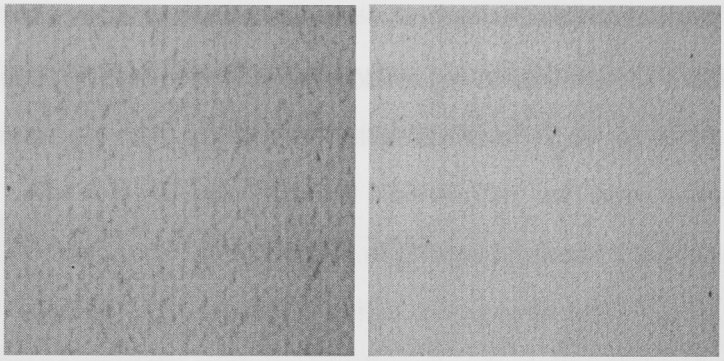

(a)

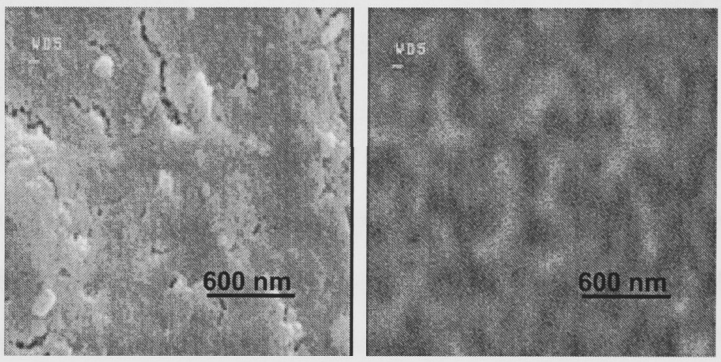

(b)

Figure 3.5: Morphology difference between IPG after Aluminum wet etching (left) and direct wet etched IPG film (right) at the same resolution. (a) Microscope images (b) FESEM images. Normarski DIC FOV is 95x70 μm.

We also investigated the influence of deposition parameters on the film quality. Two main parameters were considered: (a) the chamber pressure and (b) the working power or voltage. As mentioned earlier, the chamber pressure is set by the Argon gas flow rate, which can be controlled from 1.0 sccm to 7.0 sccm. Figure 3.6 (a) presents the relation between deposition rate and working voltage. The voltages are varied from 250 Volts to 350 Volts (the maximum voltage for Al deposition is about 400 Volts). The deposition rate changed slightly, and reached a minimum at about 290 volts. Figure 3.6 (b) shows the effect of varying the Argon gas flow rates on the deposition rate and the voltage. Deposition rate grows almost linearly with increasing of argon flow rate. A point should be

explained here is that, if the Argon flow rate is less than 0.35 sccm, the plasma will not strike. Therefore, in the graph, the curve can not be started from the zero point. The relationship between deposition rates and RMS Roughness obtained by AFM is illustrated in Figure 3.6 (c) as well. From these graphs, the results show the low gas flow rates and voltages achieved better surface quality.

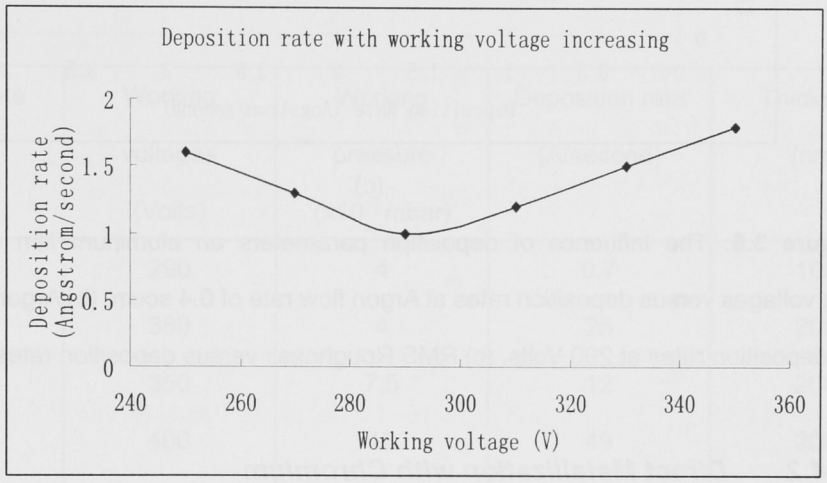

(a)

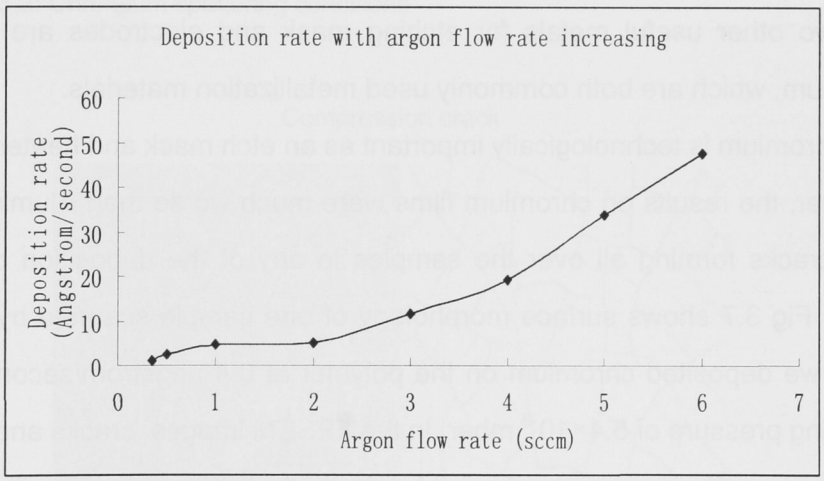

(b)

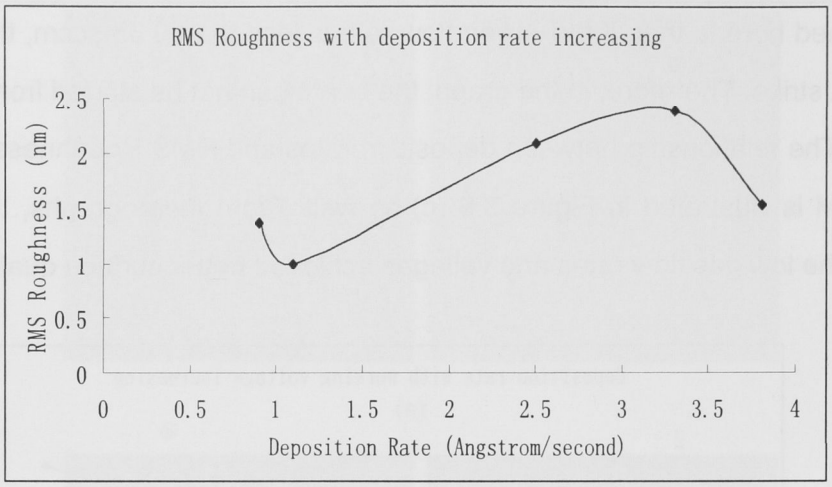

(c)

Figure 3.6: The influence of deposition parameters on aluminum film quality. (a) working voltages versus deposition rates at Argon flow rate of 0.4 sccm. (b) Argon flow rates versus deposition rates at 290 Volts. (c) RMS Roughness versus deposition rates.

3.4.2 Direct Metallization with Chromium

Two other useful metals for etching mask and electrodes are gold and chromium, which are both commonly used metallization materials.

Chromium is technologically important as an etch mask and heater element. However, the results on chromium films were much worse than Aluminum, with large cracks forming all over the samples in any of the deposition conditions trialed. Fig 3.7 shows surface morphology of one sample scanned by FESEM, where we deposited chromium on the polymer at 0.4 angstrom/second and an operating pressure of 5.4×10^{-3} mbar. In the FESEM images, cracks and "hills" on the sample surface were clearly visible. We believe it is an issue with stress in the film interacting with the softness of the IPG. The other micrograph shows a tensile cracking regime, where the IPG has clearly torn underneath the chrome. Interestingly, the individual "platelets" of chrome have rather smooth surfaces indicating that the chrome itself did not otherwise undergo deformation in the way the aluminium did. We tried a range of conditions to try and adjust the film

stress. There are laid out below in the Table 3.2. In the time available we were unable to find a condition which results in low enough stress to prevent cracking, although such a condition is likely possible. It is also worth noting that whilst chromium has the highest yield strength of the materials tested, it has the lowest coefficient of thermal expansion (CTE) which may have been an important factor in the cracking.

Ar flow rate (sccm)	Working voltages (Volts)	Working pressure ($\times 10^{-3}$ mbar)	Deposition rate (A/second)	Thickness (nm)
0.3	290	4	0.7	100
1	380	4	25	200
3	350	7.5	12	200
5	400	12	49	200
2.5	430	4	58	300

Table 3.2: Chromium sputtering conditions

Compression crack

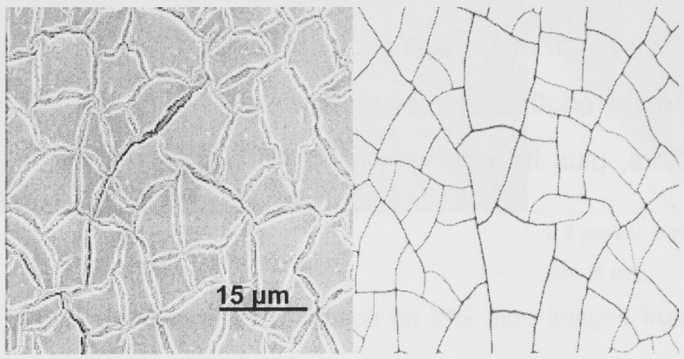

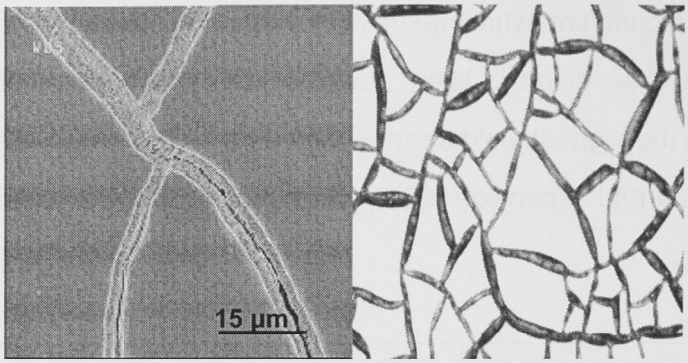

Figure 3.7: Chromium sputtered on IPG film. Normarski DIC FOV is 95x70 µm.

3.4.3 Direct Metallization with Gold

Gold metallization was much more successful. Firstly, we deposited an Aluminum buffer by using the previously optimized process under the gold film to increase the gold adhesion. This buffer layer thickness was around 50 angstrom. Then, Au was sputtered with working pressure of 9×10^{-3} mbar, working voltage of 255 Volts, and argon flow rate of 4.5 sccm. The deposition rate was 1.3 angstrom/second. The deposition results shows Au can be deposited with smooth surface and survives moderate thermal processing. However, gold is of limited usefulness as an etch mask or heater element. As far as we know, gold has superior yield strength to aluminium whilst still having a reasonably big CTE, and these factors, plus its well known ductility may be why the films did not wrinkle.

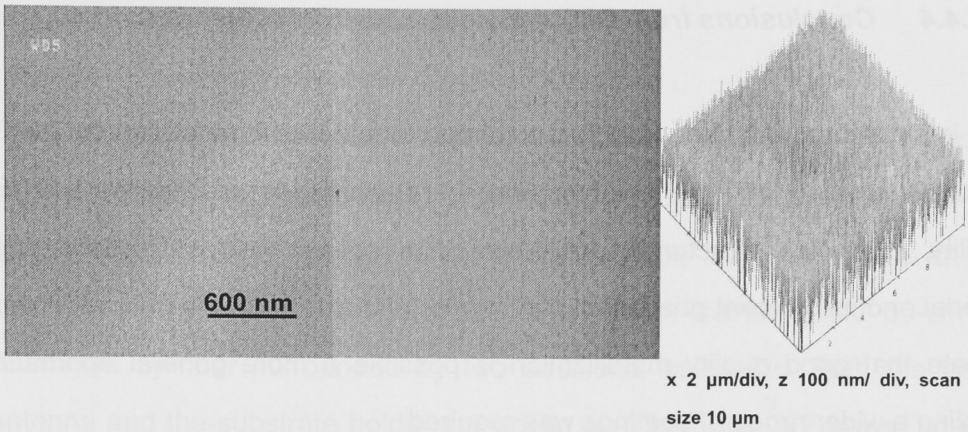

Figure 3.8: Gold metallization on IPG film. Images from FESEM (left), AFM (right) and microscope (middle). The AFM scan rate is 5 Hz. Normarski DIC FOV is 95x70 µm.

Figure 3.9 shows the thermal tests on gold metallization films at 150 ℃ for half an hour in a vacuum oven and cooled down to room temperature. The results revealed gold could pass the rigid thermal cycling tests without any wrinkles like aluminum or chromium.

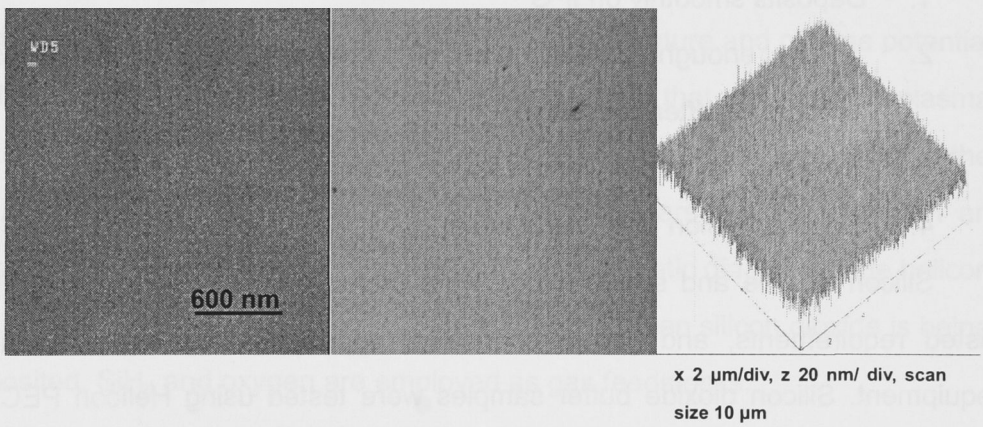

Figure 3.9: Post-heating gold metallization on IPG film. Images from FESEM (left), AFM (right) and microscope (middle). The AFM scan rate is 5 Hz. Normarski DIC FOV is 95x70 µm.

3.4.4 *Conclusions from Direct Metallization Experiments*

It is clear that a number of factors are important in direct metallization of IPG and the survival of the films in subsequent thermal processing. Clearly the CTE, ductility, crystalline structures, grain size, film stress, yield strength of the material and its different phases all play a role. Whilst the experiments with gold indicate that good quality metallization is possible a more general approach enabling a wider range of coatings was required.

3.5 Buffer Layer Deposition and Metallization

One method to alleviate the problems discussed in the precious section is to insert a buffer layer between the IPG and the metal. The requirements for the buffer layer are:

1. Deposits smoothly on IPG
2. Strong enough to resist thermal processing used in photo resist processing after deposition
3. High selectivity to dry and wet etch processes
4. Good adhesion to IPG and metal

Silicon dioxide and silicon nitride were trialed as they certainly meet the listed requirements, and had a chance of depositing well using available equipment. Silicon dioxide buffer samples were tested using Helicon PECVD system (it is not an industrial standard system). [7]; low temperature parallel plate PECVD; and by ion assisted RF sputtering. Silicon nitride was deposited in the low temperature parallel plate PECVD system only.

Deposition by using helicon system

The helicon system used in this work consists of two joined chambers: the source and diffusion chambers. The source chamber is a 15-cm-diameter, 25-cm-long glass tube surrounded by a "Boswell-type" helicon antenna and two solenoids [23]. The diffusion chamber is a 30-cm-diameter and 30-cm-long Aluminum cylinder surrounded by two additional solenoids. Both the source antenna and the substrate holder are driven by 13.56 MHz RF power sources. The currents in the 4 solenoids are adjusted to produce a transverse RF magnetic field of 100 G in the source and 60 G in the diffusion chamber, which is perpendicular to both tube axes. The plasma is allowed to diffuse from the source chamber to the diffusion chamber controlled by the extra solenoids. This produces very uniform dense plasma over a 30-cm-diameter region for deposition and etching. In this reactor, the source can be operated in the pressure range 0.1 – 10 mTorr. The useful pressure range of the source is limited at the lower end by increasing electron temperature and plasma potential, and at the upper end by the reduced collision length that prevents the plasma diffusing out of the source. The substrate holder is mounted at the bottom of the diffusion chamber, and is water-cooled. The chambers are pumped with an Alcatel ATP 400 HPC turbo molecular pump. A schematic diagram of the helicon diffusion plasma reactor is given in Figure 3.10. [7] When silicon dioxide is being deposited, SiH_4 and oxygen are employed as gas feedstocks.

Silicon dioxide deposition in this helicon system was reported previously. [7] These experiments were performed on silicon substrates, not on any kind of polymer film. Although IPG film is much softer than silicon, the deposition parameters used for Silicon dioxide depositions still provided a good starting point. The working conditions are oxygen/silane= 60/30 sccm, RF power= 800 watts, chamber and source coil current: Is.top (top source coil currents) =1 A, Is.bottom (bottom source coil currents) =0.5 A, Ic.top= Ic.bottom (chamber top

and bottom source coils currents) =3 A.

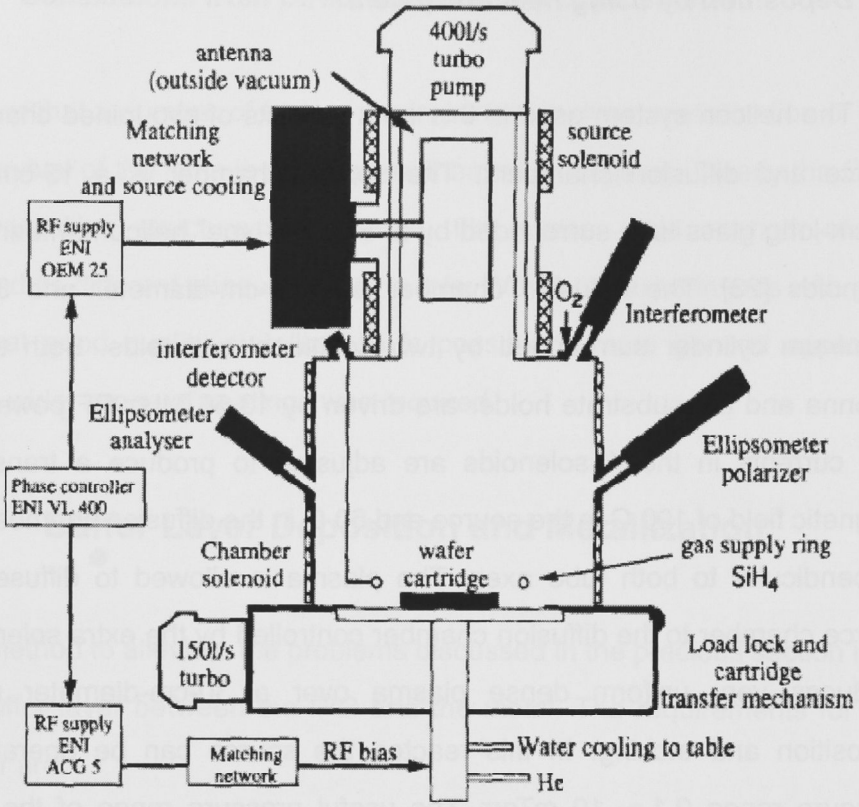

Figure 3.10: Schematic diagram of the reactor showing major components. [7]

The wafer was cooled with a helium back side cooling system. Without the helium back cooling, the wafer temperature could rise by over 200 ℃ as a result of the ion bombardment, whereas with helium back cooling the temperature was roughly twice that of ambient. [2] However, unfortunately, the efficiency of this back cooling system is questionable on IPG, since the temperature difference between the surface of the IPG film and the substrate is quite large when the surface is bombarded by plasma due to the low thermal conductivity of the IPG material. The surface morphology of a deposited silica film on IPG is shown in Figure 3.11. Given the roughness and potential for thermal management issues a move to the low temperature silicon dioxide or nitride deposition was made.

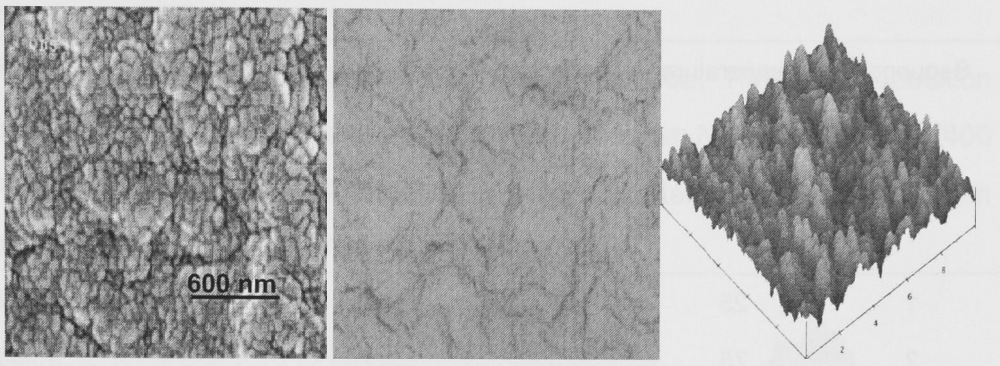

Figure 3.11: One of silicon dioxide samples made by Helicon system. Images from FESEM (left), microscope (middle) and AFM (right). The AFM scan rate is 5 Hz. Normarski DIC FOV is 95x70 µm.

Deposition by using PECVD (Plasma Enhanced Chemical Vapor Deposition)

PECVD is one of the standard material deposition methods in the micro fabrication industry. In a PECVD based process, one or several feed gases are first decomposed by the plasma. Then the decomposition products react and diffuse onto the substrate to form a film. The gases for PECVD silicon dioxide deposition are Silane (SiH_4) and NO_2. For silicon nitride deposition, the gas supply comprises Silane and Ammonia (NH_3). The ideal parameters for silicon dioxide deposition in PECVD were found to be: 710 sccm N_2O; 160 sccm SiH_4; RF power of 20 watts; pressure of 1 Torr. All These parameters were selected based on previous experience of the machine by other users. The initial substrate temperature range was from room temperature to 150℃. The thickness deposited was from 100 nm to 300 nm. The silicon dioxide deposition results are outlined in Table 3.3 below:

Sequence number	Temperature (°C)	Expected thickness (nm)	Real average thickness on silicon (nm)	Refractive index (800nm)	RMSR(Root Mean Square Roughness) (nm)
1	25	200	197.85	1.39	1.562
2	75	200	198.25	1.39	1.583
3	100	200	198.35	1.4	1.432
4	150	100	110.27	1.43	1.578
5	150	200	217.12	1.43	1.268
6	150	300	329.57	1.43	1.597

Table 3.3: PECVD silicon dioxide deposition results. FilmTek 4000 is utilized to measure the thickness and refractive index of these samples. RMS roughness is measured by AFM. The bulk silicon dioxide film Refractive Index is about 1.458.

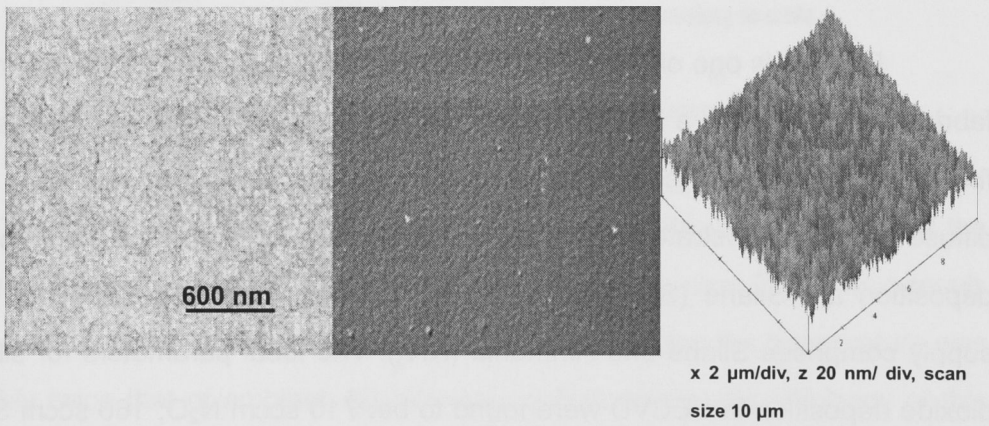

Figure 3.12: 200nm silicon dioxide sample deposited at 150℃. Images from FESEM (left), microscope (middle) and AFM (right). The AFM scan rate is 5 Hz. Normarski DIC FOV is 95x70 µm.

The results suggest the sample deposited at 150 ℃ has best quality (Lowest porosity and closest RI to bulk silicon dioxide, n_{800nm}=1.458). The final thickness selected was 200 nm, since the roughness was lower than the others. Baking at up to 180 ℃ for 30 minutes on the resist track hot plate induced no

changes in the IPG film.

Another option for the buffer film is silicon nitride. The best deposition conditions from previous experiments were known to be: NH_3 20sccm, SiH_4 400 sccm, with 20 W RF power at pressure of 1 Torr. The temperatures varied from 25 ℃ to 150℃.

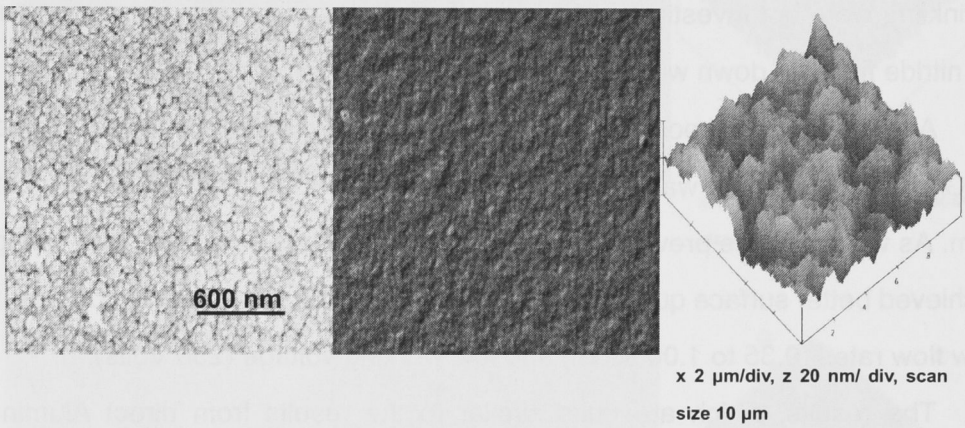

Figure 3.13: 200nm silicon nitride sample deposited at 150℃. Images from FESEM (left), microscope (middle) and AFM (right). FOV is 95x70 µm. The scan rate is 5 Hz.

Sequence number	Temperature (°C)	Expected thickness (nm)	Real average thickness on silicon (nm)	Refractive index (800nm)	RMSR(Root Mean Square Roughness) (nm)
1	25	200	200.67	1.93	8.564
2	75	200	197.85	1.93	9.332
3	100	200	203.86	1.95	8.942
4	150	100	107.66	1.98	8.967
5	150	200	208.32	1.98	8.984
6	150	300	316.94	1.98	8.948

Table 3.4: PECVD silicon nitride deposition results. FilmTek 4000 is utilized to measure the thickness and refractive index of these samples. RMS roughness is measured by AFM. The bulk silicon nitride film Refractive Index is about 2.05. And Refractive Index of PECVD silicon nitride is generally 2.00 at 250 ℃ - 350 ° C deposition temperature.

The best result from PECVD was also 200 nm at 150 °C. But the surface roughness when deposited on IPG was beyond acceptable tolerances, since there are obvious wrinkles from visual inspection. The RMS Roughness value of PECVD silicon nitride is about 8.5 nm. The reasons for the silicon nitride wrinkling were not investigated further but are likely due to the known tendency of nitride films go down with high built in stress.

After buffer film deposition, the next step was to metallize the buffer film and IPG. Firstly, Aluminum was deposited on IPG with PECVD silicon dioxide buffer film. As we know, the previous results show the low gas flow rates and voltages achieved better surface quality on IPG films. Therefore, we can only consider the low flow rates (0.35 to 1.00 sccm) and low working voltage (250 Volts).

The results, which are quite similar to the results from direct Aluminum depositions, revealed the best deposition condition were around 1.0 A/s at 2.2×10^{-3} mbar pressure, i.e. 0.4 sccm Argon, in Table 3.5. The results also suggested that the lower deposition rates can achieve better surface quality, which is quite similar to the results from Aluminum direct metallization of IPGs. Following deposition baking tests were run at 150 °C for 30 minutes on the resist track hotplate. Finally, some AFM scans were run to calculate the roughness.

Sequence number	Ar flow rate (sccm)	Working voltages (Volts)	Working pressure ($\times10^{-3}$ mbar)	Deposition rate (A/second)	RMSR(Root Mean Square Roughness)
1	0.4	250	4	1.2	1.848
2	0.6	250	4	1.7	1.973
3	0.8	250	4	2	2.089
4	1.0	250	4	2	1.985

Table 3.5: Aluminum deposition on 200 nm silicon dioxide substrate results.

FESEM and optical DIC microscope scanning of the Aluminum without and

with baking at 150 ℃ for 30 min are shown below. T he RMS roughness results are all around 2.0 nm.

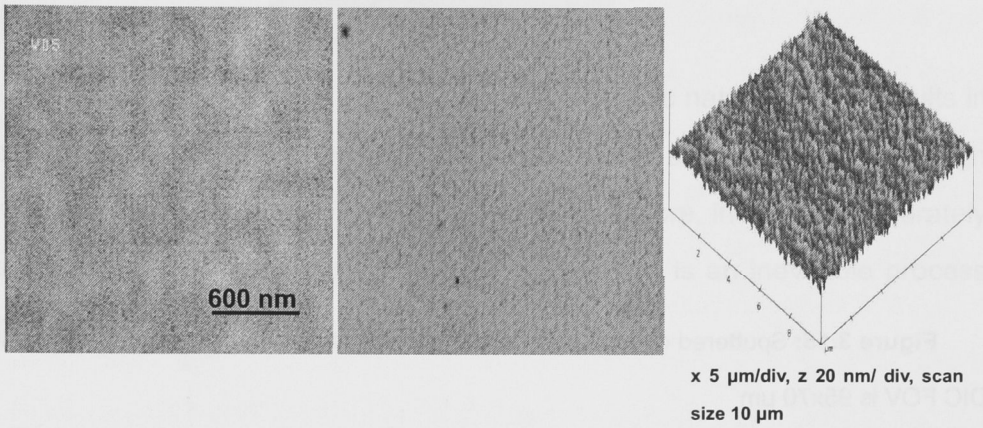

(a)

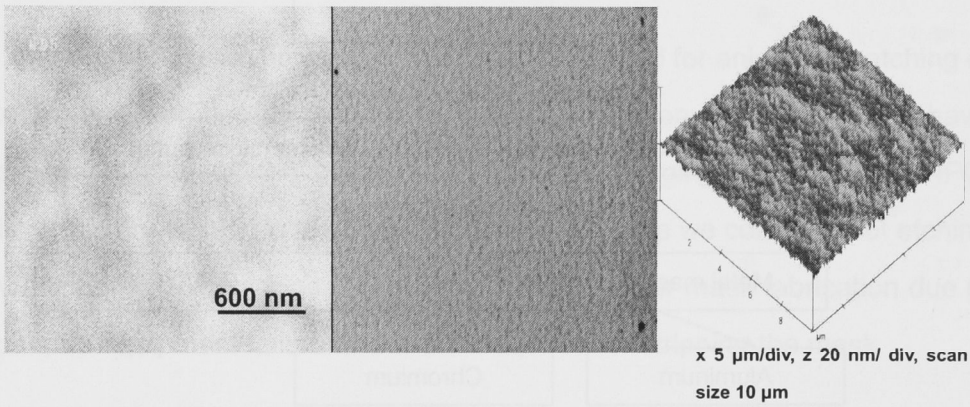

(b)

Figure 3.14: IPG/silicon dioxide/Aluminum structure sample. (a) the deposited Aluminum microstructure scanned by FESEM, Microscope and AFM; (b) samples were baked at 150 ℃ for 30 min scanned by FESEM, Micros cope and AFM. Normarski DIC FOV is 95x70 μm. The AFM scan size is 20 μm and rate is 0.5 Hz in (a), and 1um at 1 Hz in (b).

Clearly, the Aluminum film performs as desired. After Aluminum metallization, chromium was tried as well. However, the chromium still did not work on the IPG/silicon dioxide substrate. All the deposition conditions are the same as direct chromium metallization. The following image shows one result of a deposition where the results are quite similar to the samples without buffer layer.

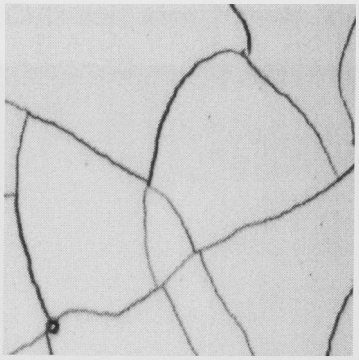

Figure 3.15: Sputtered chromium on silicon dioxide film from microscope. Normarski DIC FOV is 95x70 μm

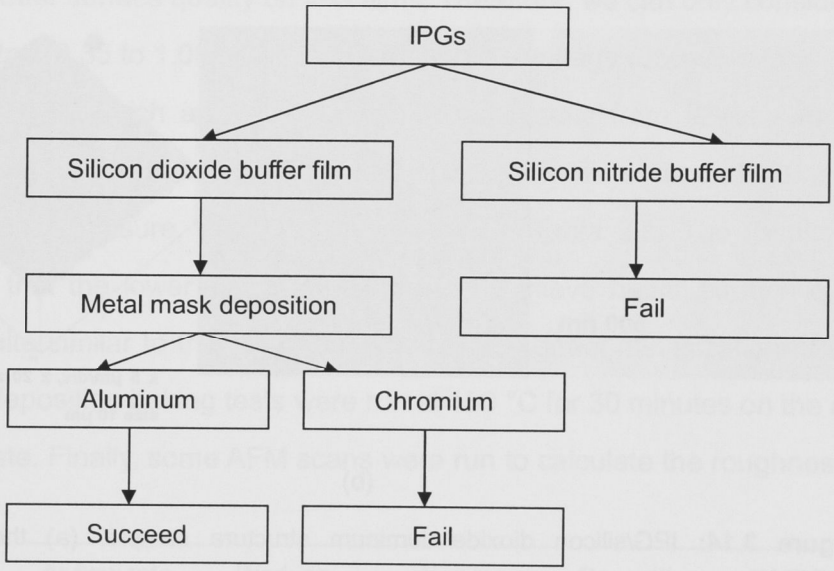

Figure 3.16: Flow chart of IPG metallization with buffer layer.

The flow chart above explains the all IPG metallization steps with buffer layers. The final conclusion from our works is that IPGs/silicon dixode/Aluminum is the only successful structure for metallization found so far. Hence, this structure is employed in etching process.

3.6 Dry Etching

The inherent limitation of wet etching is its isotropic nature, which results in severe undercutting in waveguide fabrication and in some cases also rough sidewall due to the lack of sidewall passivation. Therefore, in order to accurately control waveguide dimensions and profile, dry etching is an inevitable process for manufacturing etched IPG waveguides.

Etching

In the project, etch processes had to be developed for anisotropic etching of metal films, silicon dioxide, and the IPG itself. In addition it is necessary to have processes to strip off the metal mask without damaging the underlying IPG. Antistrophic dry etching is discussed in detail later, here we consider wet etching of Aluminum in particular as this became necessary for mask fabrication due to irreparable equipment failure and is also required for stripping the mask.

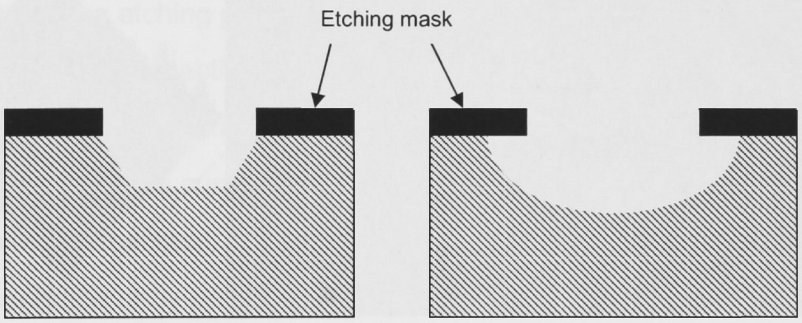

Figure 3.17: Difference between anisotropic and isotropic wet etching. The left image shows anisotropic, the right image shows isotropic.

There are several approaches for Aluminum wet etching. The simplest one is 85% concentrate phosphoric acid. However, most commercial etchants are based on 85% phosphoric acid and 70% nitric acid. Acetic acid can be added to

dilute the solution instead of water for better wetting behavior and lower viscosity. In addition, acetic acid can retard the dissociation of nitric acid in order to yield a higher concentration of the undissociated species and thereby provide some buffering of the etch solution. The mixture of Al etchant we used has a composition as HPO_4: HNO_3: CH_3OOH=16: 1: 1. The etching temperature was about 20 - 30 ℃.

Etching of Aluminum occurs in a multistep reaction in the chemistry. The nitric acid firstly consumes Aluminum to form an Aluminum oxide layer. This oxide layer is then dissolved by the phosphoric acid and water. With the concentrations given, these two processes occur at roughly the same rate, so that either one could be the rate limiting step. Because the phosphoric acid also removes the native Aluminum oxide, no additional process is needed for this purpose. There is no concern about the film under the Aluminum layer, as it is silicon dioxide layer, which will not be attacked by this sort of etchant. However, it will attack the IPG film and can result in surface roughening as shown in Figure 3.18.

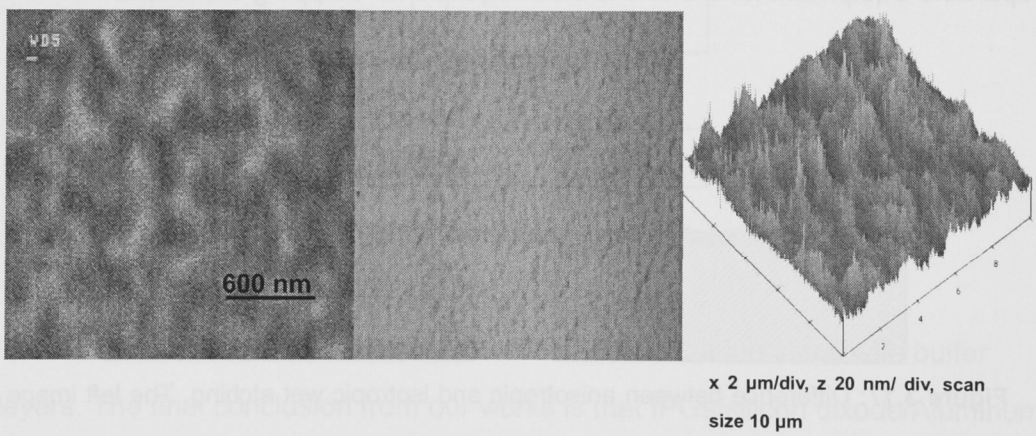

Figure 3.18: Wet etched IPG film. Images from FESEM (left), microscope (middle) and AFM (right). FOV is 95x70 µm. The scan rate is 5 Hz.

Wet etching processes are often used at elevated temperatures to increase the etch rate. For our etchant, the etch rate was 30nm/min at room temperature

and 250 nm/min at 50 ℃. However, at 50 ℃, bubbles were forming on the film surface, so a compromise temperature was chosen with the etchant heated to 30 - 40 ℃ on a hotplate whose temperature was cont rolled using a thermocouple. The heated acid enabled the 200nm etching to be completed in a safe period of 2 - 3 minutes.

However, it is still preferable to etch the Al patterns by using dry etching which results in a vertical sidewall profile on the Al mask and lower edge roughness and dimensional loss.

3.6.1 Introduction to Dry Etching

Dry etching refers to the removal of material by exposure to a reactive gas species and/or a flux of ions that dislodge portions of the material from the exposed surface. There are two dry etching methods: non-plasma based dry etching and plasma dry etching. In this project plasma dry etching was used exclusively. Both RIE (Reactive Ion Etching) and ICP (Inductively Coupled Plasma) etching are employed. A plasma is used to generate chemically reactive species (atoms, radicals and ions) from molecular gases. There are six major steps in the plasma etching process:

A) Generation of reactive species

B) Diffusion to the surface

C) Absorption on a surface

D) Chemical reaction

E) Desorption of by-products

F) Diffusion into bulk gas/plasma

In dry etching of silicon dioxide, aluminum, and organic materials, several gases are commonly employed: O_2 (Oxygen), CF_4 (Tetrafluoromethane), CHF_3 (Trifluoromethane), $SiCl_4$ (tetrachlorosilane) and Ar (Argon).

The purposes of oxygen in dry etching are diverse. Pure oxygen in plasma etching will remove or etch photo resist and other pure organics. In plasmas

involving CF_4 or CHF_3, oxygen is also used to displace F in the CF_4 or CHF_3 molecule, generating more free F. This can increase the etch rate and alter the selectivity to silicon for example. Further it is sometimes added in small quantities to CHF_3 based etches under certain conditions to prevent polymerization occurring.

CF_4 is a popular etching gas in industry or laboratory applications. It is a plentiful source of F and can therefore be used to etch silicon or silicon dioxide isotropically or anisotropically as desired. The lack of native hydrogen and the low C to F ratio means that CF_4 based etches do not generally benefit from polymer deposition on the etched sidewalls to enhance anisotropy. CHF_3 is another source of F and C, but with a lower ratio of F to C, sidewall passivation is easily achieved and higher selectivities to silicon and other mask materials than with CF_4 are possible.

$SiCl_4$ is used to etch various thin metal films in RIE systems such as Al, Si, Si_3N_4 and SiO_2, etc. In particular we wished to employ it to anisotropically reactively ion etch the Aluminum films to make a hard mask with very smooth edges.

Argon is an inert gas commonly added to dilute active gasses, but also to provide some physical sputtering. This latter effect, for example in CHF_3 based etches, prevents polymer build up on the etched surface either slowing or terminating the etch process.

3.6.2 Reactive Ion Etching (RIE) of Aluminum Mask

Lithography

In experiments, standard photolithography processes were used to pattern the resist mask on the substrate. Clariant AZ MiR 701 photo resist and AZ 300 MIF developer were employed. The UV exposure system was a Karl Suss MA 6 mask aligner, operating at 365nm single mercury line. In MA 6 UV exposure system, there are three contact modes for the mask and wafer: hard, soft and

vacuum contact. Hard contact mode is exactly that, force is applied to push the wafer and mask together to achieve a good physical connection. The force insures that the pattern on the mask is as close as possible to the resist to be exposed and therefore achieves good pattern transfer. The physical nature of the hard contact mode results in masks becoming contaminated. Soft contact mode also results in the mask and wafer being in direct contact, but without as much force. The reduced force means that in some regions the wafer and mask may not be in direct contact, and it is possible to experience pattern transfer degradation (as diffraction effects may occur at the edges if a significant gap exists between wafer and mask). In vacuum contact, a vacuum is drawn between the mask and wafer prior to exposure, allowing the highest resolution since the gap is minimized. This mode permits the highest resolution levels. In our experiments, only vacuum contact exposure was used, as it is able to provide the highest resolution.

The main steps in experiments are shown below:

1. IPG film vacuum bake at 180 ℃/ 3 hours
2. Buffer layer deposition and Aluminum sputtering
3. Spin coating photo resist (AZ MIR 701) : 4000 rpm/30 seconds (which achieves about 0.9-1 μm thickness of photo resist)
4. Soft bake: 90 ℃/ 60 seconds on a hotplate
5. UV Exposure
6. Post Exposure bake 110 ℃ for 1 minute
7. Developing
8. Hard bake: 110 ℃ /80 seconds on a hotplate
9. Aluminum etching in RIE (if using Aluminum mask)
10. Silicon dioxide etching in ICP
11. IPG etching in ICP

The whole process for using silicon dioxide mask or Aluminum masks are summarized below diagrammatically as well.

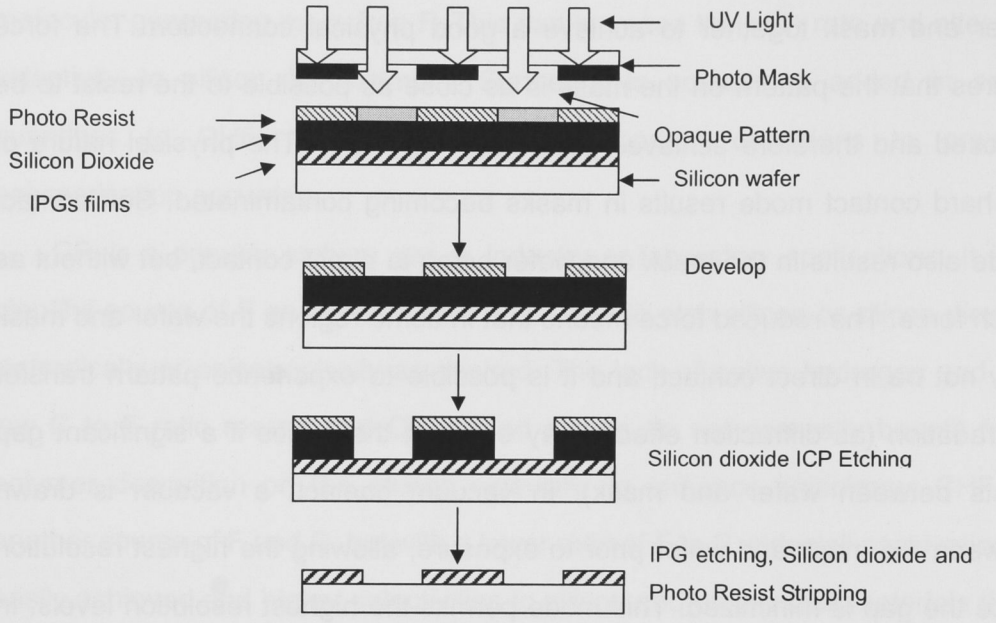

(a)

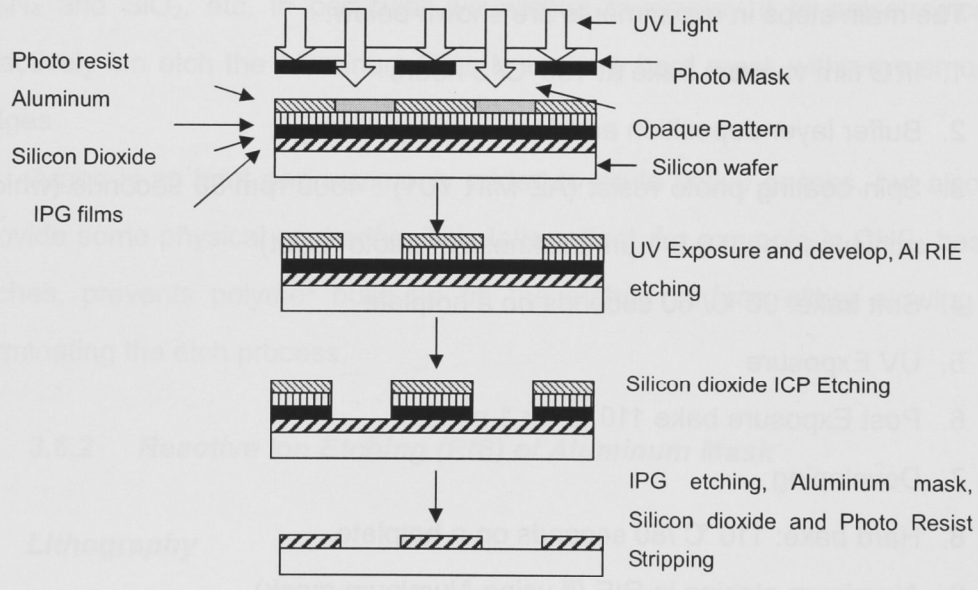

(b)

Figure 3.19. Procedure of IPG waveguide fabrication by using Aluminum mask (b) and silicon dioxide mask (a).

Reactive Ion Etching System

An RIE system (Oxford Plasmalab 80 plus) was mainly used for Aluminum mask etching.

In RIE, the substrate is placed inside a reactor in which several gases are introduced. The plasma is struck in the gas mixture using an RF power source, breaking the gas molecules into ions. The ions then are accelerated towards and react on the surface of the material being etched, forming another gaseous material. This is known as the chemical part of reactive ion etching. There is also a physical part which is similar in nature to the sputtering deposition process. If the ions have high enough energy, they can knock atoms out of the material to be etched without a chemical reaction. By changing the balance between the physical and chemical processes it is possible to influence the anisotropy of the etching, since the chemical part is isotropic and the physical part highly anisotropic the combination can form sidewalls that have shapes from rounded to vertical. A schematic of a typical reactive ion etching system is shown in the Figure 3.20. The main disadvantage of standard parallel plate RIE is that there is a conflict between etching rate and etch antistropy (if the etch rate increases, the reactive species concentration will be enhanced as well, finally resulting in larger gas pressure and collisions, which will affect the profile). In our RIE system, the process pressures can be from 5 to 150 mTorr. The available gas supplies are CF_4, Ar, O_2, and $SiCl_4$.

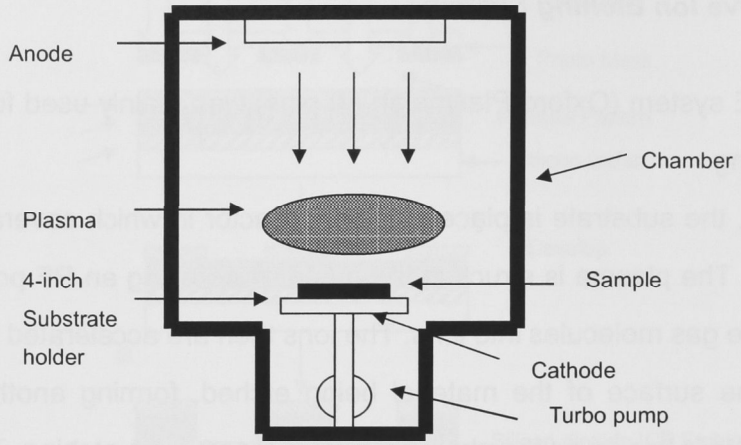

Figure 3.20: Schematic overview of a parallel plate RIE system. The substrate is placed on the powered cathode attracting the positive ions.

RIE etching experiments

The Aluminum mask etching was carried out in the RIE system to avoid the potential edge roughness that can result from wet etching.

A standard Aluminum etching recipe from Oxford Instruments Plasma Technology was investigated. The $SiCl_4$ flow rate was 23 sccm. The working pressure was 50 mTorr and working temperature is 40 ℃. RF power was set as 300 W and DC bias was 280 Volts. The etch rate of Aluminum was about 70 nm/min. The selectivity was about 2:1 (Aluminum: photo resist). Samples were given a DI water rinse immediately after etching to remove any residues in order to prevent post-etch corrosion. The etching results are shown in the figure below. The etching results show the sidewall profiles of Aluminum mask is vertical. Although imperfect lithography has created longitudinal sidewall roughness in the form of vertical striations which hide just how smooth the overall etch is.

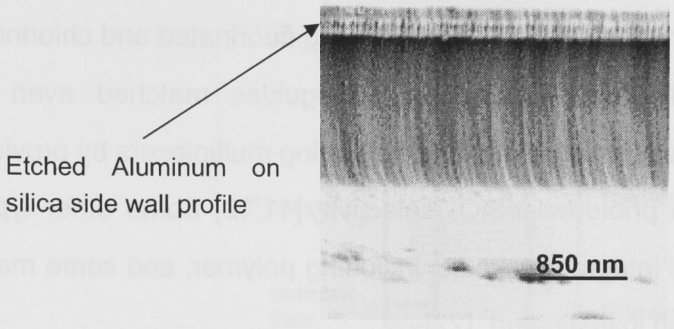

Figure 3.21: Etched Aluminum layer profile by using RIE using $SiCl_4$

3.6.3 Inductively Coupled Plasma (ICP) Etching of Silicon dioxide

Inductive Coupled Plasma System

An inductively coupled plasma reactor (Oxford Plasmalab RIE 100-ICP) was used to etch IPG waveguides. ICP was originally designed as the replacement for Magnetic Enhanced RIE (MERIE) due to the need to maintain high pressure in a parallel plate reactor to avoid extinguishing the plasma. High density plasma reactors are designed so that the plasma electrons are excited in a direction parallel to the reactor boundaries. Typical high-density plasma systems include inductively coupled plasma (ICP), [9] helicon wave plasma reactor, [10] electron cyclotron resonance (ECR) reactors [9].

In the ICP reactor, the plasma is driven by a magnetic potential set up by a coil wound outside the dielectric chamber sidewalls. [10] ECR and helicon sources can also be used to couple electromagnetic fields into the plasma. [16] When the plasma is excited in this manner, the electron mean free path can become much greater than the reactor dimensions, and the operating pressure consequently lowered.

The primary processing advantages of high density sources are better critical dimension (CD) control, higher etching rates, high selectivity, and an improved processing window as ion density and DC bias are now independently

controllable. Anisotropic dry etching performed by high density plasma has been developed for a wide range of materials mostly using fluorinated and chlorinated gases. ICP etching of deep silica/silicon waveguides matched even the demanding requirements of arrayed waveguide grating multiplexers by providing high etch rate and high photoresist/SiO_2 selectivity.[11,12] Some other typical materials used in optical integrated circuits including polymer, and some metals for masks have also been investigated. [22]

The structure of the ICP system in our laboratory is shown in Figure 3.22. The chamber consists of two joined vacuum chambers, the source and sample chambers. The substrate holder is mounted at the bottom of the sample chamber. Automatic loading is facilitated by a pin-lift mechanism capable of handling substrates or carrier plates up to 200 mm diameter and 6 mm thick. The wafer is held down on to the water cooled substrate plate by a quartz mechanical clamp plate thereby allowing Helium to be used as a heat transfer medium between the wafer and chuck. The induction coils surrounding the source tube are driven by a 5 kW 13.56 MHz RF power source (ICP generator). The substrate is biased using a separate 600 W RF source (Table generator). The configuration of this Oxford ICP source is different from other ICP systems, where the induction coils are planar and are put on the top of the source chamber. The chambers are pumped with an Alcatel ACT900HPC turbo molecular pump. The processing gases of CF_4, O_2, CHF_3, and Ar are admitted into the vacuum chamber through separate mass flow controllers. A laser interferometer (working wavelength of 677 nm) can be used to monitor the progress of the etch process in real time, hence allowing etch depth monitoring and control.

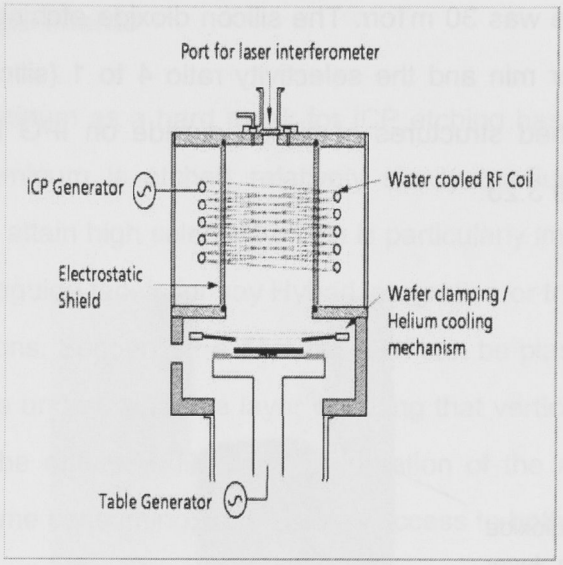

Laser interferometer working at 677 nm

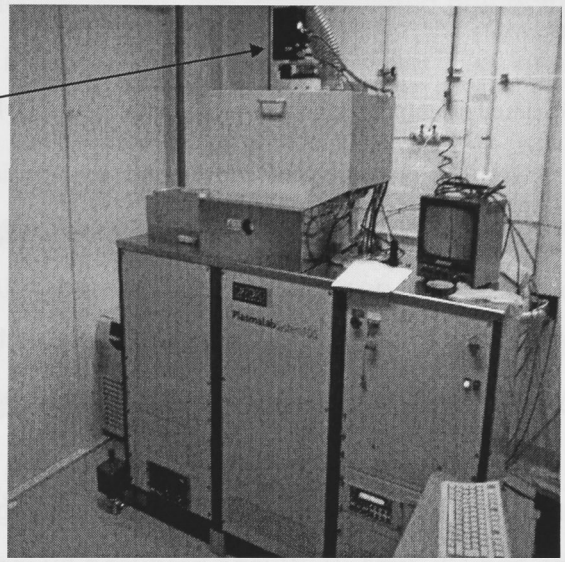

Figure 3.22. The structure of ICP system. Top image is chamber interior structure. Bottom image is exterior feature

ICP Etching experiments

The silicon dioxide mask etching was carried out in ICP system. The etching recipe is based on previous experiments provided by colleagues. The etching parameters were: 50 sccm Argon and 50 sccm CHF_3 as processing gases; RF power of 150 W and no ICP power was used (i.e., pure RIE mode etch); A helium

wafer backside cooling system controlled the wafer temperature at 20℃ and working pressure was 30 mTorr. The silicon dioxide etching rate was generally about 35 nm per min and the selectivity ratio 4 to 1 (silicon dioxide to photo resist). The etched structures of silicon dioxide on IPG films are shown by FESEM in Figure 3.23.

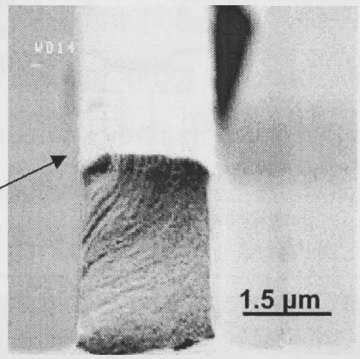

Figure 3.23: Residual silicon dioxide layer profile after IPG etch by CHF_3/Ar using ICP.

3.6.4 Inductively Coupled Plasma Etching of IPGs

An important purpose of the ICP etching studies presented in this chapter is to investigate dry etching with different process gas supplies across a range of conditions.

Fluorocarbon gases are commonly used for the etching of SiO_2 due to the activity of F atoms and CF_x (x=1, 2, 3) ions produced by ion bombardment in a plasma chamber. The addition of the source gas with Ar or O_2 can change the densities of these ions, and it was expected that due to the organic components in the IPG material that a higher proportion of oxygen would be required. The use of a silica only hard etch mask was studied in addition to an Aluminum/silica structure.

IPG etching experiments

The use of Aluminum as a hard mask for ICP etching has some attractive features. Firstly aluminum is etched relatively slowly by fluorine containing plasmas and so can attain high selectivity. This is particularly important for deep etches to make waveguide facets for say Hybrid Integration or trenches for other waveguide applications. Secondly the Al mask itself can be plasma etched with high selectivity to the underlying silica layer ensuring that vertical sidewalls and smooth edges can be obtained. However preparation of the Al hard mask is more complex and time consuming, and requires access to both Cl and F based plasma processing tools. Despite this it was pursued due to the options it may offer for deep etch in future device applications such as tunable devices and hybrid integration.

The use of a silicon dioxide/photo resist etching mask is a much simpler solution for etch depths down to about 3 micron. Several additional processes involved such as Al deposition and etching can be passed over. The major question mark over this process was whether sufficient selectivity could be achieved in the oxygen and fluorine rich etch environment.

Results and discussions

- ***Etch rates, surface roughness, RF power and selectivity***

Fluorocarbon gas plasmas have been routinely employed in selective etching of silicon dioxide over silicon [14, 15]. CF_x radicals created in the plasma diffuse onto the wafer surface and become deposited as a precursor to fluorocarbon polymer. The formation of a passivating film on the sample surface, for example Si, is thought to be a key mechanism for selective etching [17-20]. These radicals passivate silicon dioxide surfaces to a lesser degree than silicon surfaces because the carbon in the films can react with the oxygen in the silica

resulting in volatile products [21] such as CO, CO_2, COF and COF_2. One troublesome issue in high-density fluorocarbon plasmas is the high degree of molecular dissociation that produces an abundance of atomic fluorine and the consequent inadequate suppression of etching. Concentrations of fluorocarbon species and thus selectivity are controlled by source gas dilution with additives such as O_2, H_2, and Ar. As added benefits, oxygen helps in preventing excessive carbon deposition on the reactor walls and argon helps in maintaining stable discharges and physical sputtering of the polymer on horizontal surfaces thereby enhancing sidewall passivation. Among the fluorocarbon gases, ozone-friendly trifluoromethane (CHF_3) and its mixtures with other gases are commonly used in etching. Thus, CHF_3 is anticipated to be a more suitable etching gas compared to CF_4. Theoretically, although CHF_3 is evidently a better option for IPG waveguide etching, CF_4 was still trialed as a potential etching gas supply.

In this study, we firstly investigated CF_4/O_2, CHF_3/O_2 and CHF_3/O_2/Ar mixtures at gas pressures ranging from 10 mTorr to 50 mTorr. In order to analyze the chemical effect of these processing gas mixtures, the etching of 10 μm IPG (L-11) and 10 μm silicon dioxide (thermal oxide as a proxy for the PECVD silicon dioxide) were tested by in the ICP system. The standard conditions for all these etching processes were:

Table RF power: 20W

ICP power: 200W

Processing time: 10 minutes

Total gas flow: 30sccm

These parameters were chosen based on previous experience with the machine in etching other materials. The DC bias ranges from 170 Volts to 190 Volts since the RF power is constant.

Next the effect of RF and ICP powers, working pressure, and gas composition ratio, etch rate, and surface roughness was systematically studied.

The etch rates of IPG and silica were measured *in-situ* using a laser interferometer, or *ex-situ* using a Filmtek 4000. The FESEM imaging was used to

investigate the waveguide profiles, and sidewall roughness.

A) CF_4/O_2 mixture

The etch rate of IPG and silica as functions of the processing flow ratios for CF_4/O_2 are plotted in Figure 3.24. The chamber pressure was 10 mTorr. As shown in the Figure, the etch rate of IPG increases slowly with O_2 ratio at first, whilst the etch rate of silica increases slightly faster with the increase of the O_2 ratio. This is due to the addition of oxygen increasing the liberation of fluorine from the CF_4. The peak etch rates for both IPG and silica occur at around 85% O_2 before decreasing essentially to zero with further increase in the O_2 ratio. The selectivity of IPG to silica varied from 0.7 to 1.4.

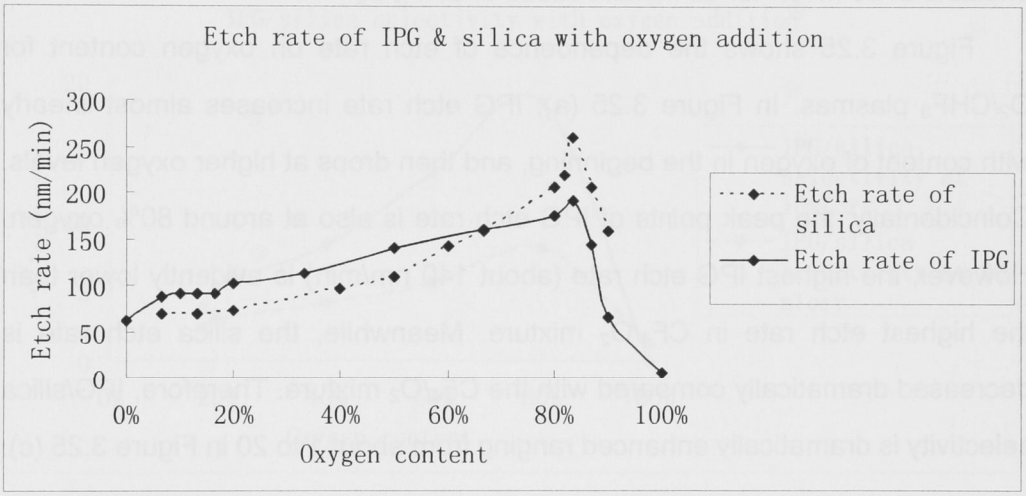

(a)

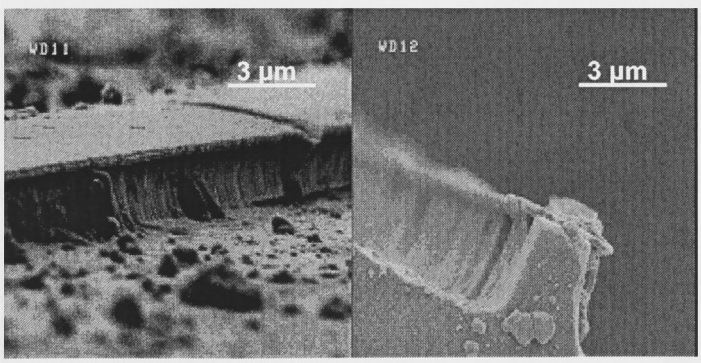

(b)

Figure 3.24. (a) Etch rates of IPG and silica with oxygen addition. Dark line is IPG, and dotted line is silica. (b) FESEM images of etching using condition of CF_4/O_2=5/25 sccm, 200

W ICP power and 10 mTorr. The thickness is about 3 μm.

For this gases mixture, silica can not be used as the etching mask. Moreover, the IPG side wall is much rougher compared with other processes using CHF_3. Therefore, this gas mixture was not pursued further.

B) CHF_3/O_2 mixture

The inductively coupled etching of IPG and silica in O_2/CHF_3 plasma has been examined as a function of working pressure, and composition of the gas mixtures. Initially pressures of 10 mTorr, 30 mTorr and 50 mTorr were to be investigated. However, in experiments, the plasma discharge was found to be unstable at 50 mTorr for all mixture ratios of CHF_3/O_2.

Figure 3.25 shows the dependence of etch rate on oxygen content for O_2/CHF_3 plasmas. In Figure 3.25 (a), IPG etch rate increases almost linearly with content of oxygen in the beginning, and then drops at higher oxygen levels. Coincidentally, the peak points of IPG etch rate is also at around 80% oxygen. However, the highest IPG etch rate (about 140 nm/min) is evidently lower than the highest etch rate in CF_4/O_2 mixture. Meanwhile, the silica etch rate is decreased dramatically compared with the CF_4/O_2 mixture. Therefore, IPG/silica selectivity is dramatically enhanced ranging from about 1 to 20 in Figure 3.25 (c).

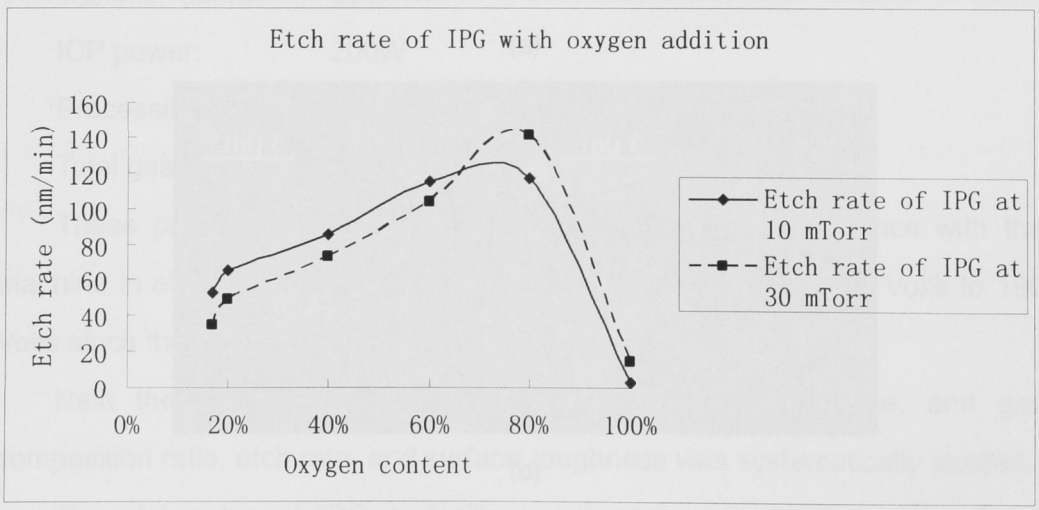

(a)

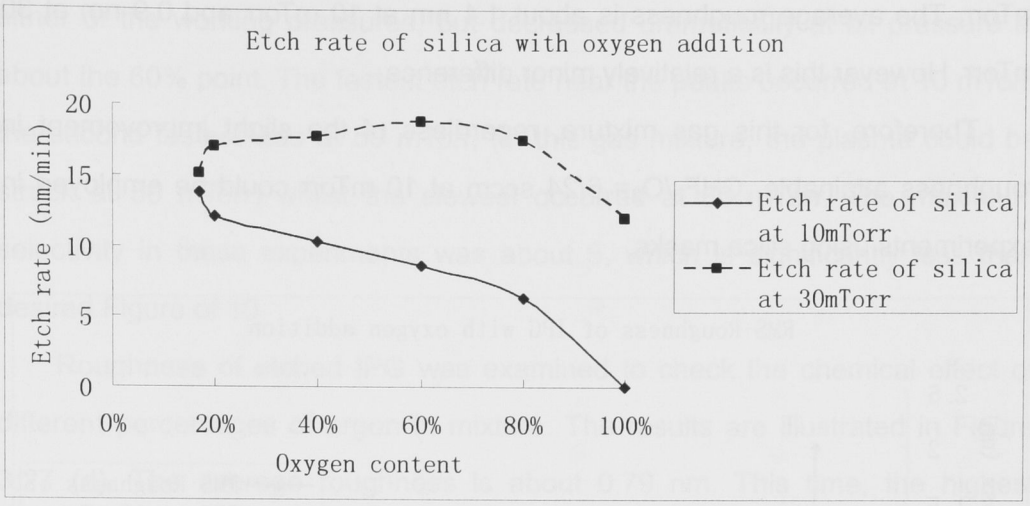

(b)

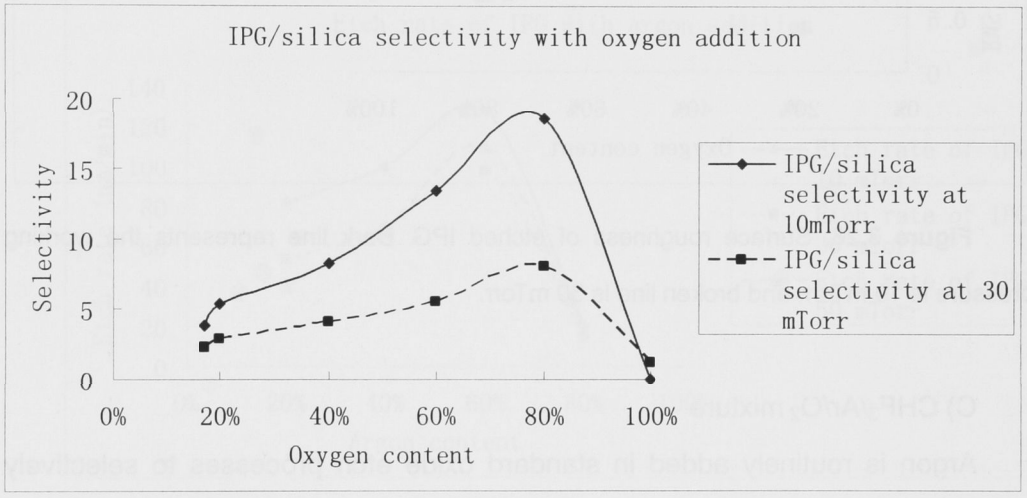

(c)

Figure 3.25. Etch rate and IPG/silica selectivity with oxygen addition. Dark lines represent the working pressure is 10 mTorr, and broken line is 30 mTorr. (a) etch rate of IPG with oxygen addition; (b) etch rate of silica with oxygen addition; (c) IPG/silica selectivity with oxygen addition.

Figure 3.26 illustrates the etched surface roughness of IPG at 10 mTorr and 30 mTorr with relation of oxygen content. We find that as the oxygen increases, the roughness oscillates in a certain range, which is most likely error in the measurements. But, at 30 mTorr, RMS Roughness is clearly smaller than at 10

mTorr. The average roughness is about 1.1 nm at 10 mTorr and 0.9 nm at 30 mTorr. However this is a relatively minor difference.

Therefore, for this gas mixture, regardless of the slight improvement in roughness attainable, CHF_3/O_2= 6/24 sccm at 10 mTorr could be employed in experiments using silica masks.

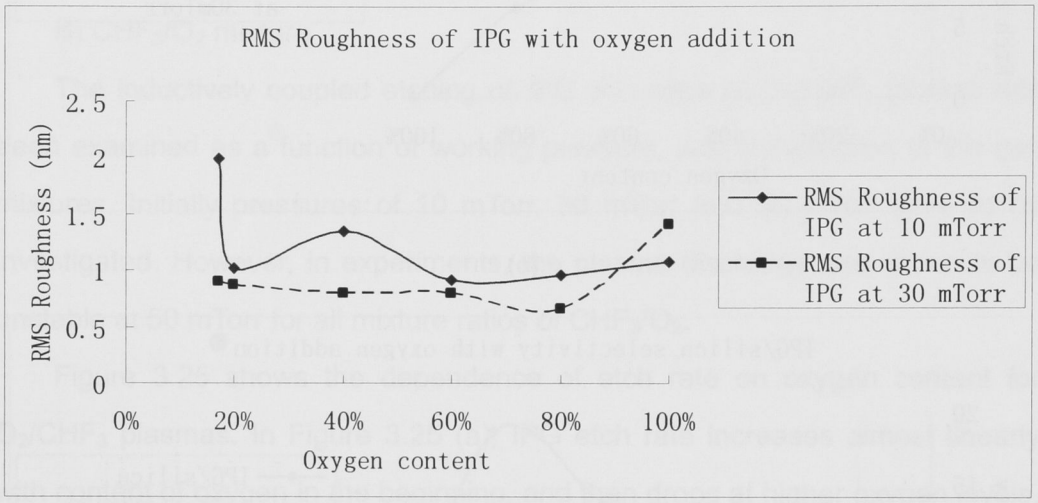

Figure 3.26. Surface roughness of etched IPG. Dark line represents the working pressure is 10 mTorr, and broken line is 30 mTorr.

C) $CHF_3/Ar/O_2$ mixture

Argon is routinely added in standard oxide etch processes to selectively sputter off polymer deposited on the horizontal surfaces in CHF_3 plasmas thereby enhancing etch verticality. Thus we decided to investigate the effect of Argon addition. Meanwhile, the oxygen content of the gas mix was varied from 20-60% in three steps, and the argon content varied inside each of these three oxygen concentrations.

Firstly, oxygen was fixed at 20% of total gas flow rates. The percentages of argon were varied from 20% to 80% and total gas flow rate was set as 30 sccm. Figure 3.27 (a) (b) shows the dependences of etch rates at different working pressures as a function of argon content for the gas mixture of $CHF_3/Ar/O_2$. As seen in Figure 3.27, the etch rates increase continuously with more argon at

either of the working pressures, but decreased dramatically at all pressure at about the 60% point. The fastest etch rate near the peaks occurred at 10 mTorr, the second fastest was at 50 mTorr, (in this gas mixture, the plasma could be struck at 50 mTorr) whilst the slowest occurred at 30 mTorr. The maximum selectivity in these experiments was about 5, which is significantly less than desired Figure of 10.

Roughness of etched IPG was examined to check the chemical effect of different percentages of argon in mixture. The results are illustrated in Figure 3.27 (d). The average roughness is about 0.79 nm. This time, the highest pressure also results into lowest surface roughness.

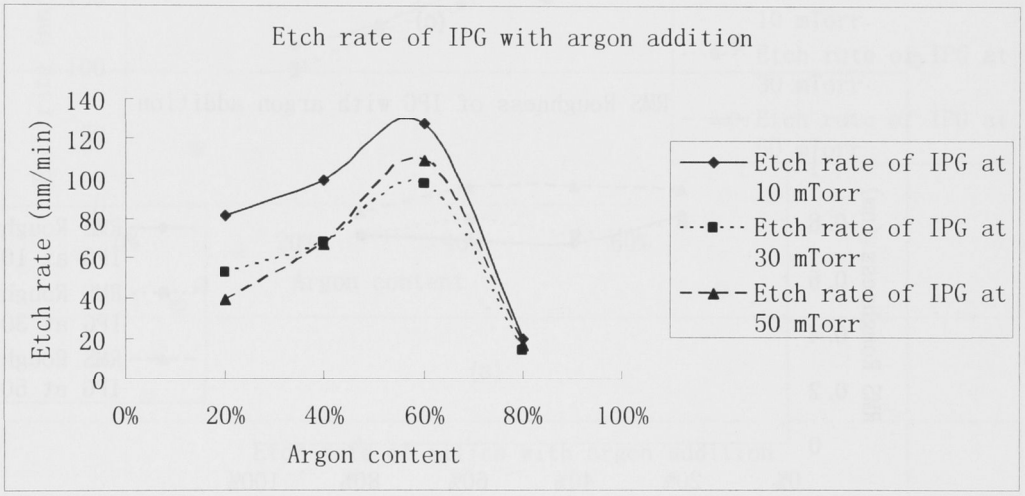

(a)

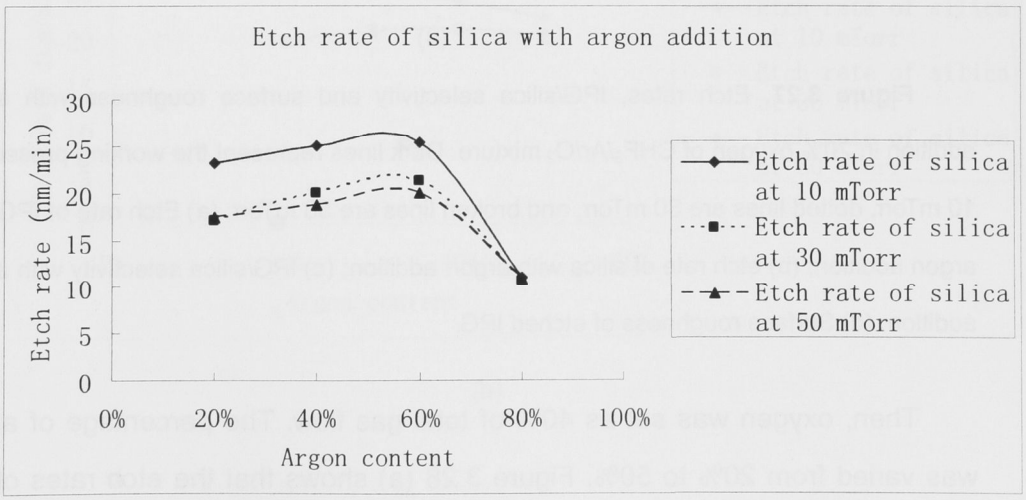

(b)

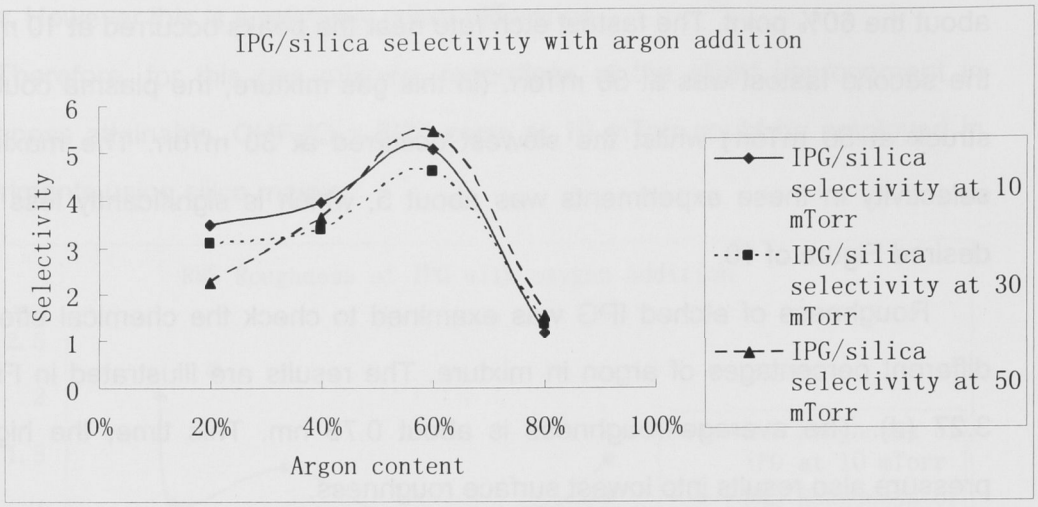

(c)

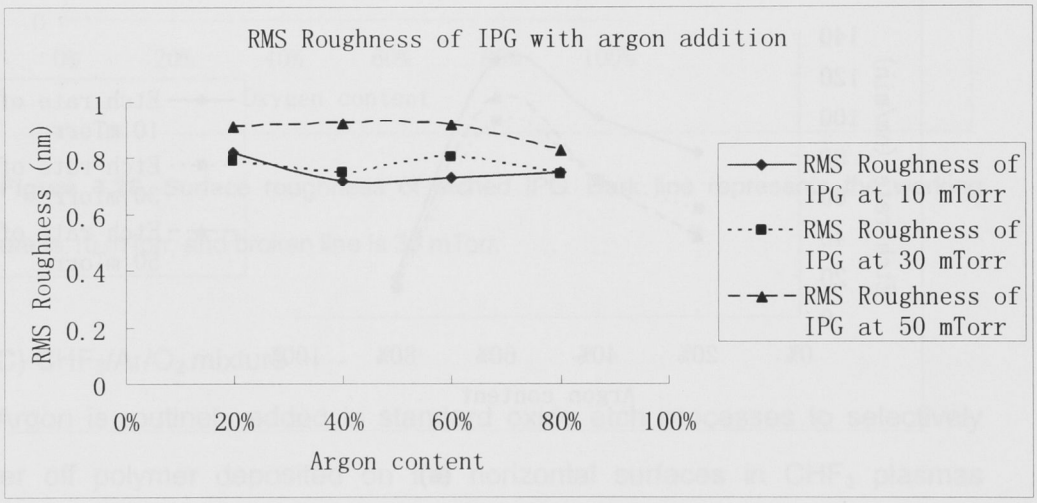

(d)

Figure 3.27. Etch rates, IPG/silica selectivity and surface roughness with argon addition in 20% oxygen of $CHF_3/Ar/O_2$ mixture. Dark lines represent the working pressure is 10 mTorr, dotted lines are 30 mTorr, and broken lines are 50 mTorr. (a) Etch rate of IPG with argon addition; (b) etch rate of silica with argon addition; (c) IPG/silica selectivity with argon addition. (d) Surface roughness of etched IPG.

Then, oxygen was set as 40% of total gas flow. The percentage of argon was varied from 20% to 50%. Figure 3.28 (a) shows that the etch rates of the

IPG films vary from 95 nm/min to 182 nm/min with increasing argon flow rate ratio. Silica etch rate decreases with increasing argon flow rate at low pressures, and is otherwise unaffected at higher pressures as shown in Figure 3.28 (b). In Figure 3.28 (c), the IPG/silica selectivity is seen to steadily increase with argon flow rate. However, in Figure 3.28 (d), RMS roughness remains approximately constant. The maximum selectivity in these experiments was about 9, which is very close to the desired 10. The average roughness was around 0.74 nm.

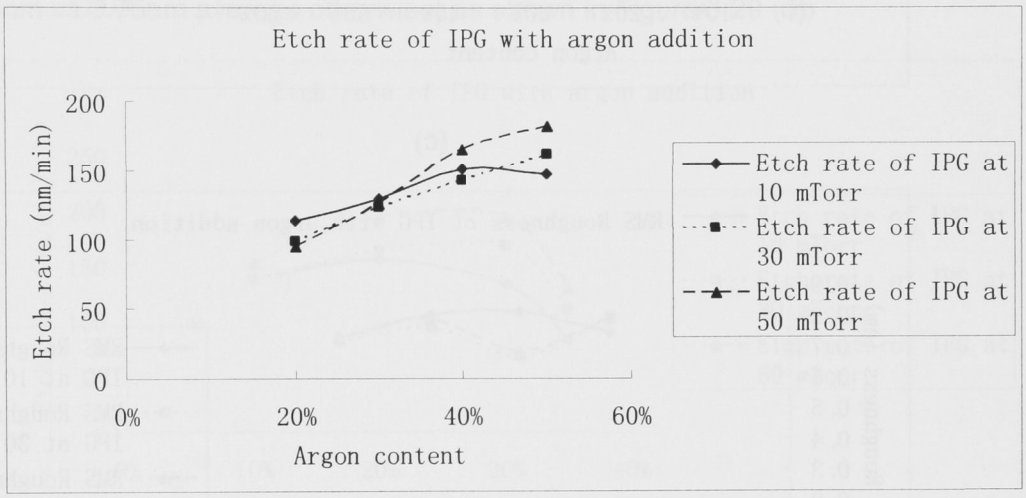

(a)

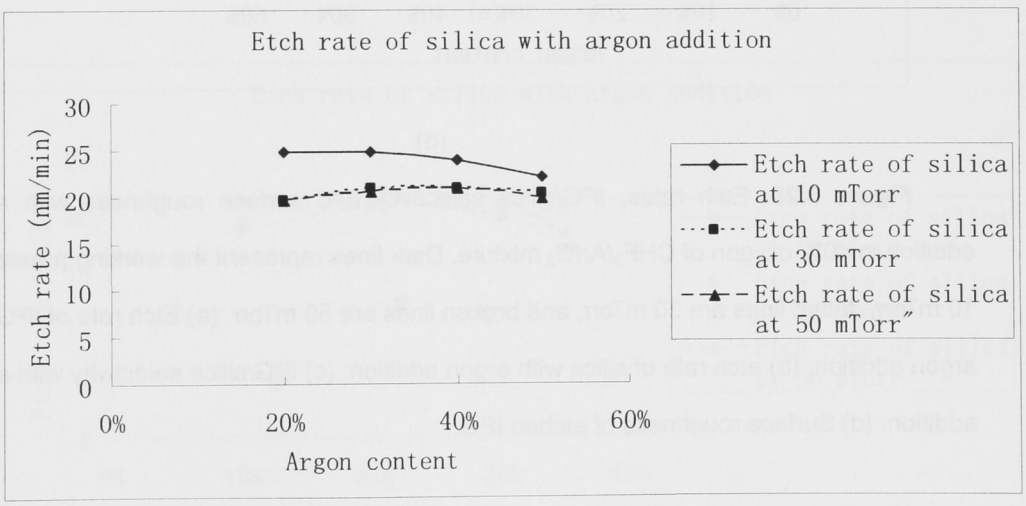

(b)

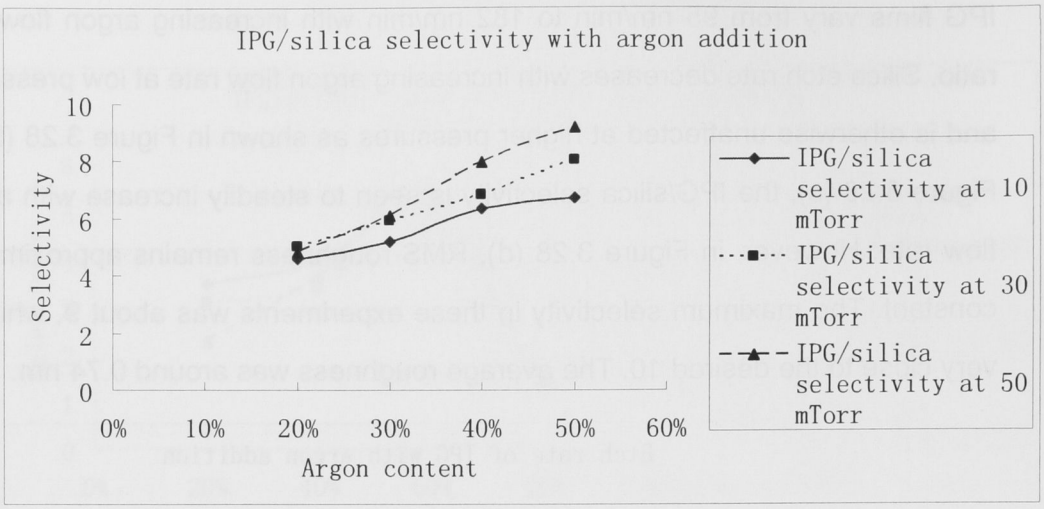

(c)

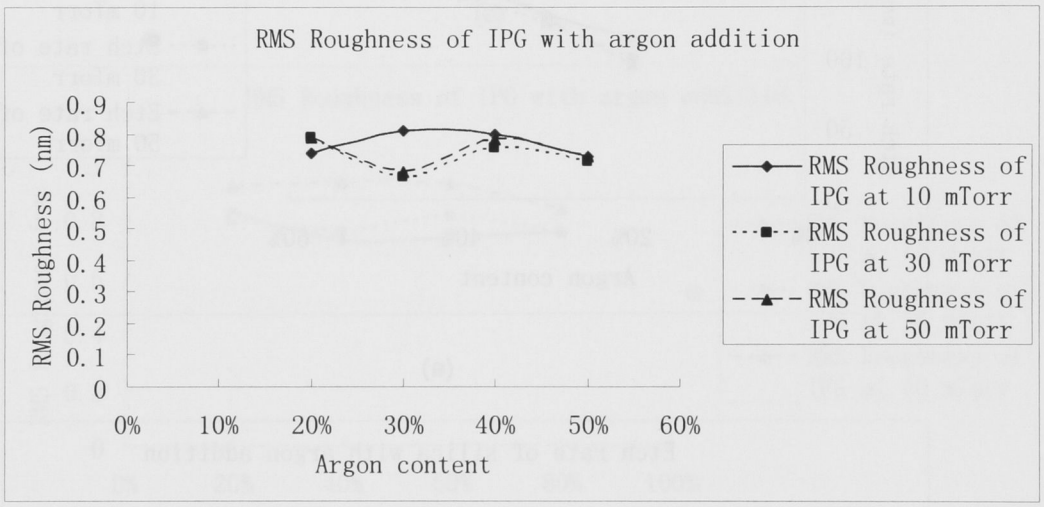

(d)

Figure 3.28. Etch rates, IPG/silica selectivity and surface roughness with argon addition in 40% oxygen of $CHF_3/Ar/O_2$ mixture. Dark lines represent the working pressure is 10 mTorr, dotted lines are 30 mTorr, and broken lines are 50 mTorr. (a) Etch rate of IPG with argon addition; (b) etch rate of silica with argon addition; (c) IPG/silica selectivity with argon addition. (d) Surface roughness of etched IPG.

Finally, the oxygen content in the gas mixture was increased to 60%. The percentages of argon are varied from 10% to 35%. Fig 3.29 (a) describes the etching characteristics of the core material with various argon contents. The

results show the etch rate peaks in the vicinity of 20-30% Argon depending on pressure. Figure 3.29 (b) shows the etch rate of silicon dioxide varies slightly between 16 and 21 nm/min with Argon concentration. Because the silica etch rates can not be reduced, further enhancement of selectivity becomes difficult. As shown in Figure 3.29 (c), the selectivity varies from 6 to 10. However the 30% argon, 60% oxygen, and 10% CHF_3 at 50 mTorr recipe which gives the best selectivity also produces the highest surface roughness (RMS Roughness is 0.98 nm vs 0.75nm average otherwise) as shown in Figure 3.29 (d).

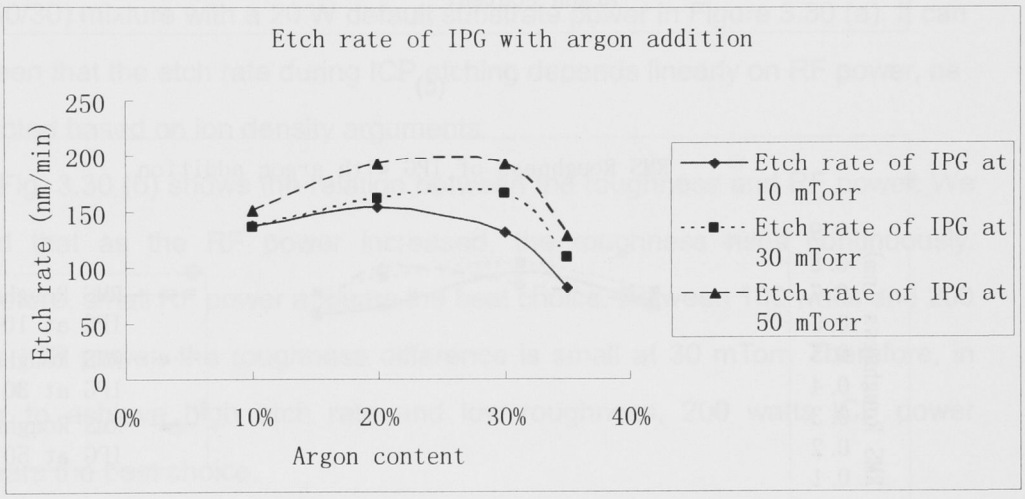

(a)

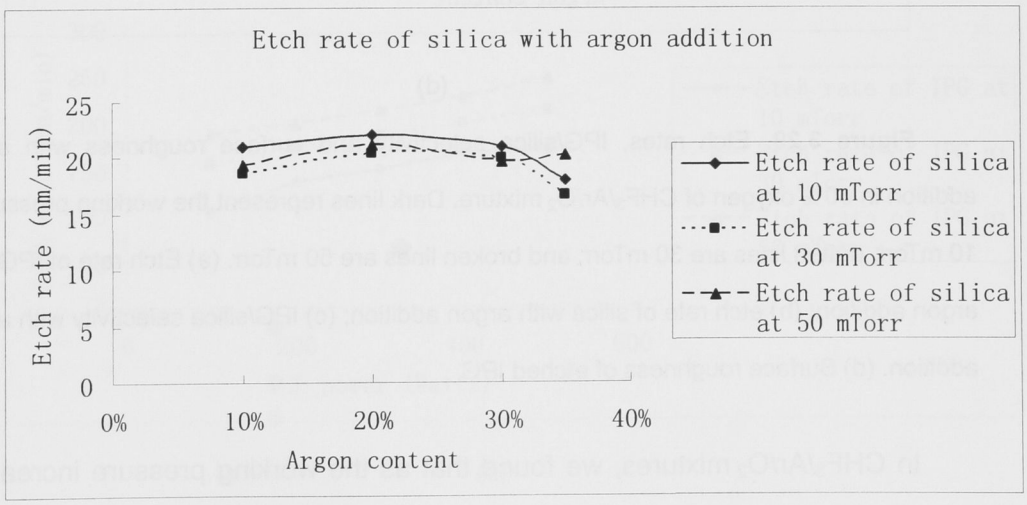

(b)

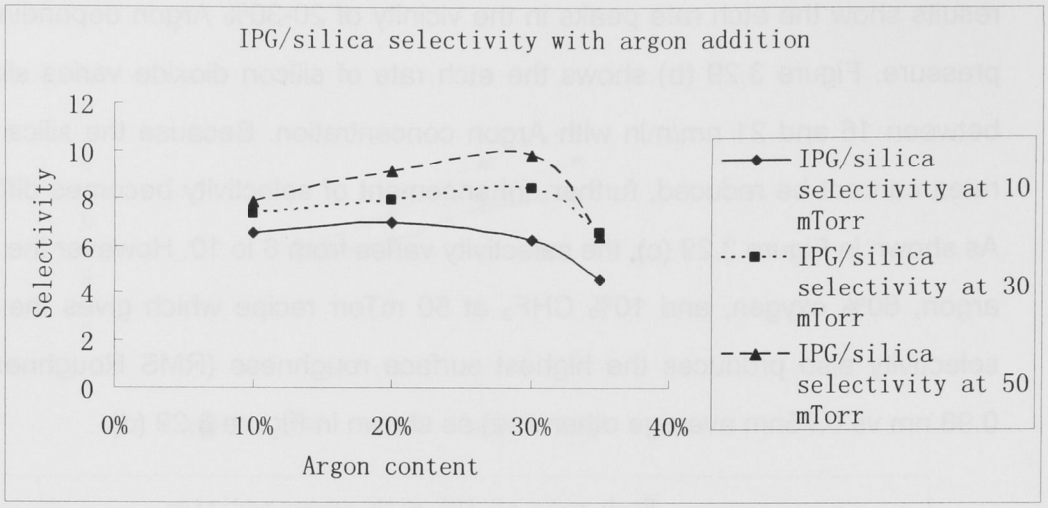

(c)

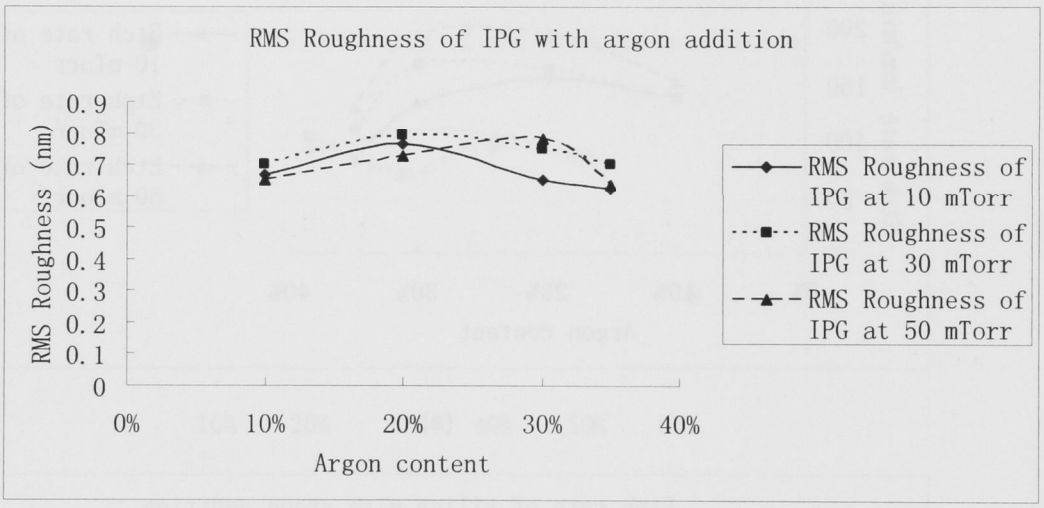

(d)

Figure 3.29. Etch rates, IPG/silica selectivity and surface roughness with argon addition in 60% oxygen of $CHF_3/Ar/O_2$ mixture. Dark lines represent the working pressure is 10 mTorr, dotted lines are 30 mTorr, and broken lines are 50 mTorr. (a) Etch rate of IPG with argon addition; (b) etch rate of silica with argon addition; (c) IPG/silica selectivity with argon addition. (d) Surface roughness of etched IPG.

In $CHF_3/Ar/O_2$ mixtures, we found that as the working pressure increases, the roughness decreases. However, the selectivity of IPG to silica is optimized at low pressure. Therefore, in order to achieve high selectivity and low roughness,

a balance working condition is required. Even within this range, the best attainable selectivity was around 10 which is marginal for the desired 3 micron high structures.

E) RF power and substrate power

In addition, the etch rate and surface roughness in inductively coupled plasma were investigated as a function of the radio frequency power.

For IPG etching, etch rate is plotted against RF power by using CHF_3/O_2/Ar (10/60/30) mixture with a 20 W default substrate power in Figure 3.30 (a). It can be seen that the etch rate during ICP etching depends linearly on RF power, as expected based on ion density arguments.

Fig. 3.30 (b) shows the relation between the roughness and RF power. We found that as the RF power increased, the roughness rises continuously. Therefore, small RF power appears the best choice. Between 100 watts and 200 watts ICP power, the roughness difference is small at 30 mTorr. Therefore, in order to achieve high etch rate and low roughness, 200 watts ICP power appears the best choice.

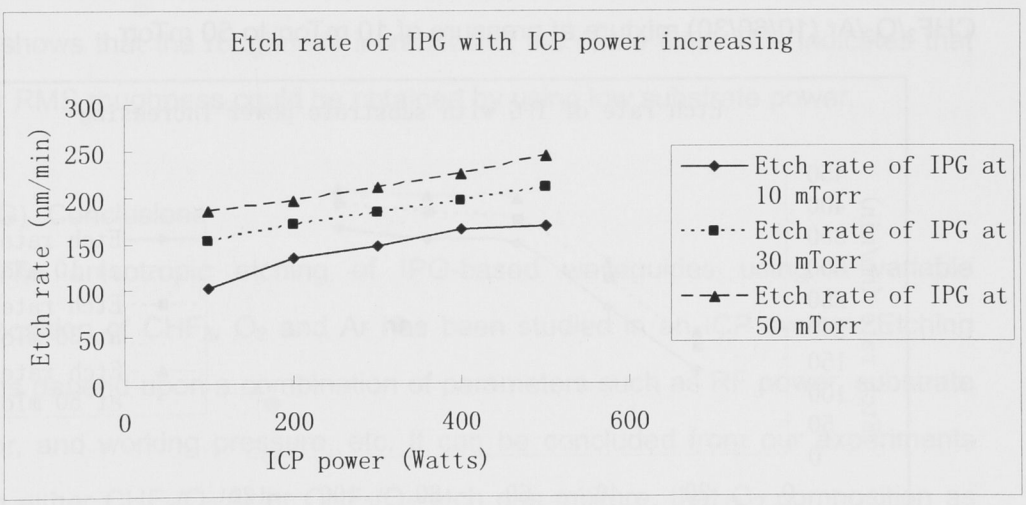

(a)

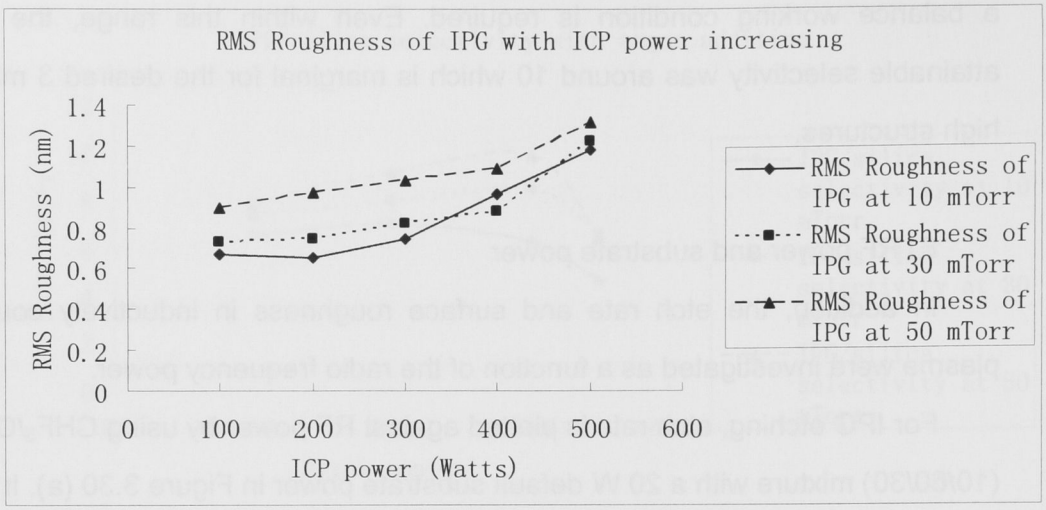

(b)

Figure 3.30. Etch rate and roughness of IPG with ICP power increasing in $CHF_3/O_2/Ar$ (10/60/30) mixture. Dark lines represent the working pressure is 10 mTorr, dotted lines are 30 mTorr, and broken lines are 50 mTorr. (a) Etch rate of IPG with ICP power increasing; (b) Surface roughness of etched IPG with ICP power increasing.

The etch rate and RMS roughness of IPG film are shown in Fig 3.31 as a function of the substrate power with applied ICP power of 200 W by using $CHF_3/O_2/Ar$ (10/60/30) mixture at pressure of 10 mTorr to 50 mTorr.

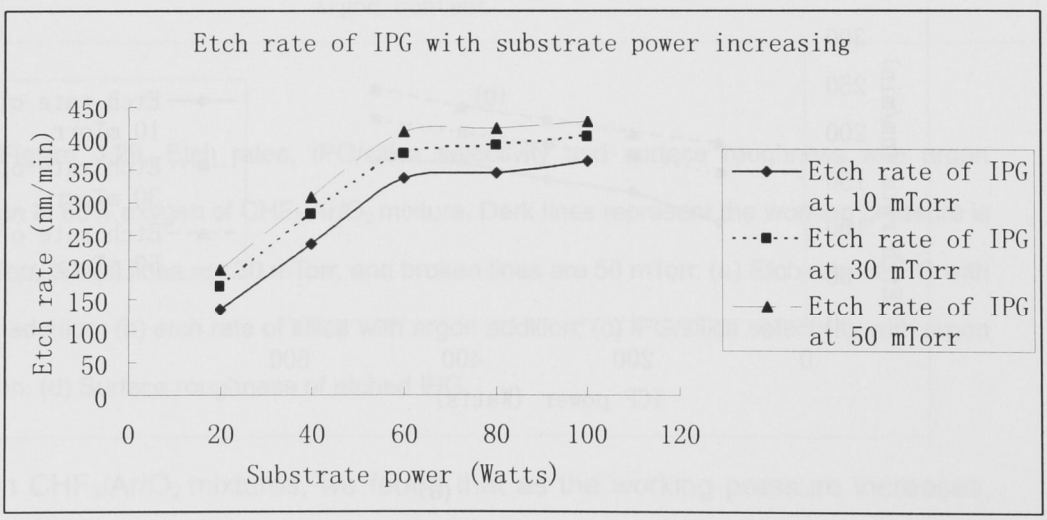

(a)

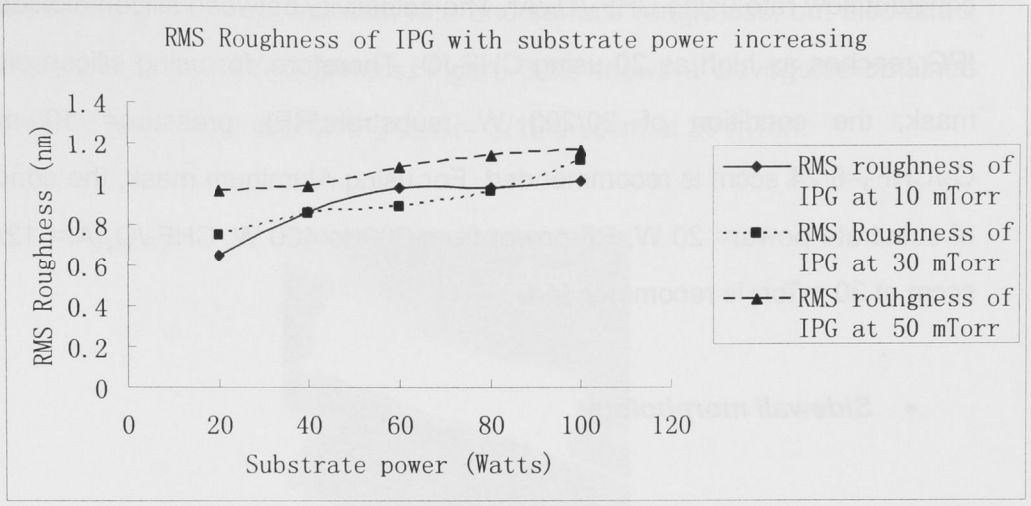

(b)

Figure 3.31. Etch rate and roughness of IPG with substrate power increasing in $CHF_3/O_2/Ar$ (10/60/30) mixture. Dark lines represent the working pressure is 10 mTorr, dotted lines are 30 mTorr, and broken lines are 50 mTorr. (a) Etch rate of IPG with substrate power increasing; (b) Surface roughness of etched IPG with substrate power increasing.

The substrate powers were varied up to 100 W. The Figure above shows that the IPG etch rate increased dramatically with increasing substrate power. It also shows that the roughness increases at the same time. This indicates that lower RMS roughness could be obtained by using low substrate power.

G) Conclusions

The anisotropic etching of IPG-based waveguides using a variable composition of CHF_3, O_2 and Ar has been studied in an ICP system. Etching results depend upon a combination of parameters such as RF power, substrate power, and working pressure, etc. It can be concluded from our experiments using either $CHF_3/O_2/Ar$ or CHF_3/O_2 etch gas mixture, that O_2 composition as well as working pressure and power principally affect the profile (surface roughness), etch rate, and selectivity between silicon dioxide and IPG. The etch rate and surface roughness also increase with RF power and substrate power at

constant flow rate using $CHF_3/O_2/Ar$. The selectivity between silicon dioxide and IPG reaches as high as 20 using CHF_3/O_2. Therefore, for using silicon dioxide mask, the condition of 20/200 W (substrate/RF), pressure= 10 mTorr, O_2/CHF_3=6/24 sccm is recommended. For using Aluminum mask, the condition of substrate power= 20 W, RF power from 200 to 400 W, $CHF_3/O_2/Ar$= 12/6/12 sccm at 30 mTorr is recommended.

- ***Sidewall morphology***

Sidewall roughness is a critical issue for optical devices, especially for planar waveguides. The sidewall roughness has a strong effect on waveguide loss. The theoretical attenuation coefficient of waveguides due to waveguide wall roughness can be expressed by.

$$\alpha = \frac{4\sigma^2 h^2}{\beta(t+2/p)} = \frac{\sigma^2 k_0{}^2 h}{\beta} \cdot \frac{E_s{}^2}{\int E^2 dx} \cdot \Delta n^2 \qquad [13]$$

Where σ is the interface roughness, t is the waveguide thickness, K_0 is the free-space wave vector, and β is modal propagation constant, while h and p are the transverse propagation constant in the core and cladding, respectively. It is seen that loss is proportional to $E_s/\int E^2 dx$ – the normalized electric field intensity at the core/cladding interface; to the square of the surface roughness; and to the square of the refractive index difference. For well-designed and well-etched IPG waveguides, improvement of sidewall roughness will help to reduce waveguide loss. [13] The sidewall roughness of the IPG waveguides mainly comes from mask roughness and the lateral etching effect of the plasma in ICP as well as from the edge roughness of the Aluminum and silicon dioxide patterns.

Etching results using Aluminum mask

It was observed that the working voltage and proportion of CHF_3, Ar and

Oxygen not only impacted the etch rate and surface roughness, but also affect the waveguide side wall roughness. Figure 3.32 shows a waveguide obtained using 200 W ICP power with $CHF_3/O_2/Ar$= 3/18/9 sccm at 30 mTorr.

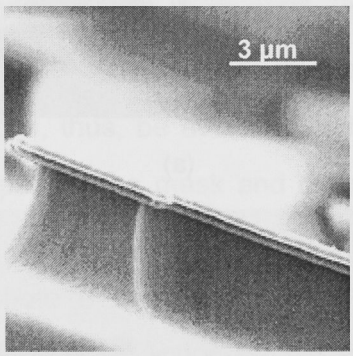

Figure 3.32. Waveguide with 2.5 wide and 3 µm high etched in ICP with 200 W, pressure= 30 mTorr, $Ar/O_2/CHF_3$=9/18/3 sccm using Aluminum mask.

The results of 400 W ICP power with $CHF_3/O_2/Ar$= 12/6/12 sccm at 30 mTorr are shown in Figure 3.33 (a). And Figure 3.33 (b) shows the sidewall morphology obtained by 400 W ICP power with $CHF_3/O_2/Ar$= 3/18/9 sccm at 30 mTorr.

The profile of waveguide made by lower ICP power in Figure 3.32 is not perfectly vertical, but its sidewall roughness is clearly better than the results obtained at higher ICP power. Furthermore, the oxygen rich gas mixture has lower sidewall roughness. The sidewall difference between 3.33 (a) and (b) is significant, higher oxygen concentration evidently benefits sidewall roughness. Therefore, the optimized ICP etching conditions for IPG waveguides using Aluminum mask are ICP power= 200 W, $CHF_3/O_2/Ar$= 3/18/9 sccm, working pressure=30 mTorr .

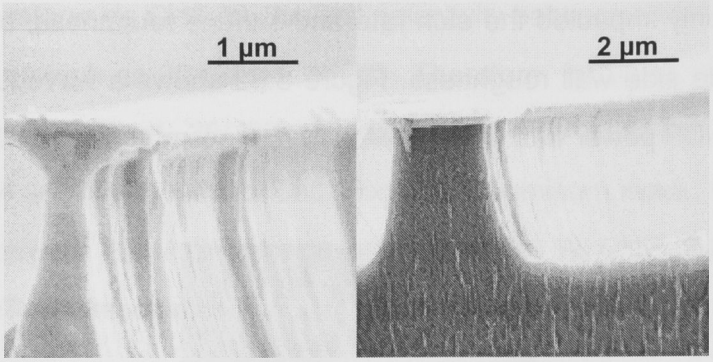

(a)

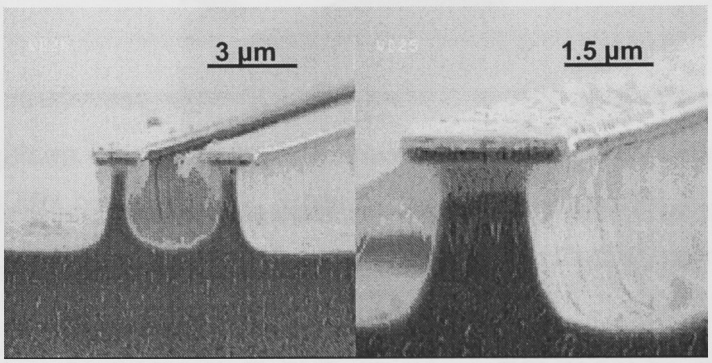

(b)

Figure 3.33. (a) Waveguide with 1 μm (left), 2 μm (rihgt) wide and 3 μm high etched in ICP with 400 W, pressure= 30 mTorr, $Ar/O_2/CHF_3$=12/6/12 sccm using Aluminum mask; (b) Waveguide with 1 μm (left), 2 μm (rihgt) wide and 3 μm high etched in ICP with 400 W, pressure= 30 mTorr, $Ar/O_2/CHF_3$=9/18/3 sccm using Aluminum mask.

Etching results using Silicon dioxide mask

Figure 3.34 shows the waveguide profile etched by using a silicon dioxide mask. Although the waveguides etched using the Al mask with the ICP system achieved quite low sidewall roughness, there were some inherent defects when using Aluminum metal masks caused by issues such as adhesion to photo resist, the forced use of wet etching for the Aluminum mask due to machine failure, etc. Moreover, the roughness of the Aluminum mask was then transferred to the waveguides during dry etching. Whilst these are not fundamental limitations,

getting around them in the available timeframe was not possible. It would also be very difficult in practice to pattern Al masks using the available equipment to a line width below about 2 μm whilst maintaining smooth line edges and good dimensional control.

These problems can be solved by replacing the Aluminum with silicon dioxide as the etch mask. Extra processes in the deposition, etching and stripping of the Al mask can, thus, be avoided. Additionally this also required only an Ar/CHF_3 etch to pattern the mask and did not require the inoperable etcher.

In the experiments, photo resist/silicon dioxide/IPG films were employed as etching structure. As discussed earlier, the silicon dioxide/IPG selectivity could be as high as 20 so that a 150-200 nm silicon dioxide was deposited using PECVD. PECVD was used for the final devices as although the RF sputtering system produced superior films, it was inoperable at the time of fabrication f the waveguides due to target exhaustion. In order to avoid over etching the mask, 200 nm thickness of silicon dioxide was selected. The conditions of photo resist spin-coating and exposure processes are as per section 3.6.2. The etching parameters of silicon dioxide are as described in section 3.6.3.

The etch results using a silicon dioxide mask are shown in Figure 3.34. The sidewall smoothness of the waveguide was significantly greater compared to the previous waveguides. The profile of waveguides also became more vertical compared to Figure 3.33.

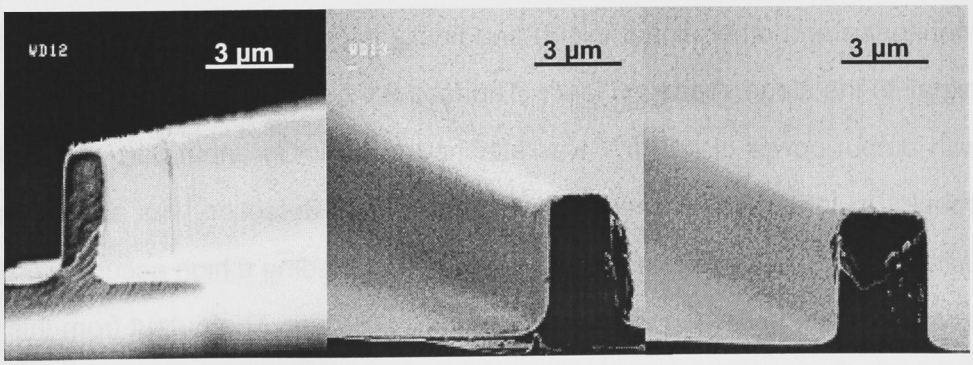

Figure 3.34. Waveguide etched in ICP with 200 W, pressure= 10 mTorr,

O_2/CHF_3=6/24 sccm using silica mask. (a) From left to right, they are 1 μm, 2μm and 3 μm width with 3 μm height waveguides respectively.

3.7 Measurements of Optical Transmission Loss

Measurement set-up

The alignment set-up comprises X-Y-Z left and right stage stacks, mounted on a vibration isolated workstation. On left and right stacks, optical fibers are mounted (Nufern UHNA-3), used for the incoupling and outcoupling. The sample is mounted on a vacuum chuck on top of a central stage which allows the sample to be horizontally translated between the fibers. Alignment in Z direction (along the waveguides) is done using a vision system, with a CCD camera. The CCD camera can move on a long linear bearing between incoupling and outcoupling to allow alignment in the Z direction. Both the waveguides and the coupling fibres are aligned to be parallel to the camera linear bearing axis. Once the incoupling and outcoupling are roughly aligned, the measured optical power can be optimized. A laser diode light source from JDS/FITEL SWS 15101 is employed for measurements at 1550 nm. Measurements are performed using an operating current of 107.5 mA and output power of 5 mW at 1550 nm. The laser feeds into an Agilent 8169 polarisation controller which has a scanning functionality to measure PDL, and then into a 50:50 fibre coupler (allows power monitoring and other signal inject) and finally into an optical isolator before the pigtail to the stage. A second laser (Thorlabs S1-FC-1310) operating at 1310 nm with output power of 1.2 mW was attached to the other input port of the 50:50 coupler to take measurements at 1310nm. Signal detection was accomplished using a 150μm SC-receptacled InGaAs detector feeding a high accuracy (<0.5% error) six decade Analog Devices logarithmic amplifier. The output from this was digitized with a 16 bit Analogue to Digital convertor card to make measurements.

To index match the waveguides, drops of core IPG material without photoinitiatior were used in the fiber ends to suppress reflections and facet imperfections.

A mask layout of the waveguides showing the waveguide path is shown in Figure 3.35.

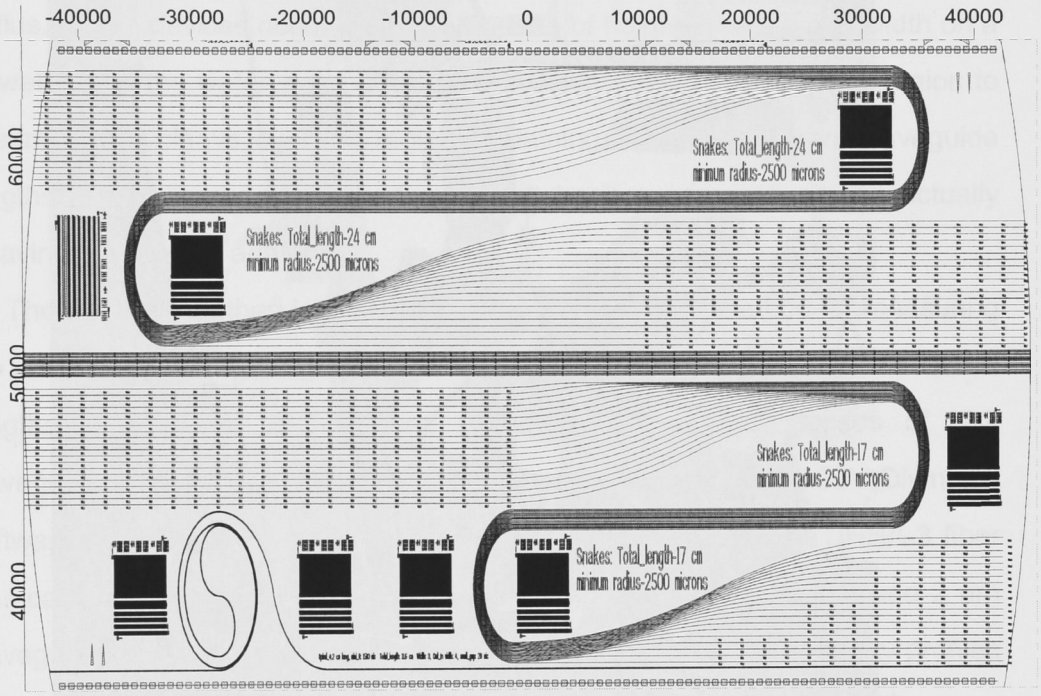

Figure 3.35. Mask layout diagram.

An image of optical loss measurement set-up is shown in Figure 3.36.

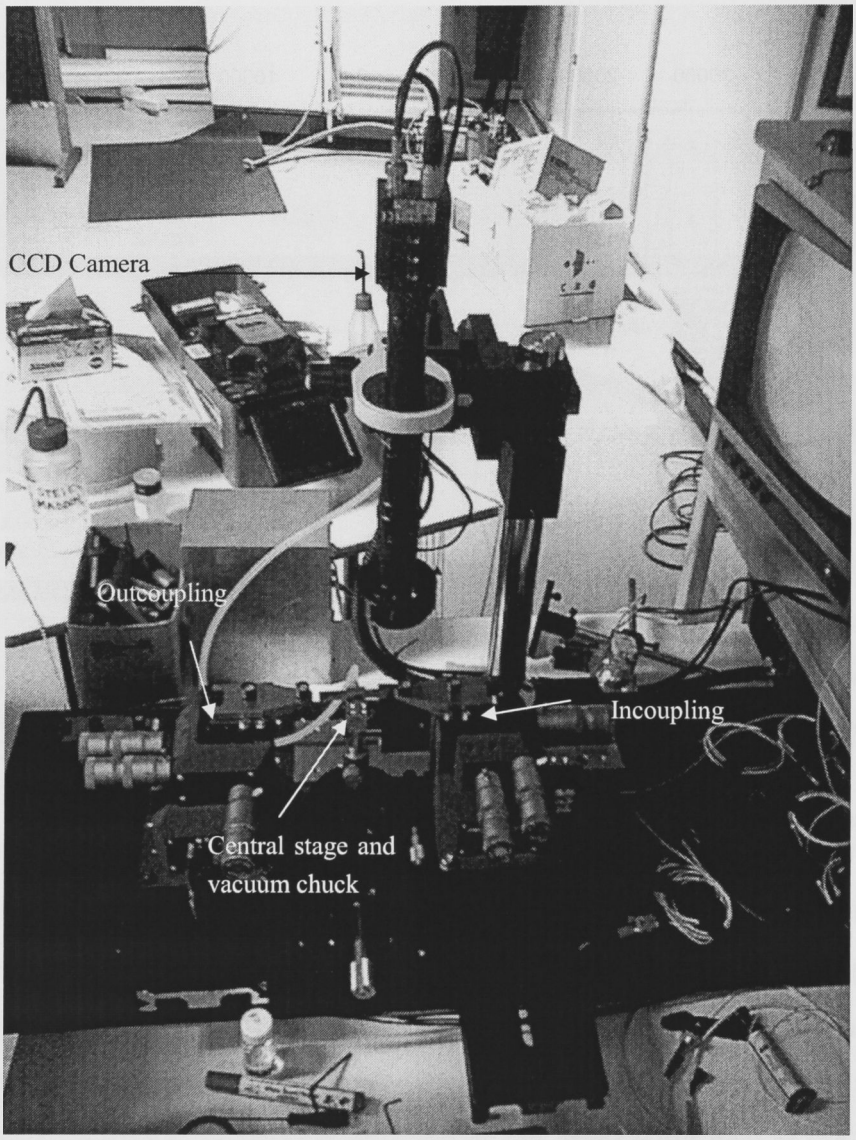

Figure 3.36. Optical loss measurement set-up.

Waveguide Propagation Loss

A sample was prepared using the final processes described above. The mask used had waveguides ranging in width from 1 to 4 microns, and lengths from 8 to 22.5 cm via a folded geometry with two 180 degree bends of 2.5 mm radius. These devices occupy the central 3cm of height and ~8cm of width on a 4" wafer, and the wafer was hand cleaved from ~2 cm back from this region to ensure a nice cleave over the region containing the three different waveguide lengths. This allowed us to perform a cut back experiment without actually cleaving the sample again.

The cut-back method is a simple, reliable and efficient method for measuring the optical loss of a waveguide. The waveguides on the sample had measured lengths of 22.5-cm, 16.5-cm and 8-cm. The propagation losses of IPG waveguides were characterized at 1550 nm and 1310 nm. Using C2V Olympios software, the mode mismatch loss between the waveguides and UHNA-3 fiber was calculated at 0.215 dB, 0.268 dB and 0.75 dB for 4 μm, 3 μm and 2 μm waveguides respectively at 1550 nm. The figures below show intensity profiles calculated using the Olympios software for the 4 μm and 3 μm waveguides.

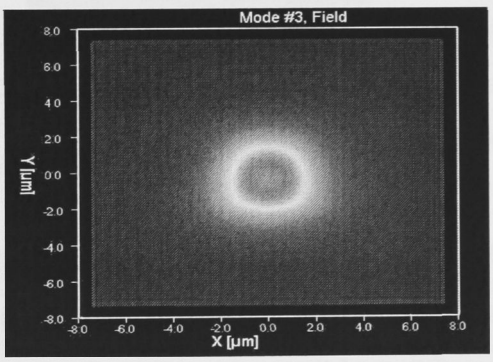

(a)

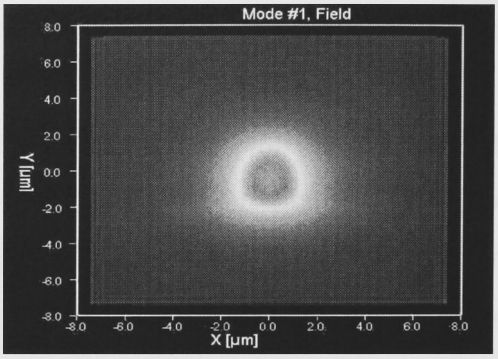

(b)

Figure 3.37. Fundamental mode field for full width of 4 µm (a) and 3 µm (b) dimensions.

Figure 3.38 shows a contrast enhanced optical microscope image of the finished waveguide for which the modeling was performed. It is clear from this image that the core was a little thicker than intended and did not get etched all the way through.

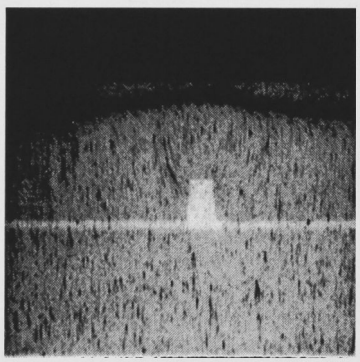

Figure 3.38. Cross-section of a 1 µm wide IPG waveguide using silicon dioxide mask from optical microscope.

The measured propagation losses of the different lengths are plotted against their lengths in Figure 3.39. The zero length point is the computed modal mismatch loss. Linear fitting of these data gave the smallest loss of 0.73 and 0.78 dB/cm at 1550 nm for the 4 µm and 3 µm wide waveguides. The 2 and 1 micron widths suffered significant bend loss, exhibiting insertion losses that were essentially identical to the wider waveguides for the straight waveguides, and

10dB more insertion loss for the 17 and 23cm bent waveguides. Ref [24] showed that a 3x3 μm waveguide of the same index contrast as those in the present work has a bend induced loss of 0.1dB for a 90 degree bend of radius 1.1mm, confirming that the 4 and 3 μm widths are not affected by the 2.5 mm radius bends used in the mask design. At 1300nm, the loss decreased to 0.40 dB/cm for the 4 μm wide waveguide in line with the lower material absorption loss.

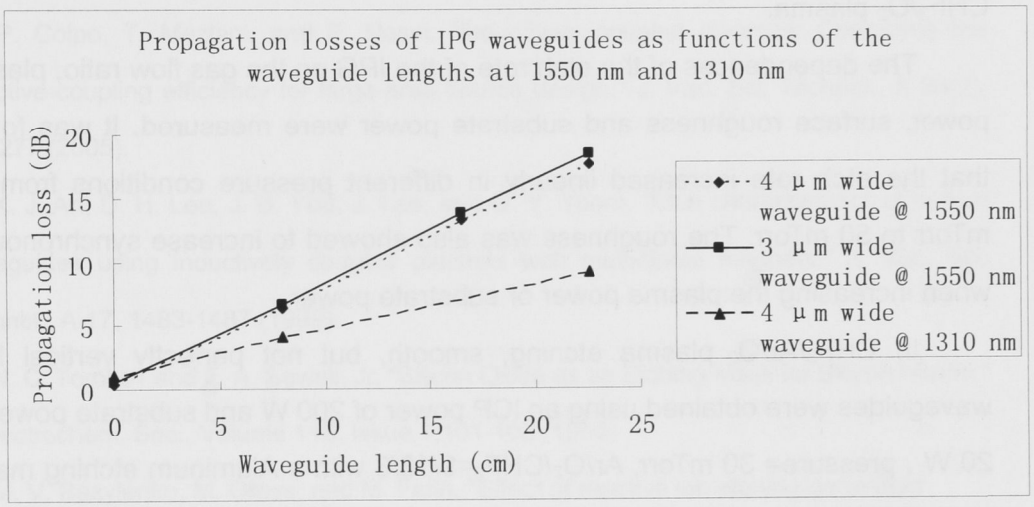

Figure 3.39. The total propagation insertion losses of IPG waveguides as functions of the waveguide lengths at 1550 nm and 1310 nm. Waveguide dimension: waveguide width = 3, 4 μm, height = 3 μm.

These figures compare favorably with the fundamental absorption loss for the material of 0.5 dB/cm at 1550nm, and 0.25 dB/cm at 1310nm.

3.8 Conclusions

Dry etching of IPG films for waveguide fabrication has been systemically studied. CF_4/O_2 mixture evidently shows the worst sidewall profiles and lower selectivity than CHF_3/O_2 and $CHF_3/Ar/O_2$ mixture, as CF_4 has much stronger chemical etching of IPG.

Through experiments, $CHF_3/Ar/O_2$ is believed as the best option for using

Aluminum as etching mask. Argon and O_2 gases were compared as the additives to dilution of the CHF_3 processing. The O_2 showed a better dilution effect than the Argon in reducing the roughness of IPG.

CHF_3/O_2 plasma generated a much lower erosion rate to the silicon dioxide mask than $CHF_3/Ar/O_2$ plasma with the same RF powers. A very high IPG/Silicon dioxide etching selectivity of almost 20 was obtained using the CHF_3/O_2 plasma.

The dependences of the etch rate of the IPG on the gas flow ratio, plasma power, surface roughness and substrate power were measured. It was found that the etch rate increased linearly in different pressure conditions from 10 mTorr to 50 mTorr. The roughness was also showed to increase synchronously when increasing the plasma power or substrate power.

In $CHF_3/Ar/O_2$ plasma etching, smooth, but not perfectly vertical IPG waveguides were obtained using an ICP power of 200 W and substrate power of 20 W , pressure= 30 mTorr, $Ar/O_2/CHF_3$=9/18/3 with a Aluminum etching mask. In CHF_3/O_2 plasma etching, the vertical and smooth IPG waveguides sidewalls were achieved using an ICP power of 200 W and substrate power of 20 W, pressure= 10 mTorr, O_2/CHF_3=6/24 sccm with silicon dioxide etching mask. The Aluminum mask results in rougher sidewall and complex processes for IPG waveguide fabrication. Comparatively, as silicon dioxide mask achieves quite satisfied etch results and relative simple processes, it could be the best method for IPG waveguide fabrication mainly due to mask fabrication limitations imposed by equipment failure. The use of silicon dioxide as an etch mask for shallow etches was successfully demonstrated and gave quite nice results.

The waveguide loss was characterized using the cut-back method which provides reasonably accurate loss values. The lowest loss obtained for IPG waveguides with 4 μm width and 3 μm widths and etched by ICP was 0.73 dB/cm at 1550 nm, and 0.40 dB/cm at 1310 nm, only a little above the intrinsic materials losses at these wavelengths. Therefore high quality waveguide fabrication has been demonstrated.

Reference

[1]. Wei-Chih Wang, Joe N. Ho, and Per G. Reinhall, "Deep reactive ion etching of silicon using an aluminum etching mask," Optics and Photonics Technologies and Applications, 633-640 (2003).

[2]. P. Colpo, T. Meziani, and F. Rossi, "Inductively coupled plasmas: Optimizing the inductive-coupling efficiency for large-area source design," J. Vac. Sci. Technol., A 23(2), 270-277 (2005).

[3]. K. J. An, D. H. Lee, J. B. Yoo, J. Lee, and G. Y. Yeom, "Etch characteristics of optical waveguides using inductively coupled plasmas with multidipole magnets," J. Vac. Sci. Technol., A 17, 1483-1487 (1999).

[4]. N. C. Tombs1 and F. A. Sewell, Jr. "Silicon Oxide as an Etching Mask for Silicon Nitride," J. Electrochem. Soc., Volume 115, Issue 1,101-102 (1968)

[5]. M. V. Bazylenko, M. Gross, and M. Faith, "Effect of reactive ion etching-generated sidewall roughness on propagation loss of buried-channel silica waveguides," Appl. Phys. Lett. 69 (15), 2178-2180 (1996).

[6]. http://www.webelements.com/

[7]. G. Giroult-Matlakowski, C. Charles, A. Durandet, "Deposition of silicon dioxide films using the helicon diffusion reactor for integrated optics applications," J. Vac. Sci. Technol A 12(5), Sep/Oct, 2754-2761 (1994).

[8]. (a) M. V. Bazylenko, and M. Gross, J. Vac. Sci. Technol. A 14, 2994 (1996). (b) B. Kim, K. H. Pkwon, and S. H. Park, J. Vac. Sci. Technol. A 17, 2593 (1999).

[9]. S. Bretoiu, D. Di Mola, E. Fioravanti, and S. Visona, "Inductively coupled plasma etching for arrayed waveguide gratings fabrication in silica on silicon technology," J.Vac. Sci. Technol., B 20(5), 2085-2090 (2002).

[10]. A. J. Perry, D. Vender, and R. W. Boswell, "The application of the helicon source to plasma processing," J. Vac. Sci. Technol., B 9(2, Pt. 1), 310-317 (1991).

[11]. S. Bretoiu, D. Di Mola, E. Fioravanti, and S. Visona, "Inductively coupled plasma

etching for arrayed waveguide gratings fabrication in silica on silicon technology," J. Vac. Sci. Technol., B 20(5), 2085-2090 (2002).

[12]. S.-T. Jung, H.-S. Song, D.-S. Kim, and H.-S. Kim, "Inductively coupled plasma etching of SiO2 layers for planar lightwave circuits," Thin Solid Films 341(1,2), 188-191 (1999).

[13]. Y. A. Vlasov and S. J. McNab, "Losses in single-mode silicon-on-insulator strip waveguides and bends," Opt. Express 12(8), 1622-1631 (2004).

[14]. Flamm D L, Donnelly V M and Ibbotson D E 1983 J. Vac. Sci. Technol. B 1 23

[15]. Kirmse K, Wendt A, Disch S, Wu J, Abraham I, Meyer J, Breun R andWoods R C, J. Vac. Sci. Technol. B 14 710 (1996).

[16]. A. J. Perry, D. Vender, and R. W. Boswell, "The application of the helicon source to plasma processing," J. Vac. Sci. Technol., B 9(2, Pt. 1), 310-317 (1991).

[17]. Flamm D L and Donnelly V M, Plasma Chem. Plasma Proc. 1 317 (1981).

[18]. Coburn J W, J. Appl. Phys. 50 5210 (1979).

[19]. Maruyama K, Sakai A and Goto T, J. Phys. D: Appl. Phys. 26 199 (1993).

[20]. Namura T, Okada H, Naitoh Y, Todokoro Y and Inoue M, Japan. J. Appl. Phys. 29 2251 (1990).

[21]. Manos D M and Flamm D L, Plasma Etching: An Introduction (New York: Academic) chq 2 (1989).

[22]. K. Han, J. Kim, and W. H. Jang, "Evaluation of halogenated polyimide etching for optical waveguide fabrication by using inductively coupled plasma," J. Appl. Polym. Sci. 79, 176-182 (2001).

[23]. A. J. Perry, D. Vender, and R. W. Boswell, "The application of the helicon source to plasma processing," J. Vac. Sci. Technol., B 9(2, Pt. 1), 310-317 (1991).

[24]. R. A. Bellman, G. Bourdon, G. Alibert, A. Beguin, E. Guiot, L. B. Simpson, P. Lehuede, L. Guiziou, and E. LeGuen, "Ultraslow Loss High Delta Silica Germania Planar Waveguides", J. of Electrochemical Society, 151 (8) G541-G547 (2004).

Chapter 4

Novel Waveguide Fabrication: Soft Lithography

Micro fabrication using non-photolithographic imprinting/molding techniques (soft lithography) has been pioneered by Whitesides et al and recently used to fabricate waveguides. [1] In this thesis, the preparation and application of Poly-dimethyl-siloxane (PDMS) stamps from an etched patterned silicon dioxide master wafer are presented. Low cost fabrication of IPG waveguides is demonstrated.

4.1 Introduction to Soft lithography

Soft lithography is a useful technology for patterning materials such as polymer, potentially including IPGs, down to resolutions of 10 nm! Soft lithography is a combination of technologies based around micro fabrication using molds. It is regarded as a complementary method to optical/e-beam/x-ray lithography and has several advantages:

1. It can generate three dimensional structures in a single process step.
2. It is able to pattern a very large area.
3. It can pattern non-planar surfaces.
4. Low cost.
5. Capable of resolution down to about 10 nm and perhaps below.
6. Not limited by the wavelength of exposure light, etc.
7. Simple fast two step process, coat then imprint

The main disadvantages of soft lithography are:

1. Defect levels potentially higher than for conventional lithography due to contact and release processes
2. Possible for mold to be distorted due to shrinking and swelling of the elastomer

3. Mold lifetime not well understood
4. Not as fast as stepper based optical systems
5. Potential for residual resist layer on surface

So far, there are several different approaches to soft lithography:

- Micro contact printing.
- Replica molding.
- Embossing.

Micro contact printing is a general and efficient method for forming patterns on surfaces on solid substrates through contact pattern transfer. The main advantage of Micro contact printing is that, once the stamp is available, multiple copies of the pattern can be produced using straightforward techniques. [2]

Replica molding is a method of duplicating the shape, the morphology, and the structure from a master. A representative method of replica molding is MIMIC (Micro Molding in Capillaries). It is a non-lithography method that forms complex structures. It is remarkable for its simplicity and its fidelity in transferring the patterns from mold to the structures that it forms. [4, 5]

Embossing is another cost-effective, high-throughput manufacturing technique that imprints microstructures in thermoplastic materials. Previous works proved that embossing could be used to make features as small as 25 nm in silicon. [9, 10]

In all these techniques, an elastomeric stamp is the primary mold used to transfer the pattern into a suitable resist on substrate via a contact based process. Each of the methods identified above uses flexible organic molecules and materials rather than rigid inorganic materials now commonly used in the fabrication of microelectronic systems (Table 4.1) [7]:

Method	Resolution	Reference
Injection molding	10 nm	[7] [8]
Embossing (imprinting)	25nm	[9] [10]
Cast molding	50 nm	[11] [12]
Laser ablation	70 nm	[13] [14]
Micromachining with a sharp stylus	100 nm	[15] [16]
Laser-induced deposition	1 μm	[17]
Electrochemical micromachining	1 μm	[18]
Silver halide photography	5 μm	[19]
Pad printing	20 μm	[20]
Screen printing	20 μm	[21]
Ink-jet printing	50 μm	[22]
Electro photography (xerography)	50 μm	[23]
Stereo lithography	100 μm	[24]
Soft lithography		[25]
(μCP) Micro contact printing	35 nm	[2]
(μTM) Micro Transfer Molding	30 nm	[3]
(MIMIC) Micro Molding in Capillaries	1 μm	[4]
(REM) Replica Molding	1 μm	[5]
(SAMIM) Solvent Assisted Micro Molding	60 nm	[6]

Table 4.1. Non-photolithography methods for micro- and nanofabrication. The lateral dimension of the smallest feature that has been generated. These numbers do not represent ultimate limits.

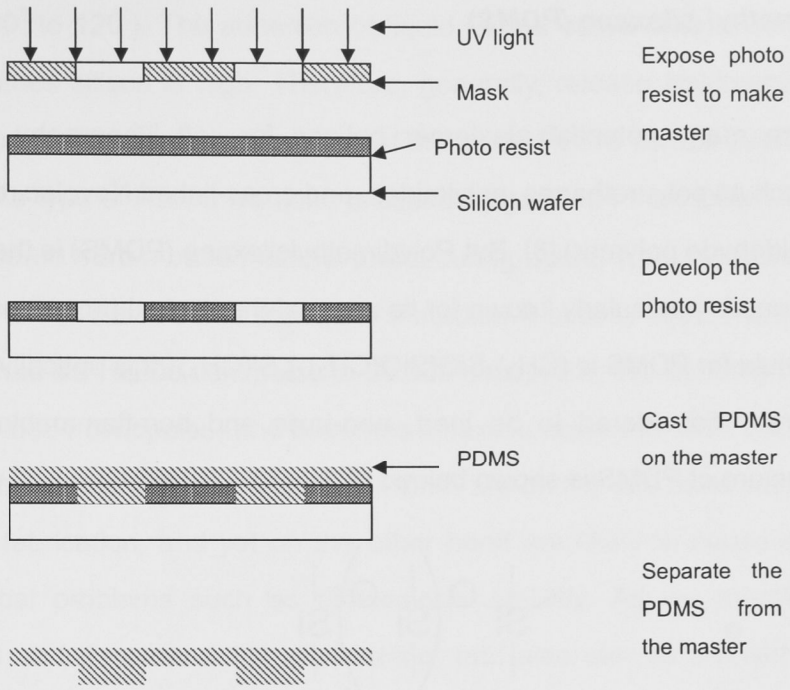

Figure 4.1. Procedure of making PDMS mold.

In soft lithography, generally, a standard lithography method and an etching process are first used to fabricate a patterned master. Then a negative image PDMS stamp is fabricated by pouring liquid PDMS over the master and curing it before the stamp is separated from this master. Figure 4.1 shows a typical procedure for making a PDMS stamp from a lithographically patterned photo resist master. Firstly, a layer of photo resist is spin-coated on a silicon wafer. Afterward, the photo resist is exposed with UV light to create the desired pattern. Secondly, the exposed photo resist is developed and baked. Before pouring the PDMS onto the master, release treatments are often undertaken to facilitate PDMS removal once cured. These treatments will be discussed in the following sections. Thirdly, the mixed PDMS (PDMS base and cure agent) is poured on the master. Then the liquid PDMS and master are baked in an oven for some time to crosslink the PDMS. Finally, the cured PDMS stamp is separated from the master.

Poly-dimethyl-siloxane (PDMS)

There are many potential elastomer options for soft lithography stamp fabrication such as polyurethanes, polyimides, and cross-linked Novolac resin (a phenol formaldehyde polymer) [8]. But Polydimethylsiloxane (PDMS) is the most widely used, and is particularly known for its unusual rheological properties. The chemical formula for PDMS is $(CH_3)_3SiO[SiO(CH_3)_2]_nSi(CH_3)_3$. It is optically clear, and is generally considered to be inert, non-toxic and non-flammable. The chemical structure of PDMS is shown below:

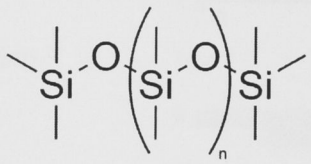

Figure 4.2. The chemical structure of PDMS

PDMS is a member of the group of viscoelastic materials (long flow times or high temperatures). It behaves to a degree over extended timeframes or at higher temperatures like a very viscous liquid. However at short flow times (or low temperatures) it acts like an elastic solid, similar to rubber. In other words, if you leave a PDMS plate on a surface overnight (long flow time), it will flow to cover the surface and mold to any surface imperfections. However if you roll the same PDMS into a sphere and throw it onto the same surface (short flow time), it will bounce like a rubber ball. The shear modulus of PDMS varies with preparation conditions, but is typically in the range of 100 kPa to 3 mPa. The loss tangent is very low ($\tan\delta << 0.001$).

The hardness of PDMS can be varied. Lowering the curing agent concentration by more than 10 percent will result in soft and weaker elastomer; increasing concentration by more than 10 percent will result in over-hardening of the cured elastomer.

Cured PDMS is regarded as a highly hydrophobic material (contact angle is

from 90° to 120°). The adhesion of liquid PDMS cured onto silicon dioxide and sometimes silicon is high. Therefore, generally, release treatments need to be used on the master to guarantee that the cured PDMS can be peeled off.

The type of PDMS we used is called Sylgard 184 from Dow Corning, which is prepared from a base material and a curing agent. It can be cured from 25 C° to 150 C°. In the uncured state, it is a medium-viscosity liquid (medium viscosity is defined as 10,000 centipoise to 30,000 centipoise; the viscosity of water at 25 C° is 0.8904 centipoise) and becomes a flexible elastomer after curing.

The inherent characteristics of PDMS are on the one hand very beneficial in micro fabrication, and yet on the other hand are likely to cause some serious technical problems such as dimensional stability. As we mentioned earlier, PDMS shrinks around 1% after curing, and also can be swelled by nonpolar solvents such as hexane. Although shrinkage can be minimized with optimized fabrication conditions, it still exists and should be taken into consideration. Therefore, in experiments discussed in this work, PDMS was cured at about 65 ºC for 4 hours to reduce the shrinkage as much as possible.

In order to understand the importance of PDMS in soft lithography, several properties of PDMS should be elucidated. Firstly, PDMS is quite a durable material; PDMS stamps have been used up to about 100 times over a period of several months without noticeable degradation in performance [27]. Secondly, the surface properties of PDMS can be easily modified by plasma processing to give appropriate interfacial interactions with materials that themselves have a wide range of interfacial free energies [28]. In its normal cured state, the surface will resist a wide range of curable materials adhering to it making an excellent stamp material. In fact even liquid PDMS cured onto an existing cured PDMS surface will not adhere! Thirdly, PDMS is deformable enough such that conformal contact can even be achieved on the surfaces that are nonplanar on the micrometer scale [29]. This characteristic permits PDMS to separate from complex structures easily. Liquid PDMS also has a relatively low viscosity meaning features fill easily, and cures in a few hours at temperatures that allow

photo resist to be used as the master. Finally, PDMS is homogeneous, isotropic, and optically transparent down to about 300 nm. It has been used to construct elastomeric optical devices for adaptive optics and to fabricate photo masks for use in UV photolithography and contact phase shift photolithography [30].

Waveguides and Photo Mask Design for Soft Lithography

One property of IPG that had to be addressed in the soft lithography waveguide fabrication process design is that it is very hard to spin IPG into thin (i.e. below about ~1 micron thick) layers. This means that it would be quite difficult to just mold a rib for the core without a substantial residual layer either side of the core. With this in mind we elected to develop an approach where we minimized the amount of fluid displaced during the imprint process.

The route to achieving this was to use a stamp where the waveguide core is defined by two protruding ribs on the stamp as shown below in Figure 4.3 (b).

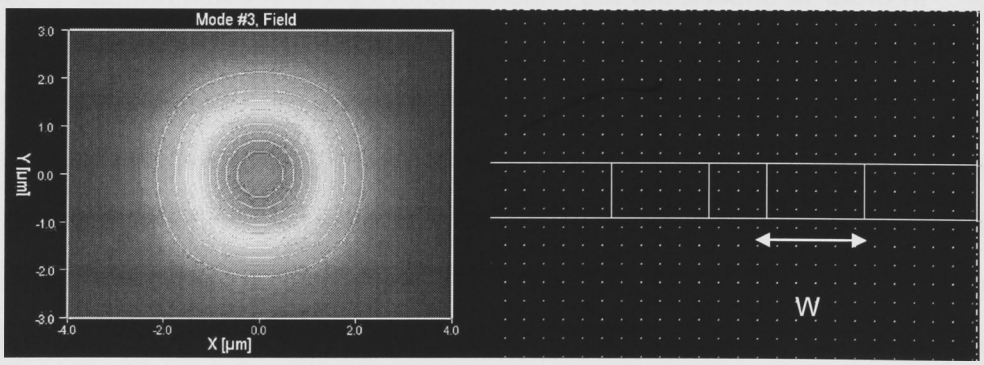

(a) (b)

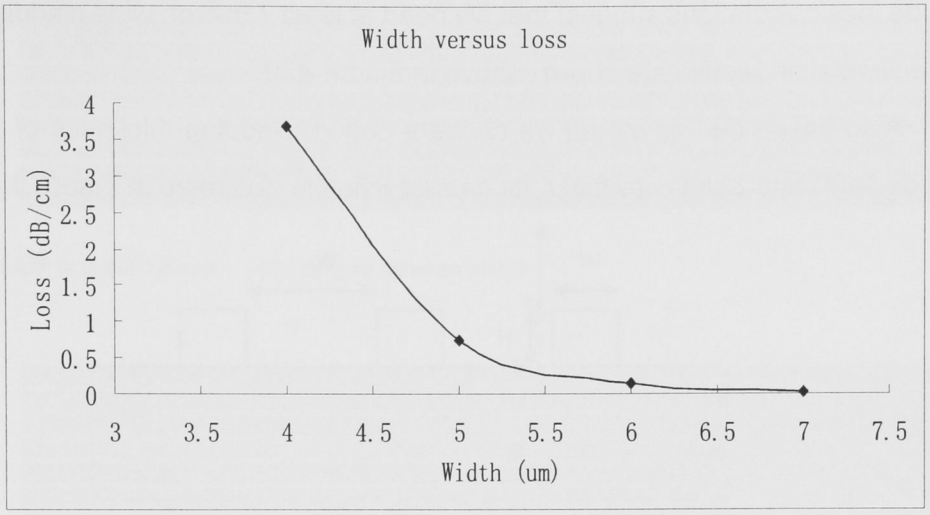

(c)

Figure 4.3 (a) The mode field distribution of TE in a 3-μm wide and 3-μm high IPG waveguide. IPGs waveguide modes (Quasi TE) (FWHM=2.44μm and FW1/e^2~3.8μm): Core 3x3 μm, n_{clad}=1.478, n_{core}=1.507, I (wavelength) =1550nm. (b) The waveguide structure. (c) Waveguide cladding ribs width versus optical radiation loss.

Using this method, only a relatively small amount of fluid is displaced at the imprint step meaning that the wet film can be the final required core height, and yet the core should be cleanly defined locally without a residual layer. So the question arises as to what width the core definition ribs need to be to avoid coupling to leaky cladding modes in the outlying slabs, and also what the optimum waveguide dimensions are. These questions were resolved using waveguide modeling with the full vector complex generic Finite-Difference method as embodied in the C2V Olympios software version 5.2. In our case the core cladding refractive index difference is fixed at 0.027 as noted earlier, so the design involves finding the optimum core dimensions for a single mode waveguide with low loss coupling to an available fiber design.

The modeling suggested that a 3x3 μm guide would be an almost perfect mode match (loss <0.1 dB) to Nufern UHNA-3 fiber (this can be spliced to SMF-28 with <<0.1dB loss with the right mode matching splicer). Radiation

mode loss calculations suggest that we need at least 7 micron wide cladding ribs. The simulation results are shown above in Figure 4.3.

Also based on this model we chose a bottom cladding thickness of 10 μm (to be safe) and 3 μm core layer. Its cross section is illustrated in Figure 4.4.

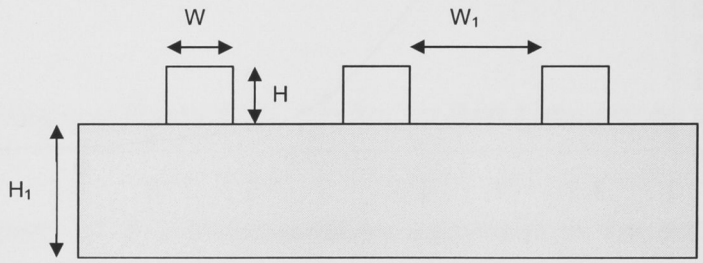

Figure 4.4 The IPG waveguides cross section structure. W is the width and H is height of rib core waveguides. They are both 3μm. And H_1 is the height of cladding, which should be larger than 7 μm. W_1 is the gap widths from 2.2 to 4.0 μm.

A new photo mask implementing this design for soft lithography was required. The details are described below in Figure 4.5.

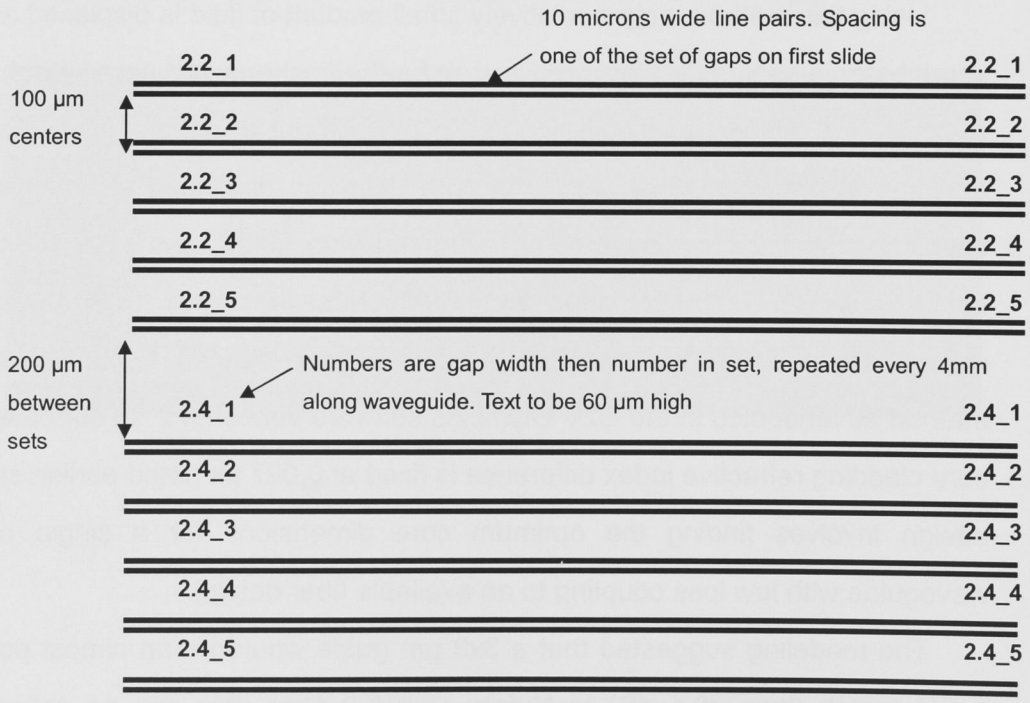

(a)

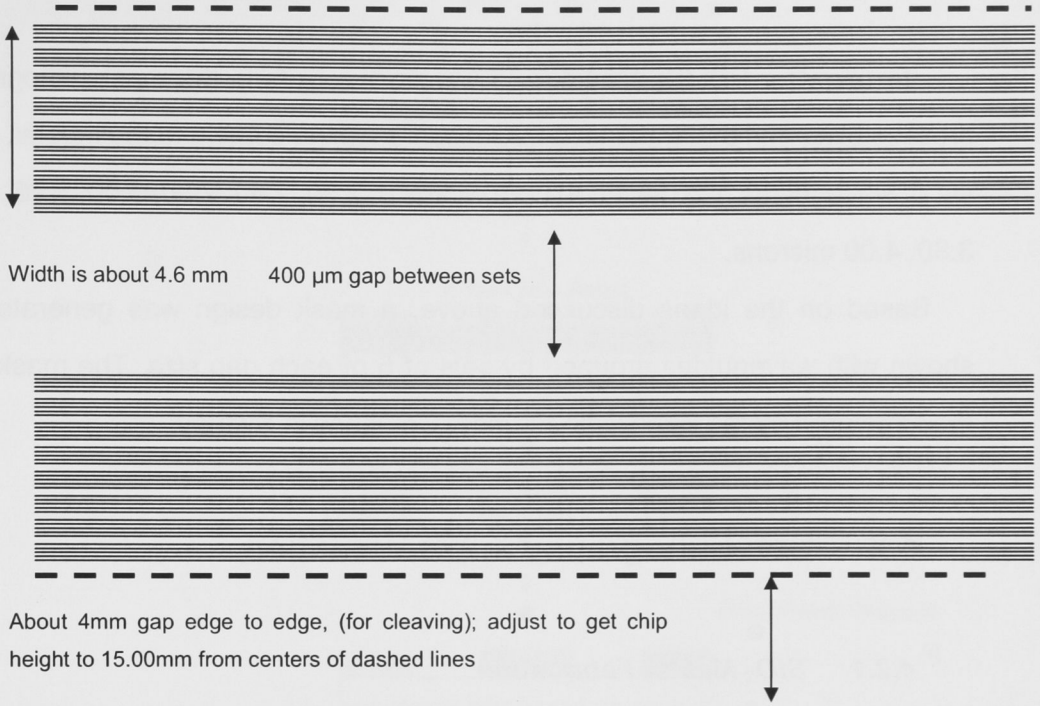

(b)

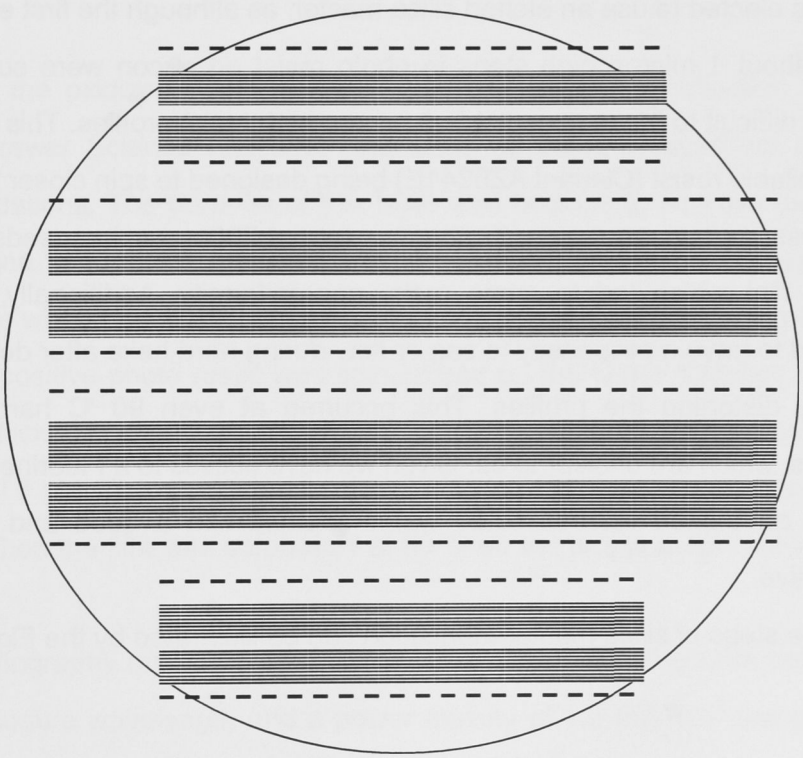

(c)

Figure 4.5 (a) Waveguide set details; (b) Chip details zoomed out to single chip level; (c) Overall mask layout.

To allow for PDMS shrinkage, dimensional errors in the mask, lithography process bias, and the option of applying a smoothing coating to the master, each set of waveguides had designed core widths of 2.20, 2.60, 2.80, 3.00, 3.20, 3.40, 3.80, 4.00 microns.

Based on the ideas discussed above, a mask design was generated as shown with waveguides grouped by sets of 5 of each gap size. The mask was manufactured by the Bandwidth Foundry Company in Sydney.

4.2 Soft Lithography Implementation

4.2.1 SiO_2 Master Fabrication

We elected to use an etched silica master, as although the first experiments using about 1 micron high steps in photo resist on silicon were successful, it proved difficult to make acceptable 3 micron high resist profiles. This was due to the available resist (Clariant AZ5241E) being designed to spin closer to 1 micron thickness, and so we required rather low (about 700nm) spin speeds to get a 3 micron film which led to some resist non-uniformity. Additionally, the resist seemed to have a propensity to sag or flow during hard bake after development, thereby distorting the profiles. This occurred at even 90 ℃ hard bake for reasons, which are unclear to us. Given we have access to a Fluorine based ICP etcher, an etched thermal oxide wafer seemed like a good and accessible alternative.

The steps of silica master fabrication can be illustrated by the Figure 4.6:

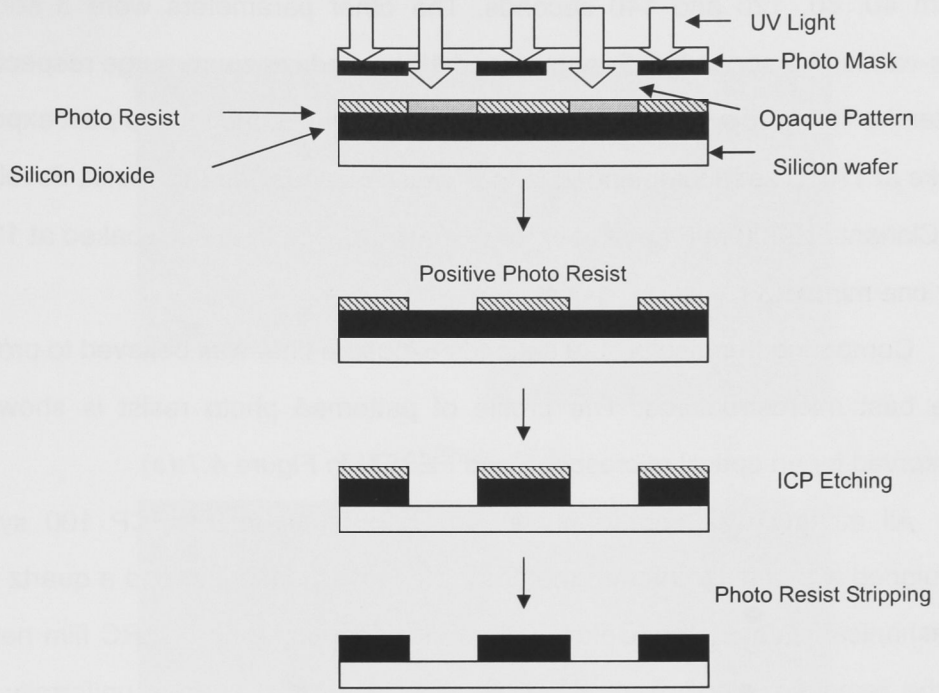

Figure 4.6. Procedure of silicon dioxide mold fabrication

Firstly, the oxidized wafer was coated with bottom anti-reflection coating (BARC). Brewer Science XhiRC-16 was used as per the datasheet process recommendations. The purpose of this layer was twofold: to improve the resist adhesion and to suppress the strong standing wave effects which degrade the resist profile when monochromatic 365nm radiation is used for resist exposure.

Then, positive photo resist was spin-coated on the wafer (Clariant AZ MiR 701). The thickness of photo resist was about 1.5 μm, and the silicon dioxide film was around 5 μm. The conditions for the photo resist spin were 1000 rpm for 45 seconds. Then the film was soft baked at 90 ℃ on the hotpla te for one and half minutes.

The lithography mode we used for this photo resist was vacuum contact at 365nm exposure wavelength and a power density of 1.5 mW/cm^2 using a Karl Suss MA6 mask aligner. The main benefit of this mode is the high resolution and better profile it gives compared to soft contact option. In order to optimize the processes, we ran several different exposure times. The exposure time was set

from 40, 80, 120 and 140 seconds. The other parameters were 3 seconds pre-vacuum, 5 seconds full vacuum and 10 seconds vacuum purge respectively. After the lithography procedure, the wafer was given a one minute post exposure bake at 110 ℃ as recommended in the process manual for this resist, developed in Clariant AZ-300 MIF developer for one minute, and then hard baked at 110 ℃ for one minute.

Comparing the results, 120 seconds exposure time was believed to produce the best microstructures. The profile of patterned photo resist is shown as observed by an optical microscope and FESEM in Figure 4.7 (a).

All etching was carried out in an Oxford Instruments ICP 100 system equipped with a laser interferometer for etch rate monitoring, and a quartz plate mechanical wafer clamp. Before silicon dioxide etching, the BARC film needed to be removed, since it could be an obstacle to final surface uniformity. The working conditions were 30 sccm O_2 with 20 W RF power and 200 W ICP power for 2 min. The chamber pressure was 10 mTorr.

In silicon dioxide etching, 50 sccm Argon gas and 50 sccm CHF_3 gas were employed as processing gases. The RF power was 150 W and no ICP power was used (i.e., pure RIE mode etch). A helium wafer backside cooling system controlled the wafer temperature at 20℃ and the wo rking pressure was 30 mTorr. The silicon dioxide etching rate is generally about 35 nm per min and the selectivity ratio is 4 to 1 (silicon dioxide to photo resist). After etching, the ICP chamber needed to be cleaned without the sample in it by oxygen plasma, since CHF_3 forms some polymers in it. Failure to clean before stripping the resist with an oxygen plasma results in the generation of free fluorine and further etching, so this step is crucial. Finally, the photo resist was stripped by 30 sccm O_2 at 20℃ with 100 W RF power and 500 W ICP power for fi ve minutes at 30 mTorr. Photo resist etch rate was 500 nm per min under these conditions. The etched structures of silicon dioxide are shown by FESEM in Figure 4.7 (b) as well. The sidewall of etched silica is almost vertical in the figure below. Furthermore, smooth and low defect ribs were formed after etching.

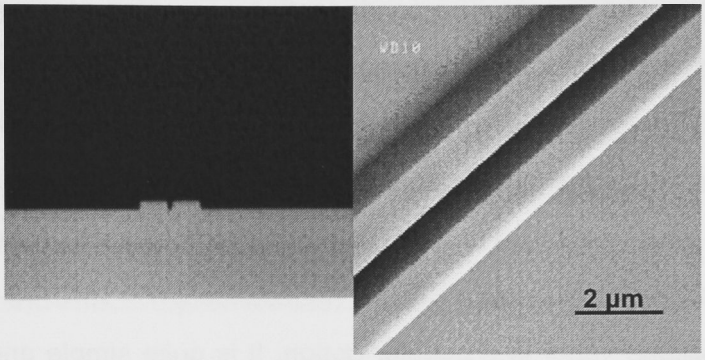

(a) Photo resist

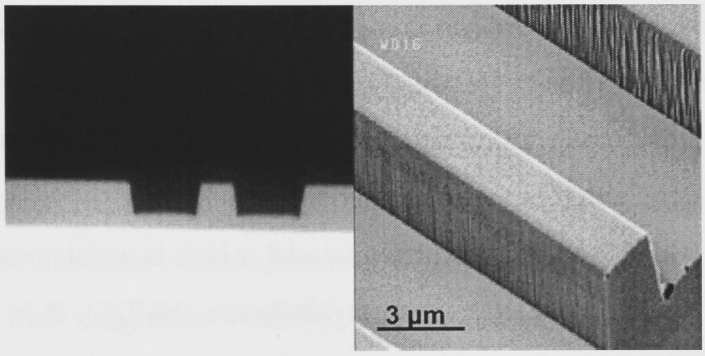

(b) Etched silicon dioxide

Figure 4.7. Cured photo resist and etched silicon dioxide microstructure images by optical microscope (left image) and FESEM (right image).

4.2.2 Release Treatments for Stamp Fabrication

As noted above, PDMS can adhere strongly to silicon dioxide. Experimentally we observed that plasma etched silica always results in non-releasable adhesion, whereas virgin thermal oxide would release more often than not. It is important to make the SiO_2 master's surface hydrophobic and free from polar species after fabrication, since PDMS (believed to be hydrophilic) reacts with the surface hydroxyl groups. This causes a covalent connection between the stamp and the master, which destroys both as the stamp can not be released when this occurs. Moreover, if the substrate is hydrophilic before curing

the stamp, capillary condensation of water can occur in narrow contact gaps, even in dry environments. The condensation generates capillary pressure that can pull surfaces into contact causing extremely high adhesion strength between two layers. To avoid destroying the stamp and mold, the mold needed to be hydrophobized by gas-phase deposition, or chemical or physical treatments.

There are several treatments commonly employed to make hydrophobic masters. Chemical treatment with (tridecafluoro-1, 1, 2, 2-tetrahydrooctyl) -1-trichlorosilane vapor is a popular option. It is quite simple and efficient. The treatment just requires the master to be placed in a vacuum vessel with a small beaker containing a few drops of (tridecafluoro-1, 1, 2, 2-tetrahydrooctyl) -1-trichlorosilane. The vessel was then evacuated to create the vapor. However, this material is somewhat hazardous, and given the lack of suitable extraction facilities in our clean room we elected not to use it.

There is also another chemical material, which is widely used in the silicon fabrication industry, called Hexamethyldisilizane (HMDS). It is considered an excellent method for chemically drying hydrated surfaces. Generally, HMDS is used as an adhesion promoter for photo resist. HMDS is also a somewhat hazardous material and so this was not tried either.

The hydrophobic method used in this work was a physical plasma treatment to form a Teflon-like film on the master surface, which is believed to be the most hydrophobic option. Actually, for thicker films, plasma polymerized fluorocarbons, which resemble PTFE (Teflon), have many good qualities such as high hydrophobicity (θ is about 109 degree), chemical inertness, smoothness and durability [31]. The advantages of plasma deposited films are the additional flexibility of controllable film thickness compared to the other hydrophobic approaches and simple stripping in oxygen plasmas.

The treatment was carried out in the ICP system described earlier. It has two generators in the chamber, one directly powering the lower electrode (table generator), and the other being the inductively coupled source (ICP generator). In IPG etching, both generators were employed. However, for polymerization

applications, judicious use of the table generator is required as it produces ion bombardment, which may inhibit or remove the film that is desired. The details of the ICP system can be found in section 3.6.3. For the experiments, trifluoromethane (CHF_3) was used as a monomer source. Although CHF_3 has a larger fluorine to carbon ratio (3 to 1) than the recommended value of 2, it is still a good candidate for this application. In fact, the presence of hydrogen facilitates polymerization and effectively lowers the fluorine to carbon ratio closer to 2 to 1. [34]

Deposition of anti-adhesive Teflon-like film

In this work, we investigated two different Teflon-like films processes in ICP, one obtained in the presence of ion sputtering (with the table generator in the ICP system), and the other by pure plasma polymerization (ICP generator in ICP system). Using both deposition methods, we deposited thin fluorinated films on both silicon and silicon dioxide substrates for a detailed comparison. In a subsequent step, etched silicon dioxide surfaces covered by both anti-adhesive coatings had PDMS cast and cured upon them to verify the release properties. During the deposition process, the influence of the operating parameters was also investigated and resulted in a better understanding of what possibilities the process offered.

Because of the tight C-F bonding in fluoro-carbon films, such materials have very low surface energy. Perhaps the best known of this class of materials is Polytetrafluoroethylene (PTFE), whose anti-stick properties are well known. Their hydrophobic properties make them excellent anti-wetting layers. However, the detailed properties of the films depend critically on the technique and the parameters of the deposition and the substrate.

PTFE (or Teflon) is arguably one of the most useful materials ever developed having found applications in a wealth of fields. It is hydrophobic and one of the most chemically resistant polymers, insoluble in practically any

solvent and non-reactive to many of the corrosive chemicals, including hydrofluoric acid. It also offers high thermal stability, excellent electrical resistance, low refractive index and is a lubricious and biocompatible coating. PTFE has a low surface energy and is an excellent choice for an anti-adhesion or release coating. Though conventionally difficult to process, CVD (Chemical Vapor Deposition) has pioneered a deposition process for producing ultra-thin PTFE coatings. This process is an effective method for producing coatings with precisely controlled thicknesses at low temperature with excellent adhesion. Since it is a vapor deposition process, coatings are conformal, or able to penetrate into and around complex structures. However, due to equipment limitations, the only possible option in this work was to utilize PECVD-type processes rather than the more conventional thermally activated CVD processes.

Two sets of experiments were run; firstly, the table generator alone was employed as deposition power source, and secondly the ICP generator alone. Operating pressures ranging from 20 to 50 mTorr and CHF_3 gas flow rate was set at 20 sccm. Films were deposited on both silicon and silicon dioxide substrates. During the experiments, the table temperature in the ICP system was set as 20 ℃ and the backside helium cooling system pressure was 10 mTorr. All processing times were 5 minutes except where otherwise indicated. The thickness of the deposited films and the underlying silicon dioxide were measured using a SCI FilmTek 4000.

Since CHF_3 is able to attack the silicon dioxide as well, this forced us to deposit PTFE films on both silicon dioxide and silicon substrates simultaneously to check how much silicon dioxide thickness might be lost during PTFE deposition.

Process nr.	TP, W	WP, mTorr	T, nm	RMSE	BV, V
1	150	20	0	0.83	375
2	300	20	0	0.75	715
3	450	20	17.8	0.51	900
4	150	30	0	0.73	375
5	300	30	16.2	0.86	715
6	450	30	19.3	0.83	900
7	150	50	0	0.64	375
8	300	50	0	0.68	715
9	450	50	0	0.61	900

(a)

Process nr.	TP, W	WP, mTorr	T, nm	EST, μm	RMSE	BV, V
1	150	20	0	0.08	1.58	375
2	300	20	0	0.0382	1.66	715
3	450	20	0	0.0407	1.54	900
4	150	30	0	0.0037	1.46	375
5	300	30	12.8	0.023	1.55	715
6	450	30	12.5	0.0204	1.41	900
7	150	50	0	0	1.59	375
8	300	50	11.7	0.0082	1.45	715
9	450	50	0	0.0066	1.48	900

(b)

Table 4.2. PTFE films are deposited by using table generator. **(a)** Different parameters and measured PTFE film thicknesses for the different plasma processes on silicon substrate (nr. 1–9). **(b)** Different parameters and measured PTFE and etched silicon dioxide film thicknesses for the different plasma processes on silicon dioxide substrate (nr. 1–9). The initial silicon dioxide thickness is 2.5041 μm by using SCI FilmTek 4000. The power values (ICP power - IP and Table/Forward power - TP), the bias voltages (BV), the working pressures (WP), the RMS errors from measurement (RMSE), the measured PTFE film

thicknesses (T) and the measured etched silicon dioxide thickness (EST) are summarized in Table 4.2.

Process nr.	IP, W	WP, mTorr	T, nm	RMSE	BV, V
1	150	20	45.1	0.67	0
2	300	20	9.6	0.82	0
3	450	20	0	0.4	0
4	150	30	64.2	0.71	0
5	300	30	24.8	0.37	0
6	450	30	8.5	0.39	0
7	150	50	47.8	0.52	0
8	300	50	47	0.43	0
9	450	50	30.6	0.31	0

(a)

Process nr.	IP, W	WP, mTorr	T, nm	EST, μm	RMSE	BV, V
1	150	20	0	0.0373	1.63	0
2	300	20	0	0	1.46	0
3	450	20	0	0.0373	1.64	0
4	150	30	29.2	0.0568	1.59	0
5	300	30	105.4	0	1.41	0
6	450	30	19.5	0.0014	1.44	0
7	150	50	0	0.0494	1.53	0
8	300	50	36.4	0.0248	1.73	0
9	450	50	26	0.0198	1.49	0

(b)

Table 4.3. PTFE films are deposited by using ICP/upper generator. **(a)** Different parameters and measured PTFE film thicknesses for the different plasma processes on silicon substrate (nr. 1–9). **(b)** Different parameters and measured PTFE and etched silicon dioxide film thicknesses for the different plasma processes on silicon dioxide substrate (nr. 1–9). The initial silicon dioxide thickness is 2.5041 μm by using SCI FilmTek 4000. . The

power values (ICP power - IP and Table/Forward power - TP), the bias voltages (BV), the working pressures (WP), the RMS errors from measurement (RMSE), the measured PTFE film thicknesses (T) and the measured etched silicon dioxide thickness (EST) are summarized in Table 4.3.

The dependence of the deposition thicknesses on the RF power and working pressure is shown in Fig. 4.8.

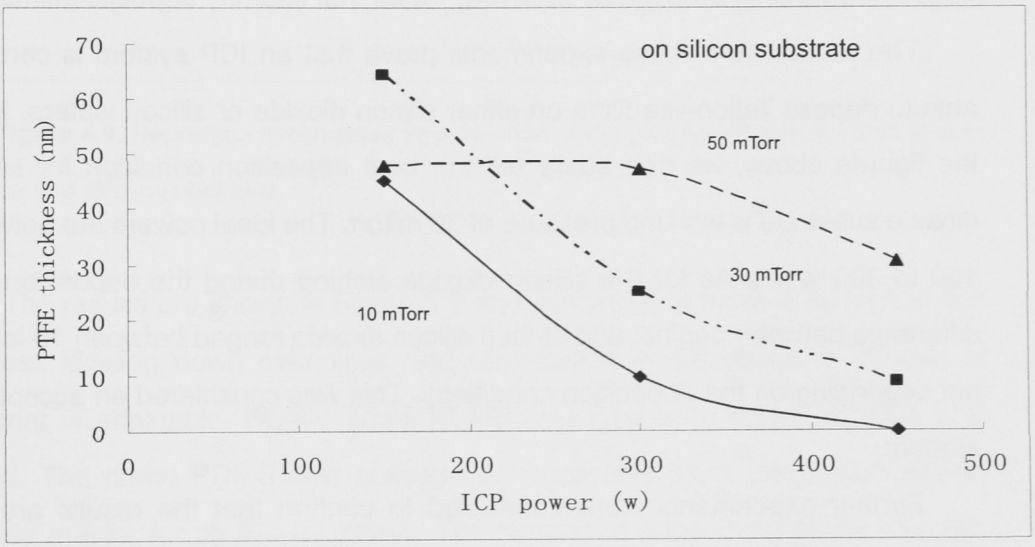

(a)

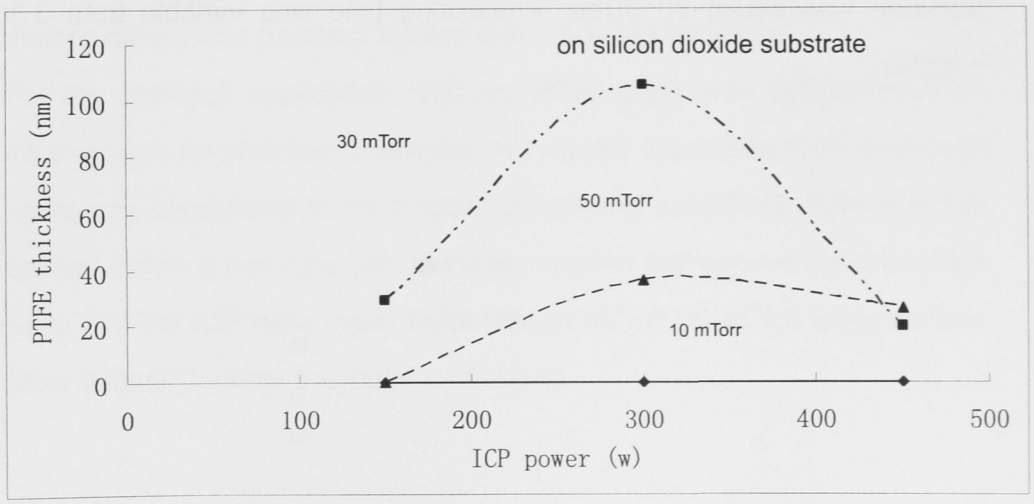

(b)

Figure 4.8. PTFE deposition thicknesses as a function of ICP RF power and working pressure. (a) Deposition on silicon by using ICP/upper generator only (b) Deposition on

silicon dioxide using ICP/upper generator only.

From the tables and Figure 4.8 above, the results are clearly better when PTFE was deposited by using ICP power alone. On the silicon substrate, increasing the ICP power leads to a decrease of the thickness at all working pressures. And on the silicon dioxide substrate, at relatively low power, the deposition thickness initially goes up with increasing power, but drops down above 300 watts. Moreover, at 10 mTorr, we cannot find any deposited films.

The results from these experiments prove that an ICP system is certainly able to deposit Teflon-like films on either silicon dioxide or silicon wafers. From the figures above, we can easily tell the best deposition condition for silicon dioxide substrate is working pressure of 30 mTorr. The ideal powers are between 150 to 300 watts. As for the silicon dioxide etching during the deposition, the difference between original and etched silicon dioxide ranged between 10 to 100 nm depending on the deposition conditions. This was considered an acceptable amount.

Further experiments were conducted to confirm that the results are not influenced by deposition time. ICP power was set at 150 watts. Working pressure was set at 30 mTorr. Processing time was variable from 3 to 40 minutes.

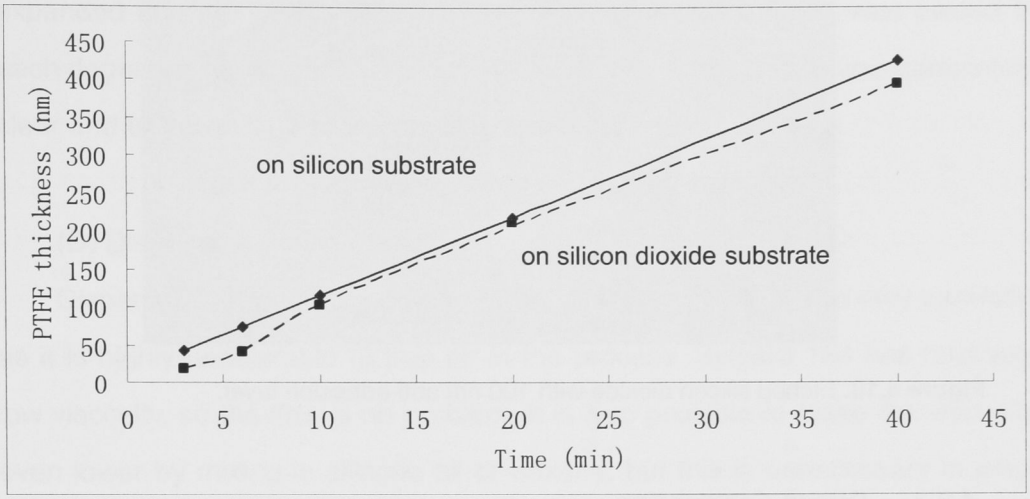

Figure 4.9. Deposition thicknesses as a function of the processing time on both silicon dioxide and silicon substrates.

The results are shown in Figure 4.9 and indicate that there is no sign of the process slowing down over time, and therefore any reasonable thickness of polymer is attainable. Finally, liquid PDMS was cast onto these samples and cured. The cured PDMS was successfully separated from the etched silicon dioxide master for all film thickness. The surface of treated silicon dioxide film was also scanned by FESEM. It was clear that there were no surface morphology differences between treated and untreated surfaces.

For the anti-stick application, 100 nm PTFE layer was considered thick enough to ensure no pinholes. Therefore, 10 minutes deposition at 30 mTorr with 150 watts was considered to be suitable processing conditions. Note that this was applied in two 5 min runs with the wafer rotated 180 degree between them to ensure that the ICP table mechanical clamps do not mask the wafer surface and allow adhesion where the wafer is clamped.

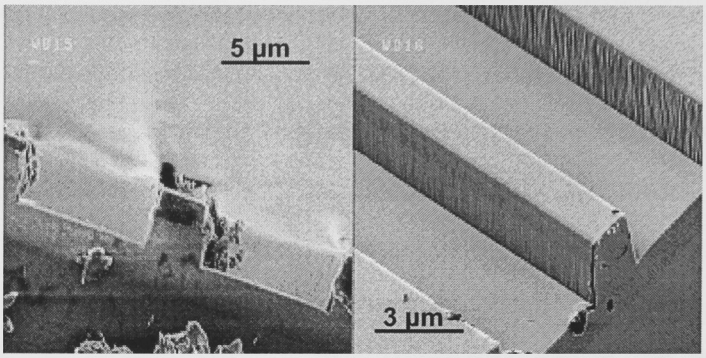

Figure 4.10. Etched silicon dioxide with 100 nm anti-adhesion layer.

4.2.3 Stamp Fabrication

The stamp fabrication is described by the following steps:

(A) Weighing

Sylgard 184 is a two-component heat-activated-curing system. It consists of a base part and a curing agent part. A plastic cup was filled with one part curing agent and ten parts of base (by weight). 7 to10 g of liquid PDMS material was sufficient to cover one 100mm diameter wafer to a depth of about 3mm, requiring 0.7 g curing agent and 7 g base. A small error in the amounts does not affect the final result.

(B) Mixing

The base and the curing agent were manually mixed using a plastic spoon for at least 5 minutes, depending on the amount of material. The mix incorporates a lot of air into the solution. The mixed materials were left to vent in clean air for half an hour to let the air bubbles settle.

(C) De-gas

Removal of the air bubbles was accomplished by vacuum degassing in a vacuum oven, but at room temperature. During the degassing the mixture

expanded and started foaming, so only a small (<5 g) amount was placed in each degassing container to prevent overflow. When the silicone was completely clear and transparent this process was finished.

(D) Dispensing

Dispensing of the silicone on to the template was carried out very carefully, as it is highly undesirable to trap air in the process. Sylgard 184 has relatively low viscosity, so the flow is no problem. It is also possible to make the viscosity even lower by mixing in silicone oil or hexane, but this is unnecessary in most cases. Normally, we slowly dispensed the material at the center of the master from just above its surface to minimize the risk of trapped air. Another point to note is that the master should remain horizontal during dispensing.

(E) Spreading

Spreading was accomplished by tilting the master at a small angle. The material flows and by varying the direction of tilt was spread over the whole surface. When coverage was completed, the master was left horizontal for several minutes in order to get a flat top surface. Stamp thickness can range from about 0.1 to 5 mm or more depending on the amount of liquid dispensed.

(F) Curing

PDMS is cured by an organometallic cross-linking reaction. In curing, the liquid mixture becomes solid via a hydrosilation reaction between vinyl groups and hydrosilane groups forming Si $-CH_2-CH_2-$ Si linkages. Sylgard 184 is heat cured. It is curable from below room temperature to over 150℃. Three recommended curing schedules are as follows; 4 hours at 65 ℃, or 1 hour at 100 ℃, or 15 minutes at 150 ℃. But, Sylgard 184 a lso displays temperature dependant shrinkage as illustrated below [14]. Curing at 100℃ for about 1 hour will make the stamp shrink almost exactly 2.5 %. Therefore, according to our requirements, 65 ℃ for about 4 hours was the best option, since there is only

about 1 % shrinkage and the curing time is acceptable. Before the coated master was placed into a pre-heated oven, it was checked visually to ensure there were no remaining air bubbles. If present these were removed using an additional degassing step to prevent the bubbles being incorporated into the stamp.

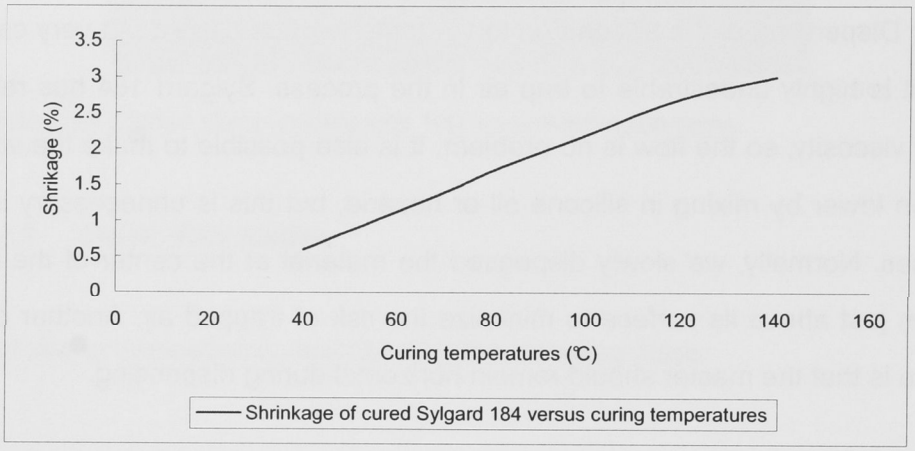

Figure 4.11. Curing time versus Shrinkage of Sylgard 184

(G) Peeling Off

The final step is to peel off the stamp from the master. Generally, a sharp and curved pair of tweezers was used to do this. Peeling off started by releasing the entire periphery and then continued slowly in a direction parallel to the largest number of structures. The stamp was stored in a flat plastic container with the pattern facing upwards, i.e. away from the container base.

4.3 Soft Lithography Methods for IPG

The available soft lithography options are listed in Table 4.1, but not all of them are suitable for IPG-based waveguides fabrication.

Soft Embossing

Soft embossing is a cost-effective, high throughput manufacturing technique that imprints microstructures in thermoplastic or light curable materials. However, embossing is not yet a mainstream method for fabricating microstructures in semiconductor manufacturing and other micro devices. It is reported that embossing can be used to make features as small as 25 nm on silicon, and has a very attractive future in the application of micro fabrication industry [9, 10].

Soft embossing has a drawback that there is a thin layer left on the substrate where none is desired. In most cases, this is not a serious problem, as it is easily stripped. The main steps in soft embossing are illustrated in Figure 4.12.

The first step is to spin the polymer layer. Optimally the thickness of the layer will be chosen based on the volume into which the fluid is expected to flow. In the case of isolated waveguides, this would require a very thin layer indeed as the total volume is small. As noted previously this is not an option with IPG as it is very hard to spin such thin layers, and also the flow required would be problematic due to the relatively high viscosity of IPG. We used a minimum displacement type stamp so that the waveguide core layer is spun on at approximately the desired thickness, i.e. 3 microns. This was accomplished in the L-3 IPG by spinning for 180 seconds at 9500 rpm.

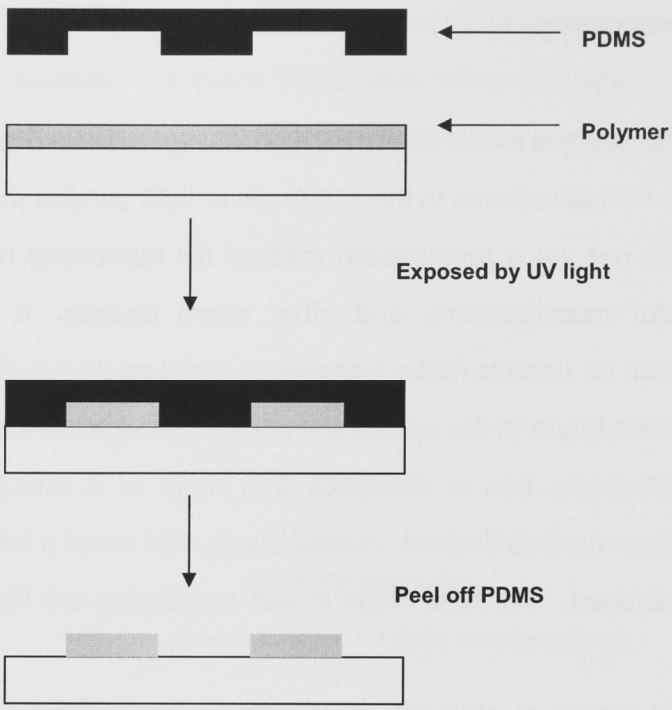

Figure 4.12. The basic steps in embossing procedure

Next the stamp has to be applied to the liquid IPG layer. In soft embossing, the stamp generally does not need to be plasma treated. The stamp is placed in conformal contact with the IPG film. Specially, for thermoset or thermocure materials, the substrate is heated to make the film soft (that is why sometimes this method is called soft embossing) while a uniform pressure is applied on the stamp by vacuum chamber. For IPG films, the heating step is not required.

In our work after exposure by UV light, the IPG is cross-linked. The stamp can then be removed. The whole process is simple and efficient. Generally this process is carried out in a specialized nanoimprint tool, which resembles a standard contact aligner with some extra features. However, we did not have access to such a tool and had to resort to applying the stamp by hand.

The initial results of embossing IPG on silicon wafer without using an embossing tool were observed by microscope and FESEM in Figure 4.13 and 4.14. The widths of these waveguides were 3 and 1 μm. Some submicron

features are also illustrated as well. As shown below, the microstructures achieved smooth and straight cross-section.

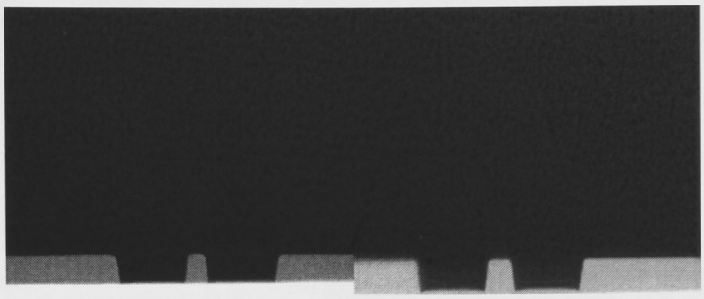

(a) By microscope

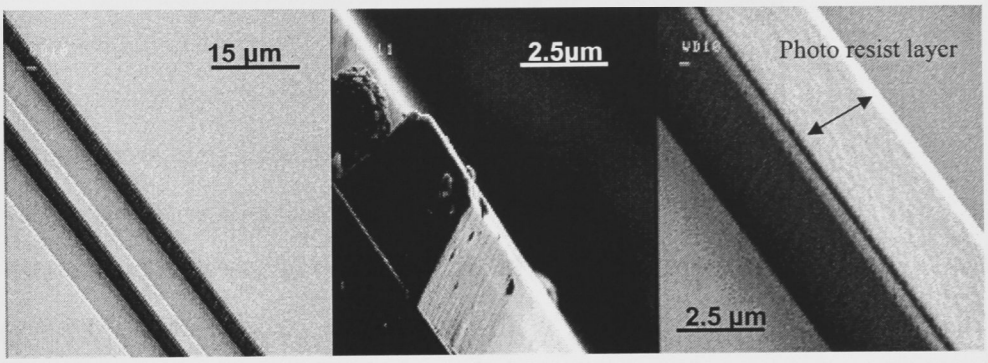

(b) Waveguides scanned by FESEM

Figure 4.13. (a) Left optical image is 3 μm waveguide without residual layer. Right optical image is 3 μm waveguide with about 1 μm residual layer. (b) The right FESEM image is top view of waveguide. The middle FESEM image is sidewall view of this waveguide (an extra layer on waveguide is incomplete etched photo resist remain left on the stamp before casting stamp from mast, which is supposed to be stripped but is unfortunately left.)

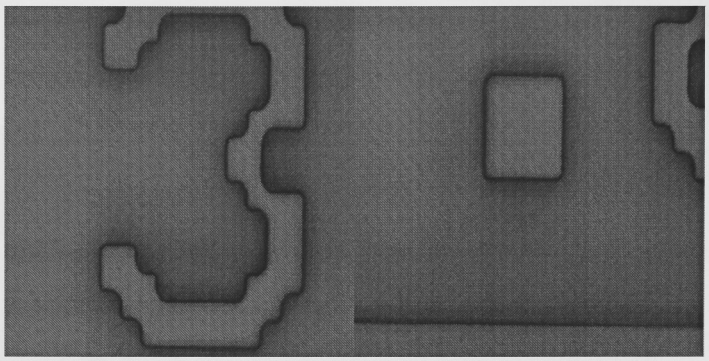

(a)

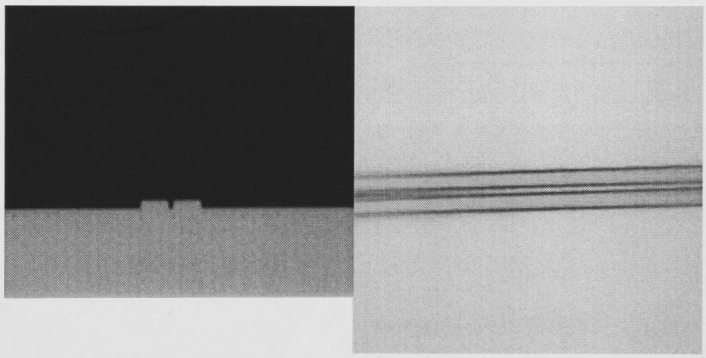

(b)

Figure 4.14. (a) The left image shows the pattern on IPG film and the right image presents the dot beside the number "3" on patterned IPG film. All these features are submicron. (b) 0.5 micron gap between 1 micron waveguide lines in IPG (left image) and PDMS (right image).

In addition, the IPG thickness is flexible and non-critical and can be controlled by different spin speeds from 3 μm to over 10 μm. However, because of equipment limitations, the stamps have to be loaded onto IPG film by hand, which raises the issues of thickness non-uniformity and residue of embossed features (several nanometers) on patterned IPG films shown in Figure 4.15.

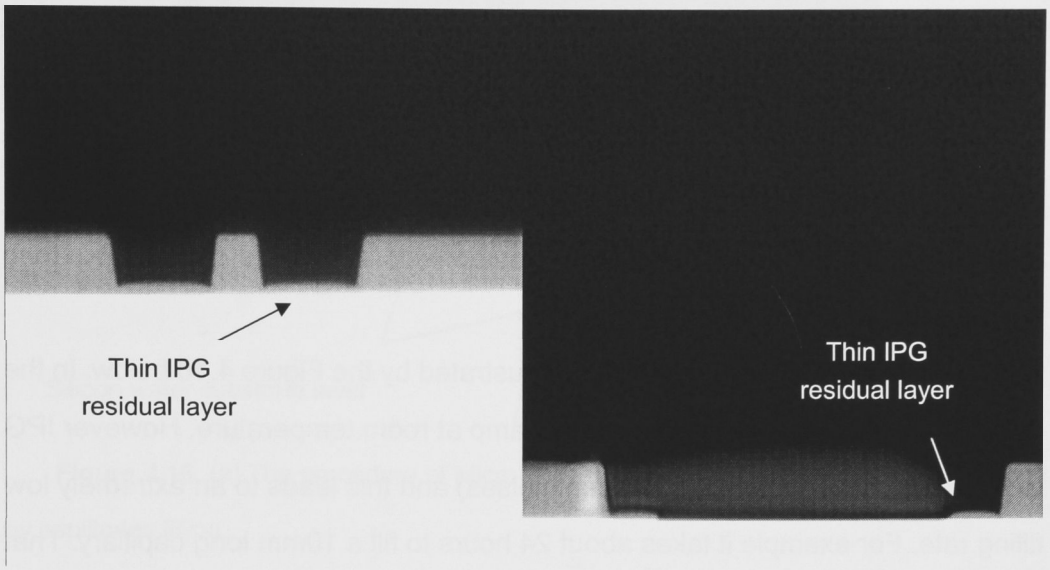

Figure 4.15. The thin residual layers on IPG after soft embossing.

Micro molding in Capillaries

Given the limitations of hand application of the stamp in soft embossing, we experimented with MIMIC. Capillary filling is a very simple and well-known phenomenon [32], and the dynamics of the wetting and spreading of liquids in capillaries has been studied systematically [33]. Different geometries of liquid flow pathways may result in different capillary filling behavior including the possibility of trapping air bubbles, etc. In circular capillaries, the flow of a wetting liquid occurs initially for films that wet the capillary symmetrically; in noncircular capillaries the most rapid flow usually occurs in the corner regions. [33]

Micro molding in capillaries is able to generate microstructures down to one micrometer [4], beyond which the limitation is the filling of the capillaries. The normal steps are: firstly, place the stamp on a substrate with the relief facing towards the substrate. This way allows capillaries to be formed. Then these capillaries are filled with the material to be molded by submerging one end of the capillaries in the liquid. The capillary force makes the liquid flow into the capillaries. Once the material has entered the capillaries it is cured by UV light.

Sometimes, it can also be cured chemically using a curing agent or by heating. The stamp is then removed.

Micro molding in capillaries has the ability to form complex microstructures on both planar and nonplanar surfaces. However, there are also several limitations in the MIMIC method. For example, the efficiency of this method decreases for long structures since viscous effects in the fluid can result in long fill times.

The MIMIC processing details are illustrated by the Figure 4.16 below. In the experiments, we filled IPG into PDMS stamp at room temperature. However IPG is a high viscosity material (2300 centipoises) and this leads to an extremely low filling rate. For example it takes about 24 hours to fill a 10mm long capillary. That is to say, in order to cover a 4-inch wafer, it could cost ten days.

Another issue is the uniformity of the IPG film. The IPG film and waveguides formed by MIMIC were found to vary significantly in thickness across the structure. The details are illustrated by the images below.

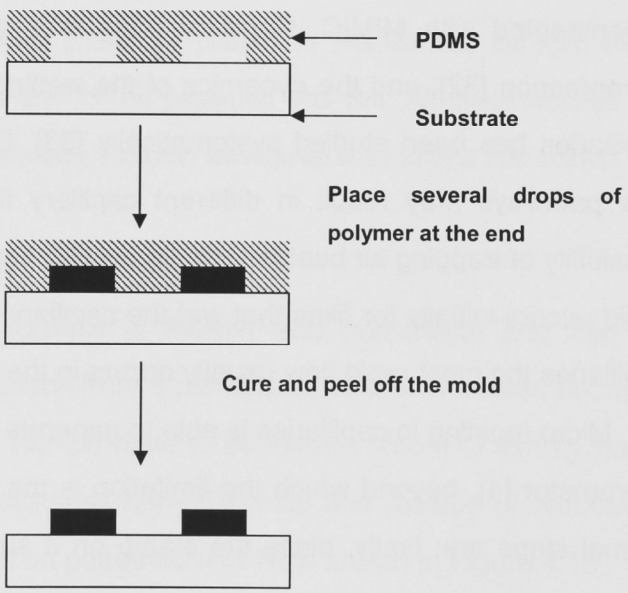

(a)

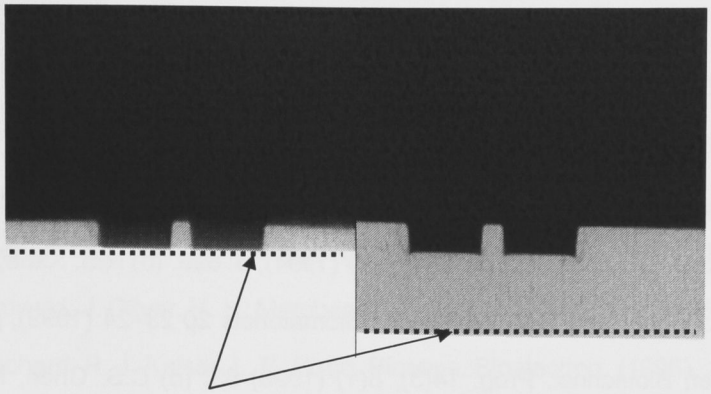

Silicon wafer substrate level

(b)

Figure 4.16. (a) The procedure of Micro molding in capillaries. (b) Waveguides formed by capillaries filling.

4.4 Conclusions

We have described a soft lithography demonstration for the fabrication of IPG-based waveguides. The applied procedures are relatively simple and efficient and apper to result in high quality structures which look very suitable for low loss waveguides. Furthermore, we have demonstrated the ability to control the deposition of Teflon-like films by ICP system, which benefits soft embossing applications by providing a release layer, and even a smoothing film option. We successfully demonstrated all the possible soft lithography processes for IPG waveguide fabrication, and the previous soft embossing experiments suggest that our approach may be viable at nanometer length scales as well.

Unfortunately, as we do not have a nanoimprint/soft embossing tool, we were unable to demonstrate the end results (We could not apply the stamp just by hands and obtain uniform waveguides more than 1 cm length.). The same issue is also raised in Micro molding in capillaries experiments. However, considering the ease of processing of IPG materials into optical waveguides, the suggested soft lithography methods could be a basis for cheap and disposable methods for IPG waveguide fabrication.

Reference

[1]. (a) R. Singhvi, A. Kumar, G.P. Lopez, G.N. Stephanopoulos, D.I.C. Wang, G.M. Whitesides and D.E. Ingber Science 264 5159 (1994), p. 696. (b) R.S. Kane, S. Takayama, E. Ostuni, D.E. Ingber and G.M. Whitesides Biomaterials 20 23–24 (1999), p. 2363. (c) A. Folch, M. Toner, Biotechnol. Prog. 14(3), 8(1) (1998) 63. (d) C.S. Chen, M. Mrksich, S. Huang, G.M. Whitesides and D.E. Ingber Science 276 (1997), p. 1345.

[2]. A. Kumar, G. M. Whitesides, Appl. Phys. Lett. (1993), 63, 2002-2004

[3]. X.-M. Zhao, Y. Xia, G. M. Whitesides, Adv. Mater. (1996), 8, 837- 840

[4]. E. Kim, Y. Xia, G. M. Whitesides, Nature (1995), 376, 581-584

[5]. Y. Xia, E. Kim, X.-M. Zhao, J. A. Rogers, M. Prentiss, G. M. Whitesides, Science (1996),273, 347 -349

[6]. E. Kim, Y. Xia, X.-M. Zhao, G. M. Whitesides, Adv. Mater. (1997), 9, 651- 654

[7]. P. E. J. Legierse, J. H. T. Pasman in Polymers in Information Storage Technology, Plenum, New York, (1989), p. 155.

[8]. P. Hoyer, N. Baba, H. Masuda, Appl. Phys. Lett. (1995), 66, 2700-2702.

[9]. J. S. Winslow, IEEE Trans. Consumer Electron. (1976) (Nov.), 318 - 326.

[10]. S. Y. Chou, P. R. Krauss, P. J. Renstrom, Appl. Phys. Lett. (1995), 67, 3114 -3116.

[11]. H. C. Haverkorn van Rijsewijk, P. E. J. Legierse, G. E. Thomas, Philips Tech. Rev. (1982), 40, 287 - 297

[12]. B. D. Terris, H. J. Mamin, M. E. Best, J. A. Logan, D. Rugar, Appl. Phys. Lett. (1996), 69, 4262 - 4264.

[13]. M. A. Roberts, J. S. Rossier, P. Bercier, H. Giault, Anal. Chem. (1997), 69, 2035 - 2042.

[14]. D. Y. Kim, S. K. Tripathy, L. Li, J. Kumar, Appl. Phys. Lett. (1995), 66, 1166 - 1168

[15]. N. L. Abbott, A. Kumar, G. M. Whitesides, Chem. Mater. (1994), 6, 596 - 602

[16]. A. Miehr, R. A. Fisher, O. Lehmann, M. Stuke, Adv. Mater. Opt. Electron. (1996), 6, 27 - 32.

[17]. M. Datta, J. Electrochem. Soc. (1995), 142, 3801 - 3806.

[18]. H. Tabei, S. Nara, K. Matsuyama, J. Electrochem. Soc. (1974), 121, 67- 69.

[19]. S. Leppävuori, J. Väänänen, M. Lothi, J. Remes, A. Uusimäki, Sens. Actuators A (1994), 41/42, 593 - 596.

[20]. H. Moilanen, J. Lappalainen, S. Leppävuori, Sens. Actuators A (1994), 43, 357 - 365.

[21]. E. Anczurowski, J. Oliver, R. H. Marchessault, CHEMTECH (1986), 16(5), 304 - 310.

[22]. A. P. Blanchard, R. J. Kaiser, L. E. Hood, Biosens. Bioelectron. (1996), 11, 687 - 690.

[23]. Q. M. Pai, B. E. Springett, Rev. Mod. Phys. (1993), 65, 163 -211.

[24]. T. M. Bloomstein,D. J. Ehrlich, Appl. Phys. Lett. (1992), 61, 708 - 781

[25]. X.-M. Zhao, Y. Xia, G. M. Whitesides, J. Mater. Chem. (1997), 7, 1069 - 1074

[26]. Y. Xia, G. M. Whitesides. Angew. Chem. Int. Ed. (1998), 37, 550-575

[27]. A. Kumar, H. Biebuyck, G. M. Whitesides, Langmuir (1994), 10, 1498 - 1511.

[28]. M. K. Chaudhury, Biosens. Bioelectron (1995), 10, 785 - 788.

[29]. Y. Xia, N. Venkateswaran, D. Qin, J. Tien, G. M. Whitesides, Langmuir (1998), 14, 363 - 371.

[30]. J. A. Rogers, K. E. Paul, R. J. Jackman,G. M. Whitesides, Appl. Phys. Lett. (1997), 70, 2658 - 2660.

[31]. Ferencz S. Denes, Sorin Manolache, Prog. Polym. Sci. 29 (2004) 815 - 885

[32]. D. Myers, Surfaces, Interfaces, and Colloids, VCH, New York, pp. 87-109, (1991).

[33]. M. Dong, F. A. Dullien, I. Chatzis, J. Coll. Interf. Sci.172, 21- 31 (1995).

[34]. B. Kim, S.-K. Kwon, Solid-State Electronics 47 (2003) 1799 - 1803

Chapter 5

Conclusions and Outlook

5.1 Conclusions

The main objective of this work was focused on the fabrication and characterization of advanced polysiloxane waveguides in inorganic polymer glasses (IPGs) using processes targeted for low cost applications.

Given that it was previously known that the metallization of soft polymers is difficult, we made a systematic study of metallization of IPG films. Whilst it proved possible to sputter good quality Aluminum and Gold films, thermal treatment of the Aluminum (such as that used in photo resist processing) resulted in a rippling of the IPG underneath the film. Chromium could not be deposited due to excessive film tension tearing the IPG. At the use of a 200 nm silicon dioxide buffer layer on top of the IPG was shown to allow the Aluminum film to survive the required thermal processing, though it did not help the Chromium. However an Aluminum film can be used rather nicely for deep RIE etching of IPG films and was therefore adopted.

Optimized dry etching processes were developed allowing the fabrication of IPG waveguides using ICP plasma reactors with $CHF_3/O_2/Ar$ gas mixture for Aluminum/silicon dioxide/IPG structures and CHF_3/O_2 gas mixture for silicon dioxide /IPG structure. It was found that the $CHF_3/O_2/Ar$=6/18/6 at 20/200 W and 30 mTorr in processing leads to relative smooth sidewall IPG waveguides. It was also discovered that CHF_3/O_2 = 6/24 at 20/200 W and 10 dmTorr provides a high selectivity of ~20 between silicon dioxide and IPG films and smooth vertical sidewalls.

Standard semiconductor device processes have been used for fabricating IPG waveguides based on the silicon dioxide mask and CHF_3/O_2 etch process. The minimum achievable loss for a 4 μm wide IPG waveguide using a silicon dioxide mask was 0.73 dB/cm at 1550 nm and 0.34 dB/cm at 1316 nm compared to intrinsic material absorption losses of 0.5 and 0.25 dB/cm respectively. Given

that the silicon dioxide film used for this result was deposited by the inferior (compared to RF sputtering) PECVD technique, there are real prospects for further improvements to these figures.

A novel and highly accurate IPG waveguide fabrication method was also trialed making use of soft embossing with a PDMS stamp in non critical thickness spin on films. We have demonstrated that soft lithography, such as soft embossing, can achieve submicron and micron feature size, vertical and smooth sidewalls, nearly 90° corners in a single process s tep requiring no development, clearly an attractive high throughput low cost option. Our study also indicates that soft embossing can also potentially print very high resolution features. A process was also developed to enable fabrication of the stamp templates in silicon dioxide and for the stamps themselves. Processes to reliably deposit Teflon-like films for mold release on silicon dioxide master using the ICP etch system with CHF_3 were also demonstrated. The films are very hydrophobic and have the ability to penetrate into narrow openings beneath microstructures. Using this technology high quality stamps were routinely fabricated using PDMS.

5.2 Future Work

There are three main areas where follow up work would yield benefits.

Firstly for the etched waveguides, it would be worth repeating the Silicon dioxide mask etch using a sputtered film to see if the results are better. Likewise trialing of the Aluminum etch mask would be worthwhile to demonstrate deep etch capability.

Secondly, work remains to be done on the metallization problem. Chromium is an important material to be able to deposit reliably due to its use as both an etch mask and a thin film heater for active devices. Clearly further work is needed to find low film stress deposition conditions and to see if this results in a successful implementation on IPG.

Lastly, a suitable tool is required to enable reliable contacting of the PDMS stamp onto a wet IPG film to enable waveguide fabrication by the imprint technique. This is a particularly interesting approach as it is a single step method for waveguide fabrication which can produce very high quality devices. It eliminates a number of process steps saving both time and money and is therefore a potential breakthrough process for low cost components. This is therefore perhaps the most important of the three areas for future development.